

# Protoplanetary and Transitional Disks in the Open Stellar Cluster IC 2395

Zoltan Balog<sup>1</sup>, Nick Siegler<sup>2</sup>, G. H. Rieke<sup>3</sup>, L. L. Kiss<sup>4</sup>, James Muzerolle<sup>5</sup>, R. A. Gutermuth<sup>6</sup>, Cameron P. M. Bell<sup>7</sup>, J. Vinkó<sup>8</sup>, K. Y. L. Su<sup>3</sup>, E. T. Young<sup>9</sup>, András Gáspár<sup>3</sup>

balog@mpia-hd.mpg.de

## ABSTRACT

We present new deep UBVR<sub>I</sub> images and high-resolution multi-object optical spectroscopy of the young ( $\sim 6 - 10$  Myr old), relatively nearby (800 pc) open cluster IC 2395. We identify nearly 300 cluster members and use the photometry to estimate their spectral types, which extend from early B to middle M. We also present an infrared imaging survey of the central region using the IRAC and MIPS instruments on board the *Spitzer Space Telescope*, covering the wavelength range from 3.6 to 24  $\mu\text{m}$ . Our infrared observations allow us to detect dust in circumstellar disks originating over a typical range of radii  $\sim 0.1$  to  $\sim 10$  AU from the central star. We identify 18 Class II, 8 transitional disk, and 23 debris disk candidates, respectively 6.5%, 2.9%, and 8.3% of the cluster members with appropriate data. We apply the same criteria for transitional disk identification to 19 other stellar clusters and associations spanning ages from  $\sim 1$  to  $\sim 18$  Myr. We find that the number of disks in the transitional phase as a fraction of the total with strong 24  $\mu\text{m}$  excesses ( $[8] - [24] \geq 1.5$ ) increases from  $8.4 \pm 1.3\%$  at

---

<sup>1</sup>Max Planck Institute for Astronomy, Heidelberg, D-69117, Germany

<sup>2</sup>NASA Exoplanet Exploration Program, Jet Propulsion Laboratory, 4800 Oak Grove Drive, Pasadena, CA 91109

<sup>3</sup>Steward Observatory, 933 N. Cherry Ave, University of Arizona, Tucson, AZ 85721, USA

<sup>4</sup>Konkoly Observatory, Research Center for Astronomy and Earth Sciences, P.O. Box 67, H-1525 Budapest, Hungary

<sup>5</sup>Space Telescope Science Institute, 3700 San Martin Drive, Baltimore, Maryland 21218, USA

<sup>6</sup>Department of Astronomy, University of Massachusetts, Amherst, MA, USA

<sup>7</sup>Institute for Astronomy, ETH Zürich, Wolfgang-Pauli-Str. 27, 8093, Zürich, Switzerland

<sup>8</sup>Dept of Optics and Quantum Electronics, University of Szeged, H-6720, Szeged, Hungary

<sup>9</sup>NASA Ames SOFIA Science Center, N211, Mountain View, CA 94043, USA

$\sim 3$  Myr to  $46 \pm 5\%$  at  $\sim 10$  Myr. Alternative definitions of transitional disks will yield different percentages but should show the same trend.

*Subject headings:* stars: pre-main-sequence – circumstellar matter – infrared: stars; IC 2395

## 1. Introduction

The *Spitzer Space Telescope* (*Spitzer*; Werner et al. 2004) has significantly improved our understanding of how protoplanetary disks form, evolve, and eventually dissipate. By 15 Myr the accretion of gas onto protostars has largely ceased and most primordial disks have dissipated (eg. Haisch et al. 2001; Mamajek et al. 2004; Meng et al. 2016). By this time, planetesimals have formed and dust produced in their collisions yields planetary debris disks. These regenerated disks indirectly reveal the presence of planetary bodies required to replenish the dust and allow us to trace the evolution of planetary systems over the full range of stellar ages (e.g., Lagrange et al. 2000; Dominik & Decin 2003; Wyatt 2008; Gáspár et al. 2013; Sierchio et al. 2014).

The beginning of the transition from an optically-thick accretion disk to an optically-thin debris disk occurs from the inside-out (e.g. Skrutskie et al. 1990; Sicilia-Aguilar et al. 2005; Megeath et al. 2005; Muzerolle et al. 2010; Espaillat et al. 2014) and is marked by a characteristic spectral energy distribution (SED) with little excess at shorter ( $< 6\mu\text{m}$ ) wavelengths but still retaining strong emission at the longer ones. These “transitional” disks appear to represent the process of clearing “caught in the act”. The result is a largely evacuated inner region accompanied by an optically-thick primordial disk at larger radii. This phase is crucial to our understanding of disk dissipation and planet formation because it signals the end of stellar accretion and the consumption of nearly all the gas in the disk. Given the small number of transitional disks identified relative to the number of primordial and debris disks, it has been concluded that this phase is of short duration, on the order of a few hundred thousand years (Skrutskie et al. 1990; Kenyon & Hartmann 1995; Simon & Prato 1995; Wolk & Walter 1996; Muzerolle et al. 2010; Espaillat et al. 2014).

The key time period to observe the transitional phase is from a few to about 15 Myr. Clusters and associations are ideal laboratories for studying disk evolution as the member stars are coeval to within a few million years, of similar composition and reddening, at similar and reliably measured distance, and numerous enough to have a wide range of masses and to support drawing statistically valid conclusions. Unfortunately, there are only a few appropriately aged young clusters within a kiloparsec to support characterizing the transitional

disk phase. For more distant clusters, *Spitzer* has insufficient sensitivity in the mid-infrared to measure the photospheres of the lowest mass members and to identify complete samples of transitional disks.

The open cluster IC 2395 can augment studies of this phase of disk evolution. The cluster is 800 pc distant (Section 3.3, Claria et al. 2003). Despite its proximity, it has not been extensively studied. Claria et al. (2003) conducted the largest photometric investigation of the cluster, identifying candidate members and estimating the cluster’s age, distance, extinction, and angular size. Sensitive to a limiting magnitude of  $V < 15$  mag, their survey found 78 probable and possible members through *UBV* photometry. There have also been several proper motion studies but none combined with photometric data. The cluster age has been estimated at  $6 \pm 2$  Myr (Claria et al. 2003) on the traditional calibration for young cluster and association ages (e.g., Mamajek 2009). A revised age calibration has been proposed (e.g., Pecaution et al. 2012; Bell et al. 2013, 2015), on which we derive in this paper an age of  $\sim 9$  Myr (Section 3.3). On either calibration, IC 2395 is in the critical range to characterize transitional disk behavior.

To increase our understanding of this cluster, we have obtained  $\sim 45$  square arcmin fields of deep optical (*UBVRI*), and mid-IR (3.6, 4.5, 5.8, 8.0 and  $24\mu\text{m}$ ) photometry and high-resolution optical spectroscopy of IC 2395. We describe the new observations in Section 2 and discuss the cluster membership and age in Section 3. In Section 4, we identify and characterize the circumstellar disks in the cluster with emphasis on identifying transitional disks. We combine these results with a homogeneous treatment of transitional disks in 19 other young clusters and associations in Section 5, to probe the evolution of circumstellar disks through the transitional phase. We summarize and conclude the paper in Section 6.

## 2. Observations and Sample Selection

In this section, we discuss the *Spitzer* observations and data reduction for IC 2395, as well as our optical *UBVRI* observations and spectroscopy of selected probable members. In addition to the photometry described below, we took JHK measurements from 2MASS. We also re-examine the results of Claria et al. (2003) and include appropriate members from their work in our study.

## 2.1. *Spitzer*/IRAC

IC 2395 was observed using IRAC (Fazio et al. 2004) on *Spitzer* on 2003 December as part of a GTO program (PID 58, PI Rieke, Evolution and Lifetimes of Protoplanetary Disks) to study protoplanetary disks and dust evolution. The survey covers a  $\approx 44' \times 44'$  area (9 by 9 grid,  $\sim 0.54$  square degrees) in each of the four IRAC channels. The 12 s high-dynamic-range mode was used to obtain two frames in each position, one with 0.4 s exposure time and one with 10.4 s. The observation of each field was repeated twice with a small offset, providing 20.8 s integration time for each position. The frames were processed using the Spitzer Science Center (SSC) IRAC Pipeline v14.0, and mosaics were created from the basic calibrated data (BCD) frames using a custom IDL package, Cluster Grinder, that treats bright source artifacts and removes cosmic ray hits and spatial scale distortion during mosaic construction (Gutermuth et al. 2009). Due to the 7 arcmin offset between channels 1/3 and channels 2/4, the total area covered in all four channels is about 0.37 square degrees.

The IDL-based photometry visualization tool PhotVis version 1.10 (Gutermuth et al. 2008) was used on the reduced images to find sources and carry out aperture photometry on them. The radii of the source aperture, and of the inner and outer boundaries of the sky annulus, were 2.4, 2.4, and 7.2 arcsec, respectively. The calibration was based on large-aperture measurements of standard stars. The zero point magnitudes of the calibration were 19.6642, 18.9276, 16.8468, and 17.3909 corresponding to zero point fluxes of 280.9, 179.7, 115.0, and 64.13 Jy for channels 1, 2, 3, and 4, respectively (Reach et al. 2005). Corrections of 0.21, 0.23, 0.35, and 0.5 mag were applied for channels 1, 2, 3, and 4, respectively, to correct for the differences between the aperture sizes used for the IC 2395 sources and for the standard stars.

## 2.2. *Spitzer*/MIPS

IC 2395 was also observed using MIPS on *Spitzer* in 2003 as part of the same GTO program. MIPS is equipped with a three-channel camera with central wavelengths of approximately 24, 70, and  $160\ \mu\text{m}$  (Rieke et al. 2004). The longer wavelength channels are insensitive to stellar photospheric emission at the distance of IC 2395 and no cluster stars were detected at  $70\ \mu\text{m}$  nor  $160\ \mu\text{m}$ . This study is based on only the MIPS  $24\ \mu\text{m}$  channel.

The observations used the medium scan mode with half-array cross-scan offsets resulting in a total exposure time per pixel of 80 s. The images were processed using the MIPS instrument team Data Analysis Tool (Gordon et al. 2005), which calibrates the data, corrects distortions, and rejects cosmic rays during the coadding and mosaicking of individual frames.

A column-dependent median subtraction routine was applied to remove any residual patterns from the individual images before combining them into the final  $24\,\mu\text{m}$  mosaic. The total area mapped was nearly a square degree ( $89' \times 40'$ ).

We measured the  $24\,\mu\text{m}$  flux density of individual sources using the standard photometry routine `allstar` in the IRAF data reduction package `daophot`, and within a  $15''$  aperture. We then applied an aperture correction of 1.73 to account for the flux density outside the aperture, as determined from the STinyTim  $24\,\mu\text{m}$  PSF model (Engelbracht et al. 2007). Finally, fluxes were converted into magnitudes referenced to the Vega spectrum (with the zero point at 7.17 Jy). Typical  $1\text{-}\sigma$  measurement uncertainties for the MIPS  $24\,\mu\text{m}$  fluxes are  $50\,\mu\text{Jy}$ ; there is also a  $\sim 2\%$  uncertainty in the absolute calibration (Engelbracht et al. 2007). The MIPS image is sufficiently sensitive to detect the photospheres of  $\sim \text{A0}$  stars at the distance of IC 2395.

Figure 1 is a three-color composite image composed of IRAC wavelengths  $3.6\,\mu\text{m}$  (blue) and  $8\,\mu\text{m}$  (green) and MIPS  $24\,\mu\text{m}$  (red). The shortest wavelength channel reaches the photospheres of all stars in the cluster. In addition, however, it also picks up many background stars. The  $8\,\mu\text{m}$  image shows fewer sources and highlights dust (and associated gas). This image likely has a polycyclic aromatic hydrocarbon contribution and potentially also silicate emission at its long wavelength limit. At  $24\,\mu\text{m}$ , we see cooler extended dust and the cluster members with significant excess emission. The brightest source is EP Velorum, an M6 asymptotic giant branch, thermally pulsating star (Kerschbaum & Hron 1994), unassociated with the cluster. The  $24\,\mu\text{m}$  mosaic of the central region of IC 2395 is displayed in Figure 2, with the most prominent infrared-excess sources marked.

### 2.3. UBVRI Photometry

Our optical observations were made with the SITe 2048-#6 CCD camera on the 1.5-m telescope at CTIO on 2003 Jan 23 and 24 as part of a 3 day campaign (2003 Jan 22, 23, and 24) to provide optical data in support of *Spitzer* observations for IC 2395 and NGC 2451 (discussed in a separate paper; Balog et al. (2009)). The camera was mounted at the f/13.5 focal position, covering a  $15 \times 15\text{ arcmin}^2$  field-of-view with a resolution of  $0.43\text{ arcsec/pixel}$  for the entire  $2048 \times 2048\text{ pixel}^2$  area. The observations were made through Johnson-Cousins *UBVRI* filters, applying the Tek #1 filter set<sup>1</sup>.

The whole cluster was covered by  $3 \times 3 = 9$  CCD frames centered on and around the

---

<sup>1</sup><http://www.ctio.noao.edu/instruments/filters>

brightest inner area at R.A. = 08:42:30, DEC = -48:06:00. One off-cluster area (separated by  $\sim 1.5$  deg from the cluster center) was also imaged to sample the foreground/background object population in the same line-of-sight. Each field was imaged three times through the same filter. One frame was obtained with a short exposure time (10 s for *U* and 5 s for *BVRI*) and the other two frames were taken with longer ones (250 s for *U*, 70 s for *B* and 50 s for *VRI*).

The reduction of the raw frames was performed with standard routines using *IRAF*<sup>2</sup>. After trimming the edges of the frames and subtracting the bias level from each image, the frames were divided by a master flat field image obtained by median combining the available flat field frames for each filter. Both dome flats and sky flats were taken at the beginning of each night and combined together into the master flat frames. After flat field division, the two long-exposure frames corresponding to the same filter were averaged to increase the signal-to-noise.

The photometry of the cluster frames was conducted via PSF-fitting using DAOPHOT implemented in *IRAF*. A 2nd order spatially variable PSF (`varorder=2`) was built for each frame to help compensate for the distortions of the PSFs due to either the optical imaging artifacts in the large field-of-view, or guiding errors that occurred randomly on a few frames. The model `function=penny2` was selected to account for the slight elongation of the PSF. The PSF-stars were selected interactively from a sample of the  $\sim 100$  brightest, non-saturated, well isolated stars on each frame, omitting the ones with suspicious profiles and/or detectable neighbors within  $r = 15$  pixels. The `fitrad` parameter was set according to the value of the FWHM. The detection threshold was fixed at the  $4\text{-}\sigma$  level on each frame.

The transformation of the CTIO instrumental magnitudes into the standard Johnson-Cousins system was performed via the observations of Landolt photometric standard sequences (Landolt 1992). The description of the standard transformation is discussed in Balog et al. (2009).

We applied aperture corrections for each frame to match the PSF photometry to the aperture photometry obtained for standard stars. The aperture photometry was computed with  $r_{ap} = 8$  pixels radius. The local sky level was estimated as the mode of the pixel distribution within an annulus having inner and outer radii of 10 and 20 pixels, respectively, centered on each object. Inspecting the final instrumental magnitudes we found a very small 0.02-0.03 mag systematic offset between the long and short exposure frames and also found that there is a  $\sim 0.03$ -0.1 mag offset between the different frames of the mosaics. We tied

---

<sup>2</sup>*IRAF* is distributed by NOAO which is operated by the Association of Universities for Research in Astronomy (AURA) Inc. under cooperative agreement with the National Science Foundation

our photometry to the middle frame (which overlaps with all of the remaining fields) of the  $3 \times 3$  mosaic to ensure the consistency of our dataset.

We tested the quality and stability of the photometry, including the standard transformation, by comparing our standard magnitudes with those from Claria et al. (2003) (unfortunately, only the  $V$  and  $B - V$  data could be compared this way). We discovered  $\simeq 0.19$  mag and  $\simeq 0.015$  mag systematic offsets between the two datasets in  $V$  and  $B - V$  respectively. Claria et al. (2003) report that there were systematic differences (sometimes as large as 0.2 mag) between their photometry and earlier work. We therefore also compared our photometry with stars from the field found in the SIMBAD database. The systematic offsets were smaller; however, the scatter of the data was much larger due to the non-uniformity of the SIMBAD data. However, we used the exact same calibration in the case of NGC 2451 (Balog et al. 2009) where we found an almost perfect agreement with the previously published dataset of Platais et al (2001). In cases where an object is missing from our photometric sample we adjust its Claria et al. (2003) photometry to match ours and give that value in the summary table for all the members.

## 2.4. Spectroscopy

We acquired AAOmega spectra using the Anglo-Australian Telescope at Siding Spring, Australia on three nights (17-23 December 2009) in conditions of clear skies with 1.5-2.5 arcsec seeing.

### 2.4.1. Target Selection

To make optimal use of the telescope time, we pre-selected member candidates based on their positions on the color magnitude (CM) diagram and color-color (CC) diagram. The 2MASS near-infrared photometry in particular is useful in deselecting reddened background stars. We matched our optical photometry to the 2MASS positions and used the  $V$  vs.  $V - K$  CM diagram and the  $V - K$  vs.  $V - I$  CC diagram to separate possible cluster members from the foreground and background population. We selected stars as member candidates if their positions on the CM diagram were compatible with the cluster age, distance and reddening allowing for errors due to binarity and age spread. First we combined the pre-main-sequence isochrones with ages 3 and 10 Myr (traditional age calibration) of Palla & Stahler (1999) with the post-main-sequence isochrones of Marigo et al. (2008). We selected these isochrones because they bracket the age of the cluster ( $\sim 6$  Myr on this calibration)

and allow some room for errors in the age estimates. Then we shifted these isochrones to the distance modulus of IC2395 (800 pc) and applied additional shifts to take into account the reddening and extinction. We show the CC diagram with the selected possible members in Figure 3. We also included all objects that showed some level of IR excess in the IRAC bands even when they were not covered by our optical imaging<sup>3</sup> Altogether 710 candidates were selected based on the above criteria. We were able to obtain spectra of 675 of the candidates.

#### 2.4.2. Observations and Data Processing

In the blue arm of the spectrograph, we used the 2500 V grating, providing  $\lambda/\Delta\lambda = 8000$  spectra between 4800 Å and 5150 Å. In the red arm we used the 1700 D grating that has been optimized for recording the Ca II IR triplet region. The red spectra range from 8350 Å to 8790 Å, with  $\lambda/\Delta\lambda = 10000$ . This setup has the highest spectral resolution available with AAOmega, suitable to measure stellar radial velocities. In total, we acquired 11 field configurations centered on the open cluster. The spectra were reduced using the standard Two-Degree Field data reduction pipeline. We performed continuum normalization for the stellar spectra using the IRAF task `onedspec.continuum` and then cleaned the strongest skyline residuals using linear interpolation of the surrounding continuum (see Balog et al. 2009 for a detailed description of the data processing of AAOmega).

Balog et al. (2009) also describe the methodology for radial velocity determination. In summary, an iterative process was used to fit the atmospheric absorptions and the stellar radial velocity, based on synthetic stellar spectra. Our method is similar to that of the Radial Velocity Experiment (RAVE) project (Steinmetz et al. 2006; Zwitter et al. 2008), including use of the same library of synthetic spectra. We required three iterations to converge to a stable set of temperatures, surface gravities, metallicities, and radial velocities. We estimate the velocities to be accurate within  $\pm 1 - 2 \text{ km s}^{-1}$  for the cooler stars ( $T < 8000 - 9000 \text{ K}$ ) and  $\pm 5 \text{ km s}^{-1}$  for the hotter ones.

---

<sup>3</sup>The objects without V and I photometry (numbers 1, 2, 3, 4, 111, 134, 167, and 278) include one identified as a transitional disk (134), two as class II sources (111, 167), and one as a debris disk (278): the ratio of the number of transitional to class II sources is identical to the overall value, so the selection of these objects does not bias our results on the incidence of transitional systems.



### 3. Cluster Membership

#### 3.1. High mass members from Claria et al. (2003)

We now describe our identification of cluster members. Associating stars to stellar clusters can be challenging and is best carried out using several criteria, all of which need to be consistent with membership. The most confident membership designations are those that have photometric, kinematic, and spectroscopic measurements. In the case of IC 2395, no previous study has constructed a membership list based on multiple criteria.

Claria et al. (2003) conducted a  $UBV$  investigation of the cluster’s central  $50' \times 50'$  region to a  $V$  band limiting magnitude of 15. This survey is the starting point for our identification of the high-mass cluster members. They selected cluster members photometrically by examining the positions of the observed stars in  $UBV$  color-magnitude and color-color diagrams with respect to the theoretical models of Lejeune & Schaerer (2001). Stars lying no more than 0.75 mag above the zero-age main sequence (ZAMS) and deviating no more than 0.10 mag from the CC main sequence locus were classified as cluster members. Claria et al. (2003) presented 61 sources meeting these photometric criteria. The CM and CC diagram positions of another 16 stars were somewhat ambiguous but they were retained as possible members.

A comparison of 21 of these cluster members to a proper-motion-selected list from Dias et al. (2001) showed very good agreement; however, the uncertainties in the mean proper motion survey are sufficiently large to make the comparison inconclusive. Without a kinematic, spectroscopic, or near-infrared membership criterion to go along with the visible photometry, we believe that the Claria et al. (2003) classification is insufficient for providing a robust list of bona fide cluster members.

##### 3.1.1. Mean Cluster Proper Motion

We add a kinematic criterion to the Claria et al. (2003) photometric membership list by selecting on proper motion. There are multiple estimates of the mean proper motion of IC 2395 members, but some of the estimates are inconsistent. We re-estimated the mean proper motion using the spectroscopically confirmed sample of 14 B-type cluster members selected from Claria et al. (2003). The NOMAD catalog from USNO (Zacharias et al. 2004) provides the best available proper motion for each star (usually from Tycho-2 or Hipparcos; Hogg et al. 2000; Brown et al. 1997). Twelve of the 14 had proper motions with the exceptions being HD 74455 and HD 74436. The variance-weighted mean  $\mu_{\alpha} \cos \delta$

and  $\mu_\delta$  values were calculated and the  $\chi^2$  of each value was calculated for the sample. One star, HD 74251, was rejected due to contributing (by far) the majority of the  $\chi^2$  for both  $\mu_\alpha \cos \delta$  and  $\mu_\delta$ . Further clipping, however, had negligible effect on the final proper motion, so we calculated the mean proper motion value for the remaining 11 B-stars as representative for the group:  $\langle \mu_\alpha \cos \delta \rangle = -3.9 \pm 0.4 \text{ mas yr}^{-1}$  and  $\langle \mu_\delta \rangle = +3.0 \pm 0.4 \text{ mas yr}^{-1}$ . As the variance-weighted mean uncertainty ( $\sim 0.3 \text{ mas yr}^{-1}$ ) was close to the uncertainty in the Tycho-2 reference system proper motion ( $\sim 0.25 \text{ mas yr}^{-1}$ ), we conservatively added that term in quadrature to derive our final uncertainty estimate ( $\sim 0.4 \text{ mas yr}^{-1}$ ). The mean proper motion is consistent within the errors whether we calculate it as a true median (Gott 2001), a Chauvenet-criterion clipped mean (Bevington & Robinson 1992), or an unweighted mean, so our choice of  $\mu$  estimation matters little.

Our derived mean proper motion agrees well with most of the previously measured values as shown in Table 1 (Kharchenko et al. 2005, 2003; Loktin et al. 2003; Dias et al. 2002, 2001; Baumgardt et al. 2000), but is severely at odds with the quoted values from Gulyaev & Nesterov (1992) and Dias et al. (2006). The Dias et al. (2006) value is dominated by large numbers of faint UCAC2 stars and likely suffers from a significant amount of field star contamination. As we (and most other studies) do not agree with the mean proper motion estimated by Dias et al. (2006), we do not use their membership probabilities.

### 3.1.2. Revised High Mass Cluster Membership List

We now take the 61 probable and 16 possible cluster members from Claria et al. (2003) and further select those as members that meet the *combined* near-infrared and optical photometric and the proper motion criteria, i.e., those:

- lying near a dereddened isochrone on near-IR and optical CM and CC diagrams.
- with proper motions within two sigma of our derived cluster mean, *and*
- whose proper motion uncertainties are less than 5 mas/yr.

All of the Claria et al. (2003) objects were consistent with the photometric criterion. The second criterion was determined through a  $\chi^2$  comparison to the mean cluster motion (as measured in § 3.1.1 and presented in Table 1) which includes the objects' proper motion uncertainty along with an assumed intrinsic velocity dispersion of 1 mas/yr, where 1 mas/yr  $\approx 0.7 \text{ km/s}$  (Bevington & Robinson 1992). In equation form:

$$\chi^2 = \left\{ \frac{[\overline{(\mu_\alpha \cos \delta)^{\text{cl}}} - (\mu_\alpha \cos \delta)^*]^2}{(\sigma_{\text{int}, \mu_\alpha \cos \delta}^{\text{cl}})^2 + (\sigma_{\mu_\alpha \cos \delta}^*)^2} \right\} + \left\{ \frac{[\overline{\mu_\delta^{\text{cl}}} - \mu_\delta^*]^2}{(\sigma_{\text{int}, \mu_\delta}^{\text{cl}})^2 + (\sigma_{\mu_\delta}^*)^2} \right\} \quad (1)$$

where the “cl” superscript designates the cluster, the “int” subscript designates intrinsic, and the asterisk superscript designates individual stars. By selecting those sources with  $\chi^2 \leq 6$  and two degrees of freedom, we expect only  $\approx 5\%$  of bona fide cluster members to be rejected using this criterion ( $\sim 2 \sigma$ ).

We invoke the last criterion to reduce the chances that sources with relatively large uncertainties may unjustifiably obtain low  $\chi^2$  values and contaminate our sample of bona fide cluster members. We selected a 5 mas/yr cutoff because it is less than the typical UCAC2 uncertainty for their faintest objects ( $V \gtrsim 12$ ). The consequence of this criterion, however, is that at the distance of IC 2395, spectral types inferred from  $J$ - $H$  to be roughly later than mid-F are deselected. In our effort to reduce interlopers, we have potentially removed faint cluster members reducing both the sample size and mass range of a measured disk fraction. Incorporating later spectral types will require adding other criteria such as radial velocity, spectral classification, or youth spectral features (see §3.2).

Our proper motion criteria retained 40 of the Claria et al. (2003) sample of 61 probable cluster members. We examined the six sources that had  $\chi^2 \leq 6$  and uncertainties greater than 5 mas/yr and found that half of them had very inconsistent mean proper motions and were left deselected. The other three had mean proper motions within  $1 \sigma$  of the cluster mean ( $\chi^2 \leq 1$ ) and we reclassified them as possible cluster members. Another of the original 61 had no measured proper motion and was retained but only as a possible member. We also examined the sources that had  $\chi^2 \geq 6$  and uncertainties less than 5 mas/yr to identify any sources that were potentially penalized for having abnormally small reported uncertainties ( $\leq 2$  mas/yr). Three were retained and reclassified as possible cluster members.

Of the original Claria et al. (2003) sample of 16 possible cluster members, three were proper motion selected and hence upgraded to probable members. One possible member had no measured proper motion and remains a possible member.

After having applied the additional membership criteria, we end up with 43 probable cluster members and 14 possible members. As we discuss below, we believe that two of the possible members are probable members, increasing the reported number to 45 cluster members and 12 possible members. In the following section, we discuss the selection of members from radial velocities measured from our spectra. In addition to allowing us to extend the membership list to lower masses, we apply this test to the possible massive

members from Claria et al. (2003), eliminating a total of ten probable and possible members<sup>4</sup>.

### 3.2. Low mass member candidates from radial velocities

#### 3.2.1. Radial Velocities

The result of our radial velocity survey is shown in Figure 4. the cluster members are clearly concentrated around  $24.7 \text{ km s}^{-1}$  with  $\sigma = 1.54 \text{ km s}^{-1}$ . We accepted an object as a cluster member if its radial velocity is within  $2.4 \sigma$  ( $= 1$  full width at half maximum of the distribution) of the mean radial velocity<sup>5</sup>. Increasing this criterion to  $3 \sigma$  admits 17 additional sources, but nine are likely to be non-members, where we have estimated the number of non-members as the average for all velocities in the figure outside of  $4 \sigma$  from  $24.7 \text{ km s}^{-1}$ . Increasing the window to  $4 \sigma$  admits a total of 46 additional stars, but by the same method we estimate that 24 are likely to be non-members. Close binaries will have discrepant velocities outside our adopted criterion for cluster membership and will be rejected on this basis; it appears that there are relatively few such cases, or extending the radial velocity selection threshold would add more probable members.

We also revised the high-mass membership of the proper motion members based on radial velocities, reducing the total size of this sample to 37 members and 10 possible members. The final selection of members from Claria et al. (2003) is listed in Table 2, while the full membership list including those from Table 2 is provided in Tables 3 and 4. Figure 6 places the members on CM and CC diagrams. Altogether we identified 250 low-mass members that were not included in the proper motion sample, based on our radial velocity survey.

#### 3.2.2. Spectral Types

Spectral types were assigned as available from the literature, as indicated in Table 2. The U-B vs. B-V color-color diagram shows that the reddening is uniform across the region, such that the U-B vs. B-V sequence is well-defined and there are no obvious signs of spread (outside of expectations from the presence of binaries) (Claria et al. 2003). We estimated

---

<sup>4</sup>However, the radial velocity selection criterion is biased against close massive binaries, so some of the eliminated stars may in fact be cluster members.

<sup>5</sup>We relaxed the radial velocity requirement if the object appeared to be a member or possible member based on proper motion data. In this case we accepted a star as a member for the final analysis if its radial velocity was within  $4.8 \sigma$  of the mean radial velocity.

the  $E_{B-V}$  for the members with spectral types using the intrinsic main-sequence relation of Pecaut & Mamajek (2013). Reddening this sequence according to  $E_{U-B} = 0.73 * E_{B-V}$ , our estimate is  $E_{B-V}=0.09$  mag, as also found by Claria et al. (2003). We therefore adopt an extinction equivalent to  $E_{B-V} = 0.09$ .

Where types were unavailable, we used our photometry to estimate them. For the stars earlier than  $\sim$  K4 the preferred color for this purpose,  $V - J$  or  $V - K$ , depends on the age of the cluster and whether there is, for example, active accretion.  $V - K$  is the better choice for evolved field stars because of the longer wavelength baseline, whereas for very young star forming clusters  $V - J$  is preferred to circumvent excess emission at  $K$ . IC 2395 is in between. Therefore, before selecting the bands we did a number of tests. First, we computed trend lines of  $V$  vs.  $V - J$  and  $V - K$ . The scatter was similar (in all these evaluations, we rejected outliers in similar numbers -  $\sim 8\%$  - for both bands). However, when the scatter was weighted by the expected  $V - J$  or  $V - K$  value to create a metric for the uncertainty in stellar type that would result, the metric was a factor of 1.39 smaller for  $V - K$ . That is, the larger wavelength baseline resulted in a significant advantage for use of  $V - K$ . After identifying the Class II sources, we also tested whether  $K$  or  $IRAC1$  (hereafter [3.6]) could be contaminated by excess emission. To do so, we took all of the Class II sources and compared their observed  $K - [3.6]$  colors with those we would expect from the spectral types we assigned them as discussed in the following paragraph and using the Luhman et al. (2010) standard colors for young stars. There were no significant discrepancies, and the average was  $-0.01$ , that is the  $K - [3.6]$  color was 0.01 bluer than expected for the standard colors.

Therefore, for types earlier than K4, we made the type estimates based on the (extinction-corrected)  $V - K$  color compared with the tabulation in Mamajek (2015), while for K4 and later we used the  $J - [3.6]$  colors from Luhman et al. (2010). After a preliminary assignment of types, we determined empirical loci for the apparent  $V$  and [3.6] magnitudes vs. type. We rejected any type estimates for stars that deviated from these loci by more than 1.1 magnitudes in  $V$  or 0.8 magnitudes in [3.6]. That is, the types were only accepted if the stars were consistent in  $V - K$  or  $J - [3.6]$  *and* had apparent magnitudes consistent with cluster membership at *both*  $V$  and [3.6]. Of the 295 members, 80 failed the tests for a consistent classification, of which 13 are Class II sources (see below).

### 3.3. Age

We have put the age of the cluster on the revised age scale (e.g., Bell et al. 2013). To do so, we estimated the cluster age and distance from the Claria et al. (2003) catalog of

probable luminous members, using the Ekström et al. (2012) main-sequence interior models including the effects of rotation. Given that the photometry is in the apparent color-apparent magnitude plane, it is first necessary to transform the interior models into color-magnitude space and then also redden the model corresponding to  $E(B-V)=0.09$  mag. To transform the interior models we used the Castelli & Kurucz (2004) so-called ODFnew models. To redden the model isochrones we used the standard  $A_V = 3.1 \cdot E(B-V)$  relation (as appropriate for the low level of reddening, see e.g. Olson (1975)). The most massive star, HD 74455, provides the best age diagnostic for this method. It sits in the vertical region of the model isochrones, hence the small dependencies of the estimated age on the color and reddening combined with the small reddening of the cluster itself will have an insignificant effect on the result. This star is a likely ellipsoidal variable (Morris 1985), i.e. a binary, but given the vertical isochrones the single-star luminosity for one of the pair is still compatible with our assigned age. Using main-sequence fitting, we estimated a distance modulus of  $\sim 9.5$  mag (equivalent to  $\sim 800$  pc; as also found by Claria et al.) and an age of  $\sim 9$  Myr.

This age is confirmed by the  $V$  vs.  $V - J$  HR (CM) diagram in Figure 5, which is primarily based on the low-mass cluster members identified in our study. Both age determinations agree on  $\sim 9$  Myr. As is usually the case, the revised calibration gives a significantly older age than the traditional estimate of  $6 \pm 2$  Myr (Claria et al. 2003).

IC 2395 is in an age range where absolute ages are not well-determined but relative ones are better understood (Soderblom et al. 2014). We assign an error of 3 Myr, i.e., we take the age to be  $9 \pm 3$  Myr. This error is to be understood as a statement that IC 2395 is likely to be similar in age to Upper Sco and Ori OB1b, nominally near 10 Myr (on the revised age scale), and neither so young as classic star-forming clusters such as  $\rho$  Oph, NGC1333, NGC 2244, or IC 348 nor so old as Ori OB1a and LCC/UCL. On the traditional age scale, these clusters/associations are in the same relative sequence, but all at younger ages.

## 4. Analysis

The key result of this section is the identification of candidate IC 2395 cluster members with evidence of circumstellar disks. *Spitzer* photometry is efficient in identifying evolutionary stages for disks around young stars (e.g. Allen et al. 2004; Megeath et al. 2004; Hartmann et al. 2005; Sicilia-Aguilar et al. 2006; Megeath et al. 2005; Lada et al. 2006; Allen et al. 2007; Wang & Looney 2007). For the youngest systems, these studies have distinguished deeply embedded protostars (Class I) from accreting T-Tauri-like stars (Class II) from “normal” stars (Class III), based on placement on IRAC CC diagrams (e.g. [3.6]-[4.5] versus [5.8]-[8.0]). We build on this body of experience to separate Class II sources from the non-

or weak-excess Class III cluster members and to identify the transitional disks caught in the process of transformation between these classes. At the age of IC 2395, second-generation debris disks are also starting to appear - these are systems where the dust is not primordial, but is generated in planetesimal collisions.

We have matched the selected cluster members presented in Tables 2 and 3 to the IRAC and MIPS photometry using a  $2.5''$  radial positional threshold. Several of the Claria et al. (2003) objects are outside the areas covered with IRAC and MIPS and a handful are incomplete in the IRAC detections. Altogether 277 objects out of 297 are detected in all 4 IRAC bands and 67 of those also have counterparts at  $24\ \mu\text{m}$ . We use this body of photometry to identify the transitional, Class II, and strong debris disks in IC 2395. We find 18 Class II sources (6.5% of the sources detected in all four IRAC bands), 8 transitional disks (2.9% of the full IRAC detections) and 23 debris disk candidates (8.3%).

The most significant risk in using the longer wavelength *Spitzer* channels for identifying stars and protostars with strong infrared excess emission is contamination from thermal dust continuum from the residual natal molecular cloud, including emission from polycyclic aromatic hydrocarbon molecules (PAHs, which contribute strongly at  $8\ \mu\text{m}$ ), and confusion with background sources along the line-of-sight. After identifying the cluster members with strong emission from circumstellar disks, we discuss the extent to which contamination may influence these results.

#### 4.1. Identification of excess types among cluster members

Figures 6 and 7 show the objects with excesses on different optical-near-infrared-mid-infrared CM and CC diagrams. The locations of the identified sources are also shown in Figure 2. Two objects (#6 and #21) that have large  $K - [24]$  excess are not classified because all of our classification schemes require IRAC data and these two stars are outside the area covered by IRAC. Based on their  $K - [24]$  color they can be either transitional disks or class II sources. The identification of the other objects is explained in the next three subsections. Since we will use identical criteria for a sample of 19 clusters and associations as listed in Table 6, we discuss our approach in this general context.

##### 4.1.1. Transitional disks

Although it is desirable to identify transitional disks through infrared spectroscopy (Espaillat et al. 2014), our aim is for a large sample to investigate their incidence and how

it evolves with age. Since infrared spectroscopy is not available for all of this sample, we used photometry to test for photospheric-like colors in the  $4\ \mu\text{m}$  region and to measure the size of the excess at  $24\ \mu\text{m}$ , and also impose a requirement on the spectral type of the star for systems old enough that extreme debris disks might be confused with transitional ones.

We first derive a criterion to test for photospheric-like colors. We start with a simple physical definition, obtained from Sicilia-Aguilar et al. (2008): a transitional disk should have no excess out to  $6\ \mu\text{m}$ , but should retain a large excess at  $24\ \mu\text{m}$ , indicative of retention of much of the primordial disk in the more distant zone that dominates at this wavelength. In this regard, transitional disks can be distinguished from Class II sources, which have significant excesses already at  $6\ \mu\text{m}$  (Sicilia-Aguilar et al. 2008). The simplest way to isolate candidate transitional disks, then, is to use a color difference involving IRAC band 3 at  $5.8\ \mu\text{m}$ . We prefer  $[3.6] - [5.8]$  because we will want to apply identical criteria to many clusters and associations, some with significant reddening, and this color difference is significantly less affected by extinction than is the case for color differences involving shorter wavelengths, such as  $K$  (e.g., Flaherty et al. 2007). In addition, the measurements of  $[3.6]$  and  $[5.8]$  are obtained at the same time and hence are not affected by variability.

To determine the acceptable values of  $[3.6] - [5.8]$  to isolate candidate transitional disks from Class II sources, we show in Figure 8 the distribution of this color difference for our entire sample of stellar clusters and associations (listed in Table 6), along with a Gaussian fit to the primary peak in the distribution. There is a distinct excess over the Gaussian fit for sources with  $[3.6] - [5.8] < 0.4$ . We adopt this value as the limit for a candidate transitional disk since it defines a class of object that apparently does not belong to the population of typical Class II YSOs. The  $K - [6\mu\text{m}]$  slope quoted as the upper limit for transitional disks by Kim et al. (2013) predicts this same color, while the limits by Espaillat et al. (2014) and Muzerolle et al. (2010) are more lenient, equivalent respectively to  $[3.6] - [5.8] = 0.48$  and  $0.56$ .

In the cases of Upper Sco, Lower Centaurus Crux (LCC), Upper Centaurus Lupus (UCL), and TW Hya, we have identified transitional disks from WISE photometry. To determine a criterion similar to that we have adopted for IRAC photometry, we compared  $W1 - W2$  vs.  $[3.6] - [5.8]$  for more than 100 sources with measurements in both systems in Upper Sco, finding that the equivalent limit is  $W1 - W2 < 0.43$  with a nominal error of  $0.01$ .

We also need to define a minimum level of excess at  $24\ \mu\text{m}$ . Muzerolle et al. (2010) define “weak excess” transitional disks with a slope equivalent to  $[8] - [24] \geq 1.5$ . They also define an optically thick disk with a slope roughly equivalent to  $[8] - [24] = 3.5$ . We adopt a threshold of  $[8] - [24] = 1.5$  and compare our results at this level with those at  $[8] - [24]$



$> 2.5$  and  $[8] - [24] > 3.5^6$ . To determine similar criteria for measurements with WISE, we used measurements of sources in Upper Sco detected in both sets of photometry to set the equivalent threshold to be  $W3 - W4 > 0.8$  and  $W2 - W4 > 1.7$ .

A question remains of whether the *Spitzer* measurements should also put a limit on how strong the source infrared excess can be at IRAC4 ( $8\ \mu\text{m}$ ). We explored the implications of strong fluxes in this band using the YSO disk SED fitting tool (Robitaille et al. 2006) and found that disks with masses and accretion rates well within the range expected for transitional disks (e.g., disk masses of  $\sim 10^{-6}M_{\odot}$  and accretion  $< 10^{-10}M_{\odot}\text{ yr}^{-1}$ ) could have substantial fluxes at  $8\ \mu\text{m}$ . In addition, the broad IRAC  $8\ \mu\text{m}$  band can include silicate emission, which can be strong in transitional disks. Therefore, we imposed no requirement there.

Finally, we imposed a spectral type criterion. The great majority of transitional disks are around stars of spectral type later than F (Muzerolle et al. 2010; Espaillat et al. 2014). The evolution of protoplanetary disks is faster around higher mass stars (e.g., Kennedy & Kenyon 2009; Yasui et al. 2014). Therefore, by an age of  $\sim 10\text{ Myr}$ , we do not expect to find many transitional disks around early-type stars. To reflect this trend, we imposed the requirement that the stellar spectral type for ages  $> 6\text{ Myr}$  had to be later than F (either from spectroscopy or estimated through photometry) to accept a disk as being transitional. The transitional disks in IC 2395 resulting from these criteria are indicated in Table 5 (WT for weak transitional,  $[8] - [24] < 2.5$ , and T for transitional). Our final selection criteria are also illustrated in Figure 8.

To test the degree of debris-disk contamination in these selections, we used the list of ten extreme debris systems in Balog et al. (2009) (we excluded HD 21362 since its excess is dominated by free-free emission). These sources have excesses at  $24\ \mu\text{m}$  by at least a factor of four (i.e., 1.5 magnitudes, the threshold for our identifying a weak transitional disk) and hence can be compared directly with our candidate transitional disks, since the latter are required to have similar excesses. We used the identical approaches with these sources, first testing with *Spitzer*  $[3.6] - [5.8]$  photometry (from Balog et al. (2009); Gorlova et al. (2007); Weinberger et al. (2011)) and if that was lacking, using WISE measurements. Two of the extreme debris systems are too red in these colors to pass our transitional disk criterion; if we also impose the spectral type criterion, *only* BD 20 307 would pass our selection. Only HR 4796A has  $[8] - [24] > 2.5$ , but it is too early-type to pass our criteria. Therefore, the potential contamination appears to be small, particularly at the higher thresholds for  $24$

---

<sup>6</sup>For comparison, Cieza et al. (2012) use a roughly similar threshold of  $[3.6] - [24] = 1.5$  to identify candidate transitional disks.

$\mu\text{m}$  excess. If the  $[8] - [24] > 1.5$  threshold were allowing a significant number of extreme debris disks, we would expect the fraction of transitional disk candidates to decrease as the threshold was increased, but Table 6 shows that, if anything, there is a trend in the opposite direction. We conclude that, at least for the samples  $\leq 15$  Myr in age, debris-disk contamination is not an issue.

#### 4.1.2. *Class II Objects*

Class II objects are pre-main sequence stars characterized by SEDs with photospheric emission at visible wavelengths up to about  $2\mu\text{m}$  followed by flat or gradually decreasing slopes at longer wavelengths (e.g. Lada & Wilking 1984; Lada 1987). The mid-infrared emission is believed to be due to large amounts of heated dust dispersed in an optically-thick, gas-rich primordial disk. In some cases, there may also be an ultraviolet excess component of the SED indicating radiation emitted from an accretion shock on the star’s surface (Muzerolle et al. 2003). Class II includes classic T Tauri stars (CTTSs) and Herbig AeBe (HAeBe) stars. Their existence within a cluster, especially in large numbers, implies stellar ages on the traditional scale of less than about 10 Myr (e.g. Haisch et al. 2001; Mamajek 2005; Hillenbrand 2005). Stars older than this age have typically dissipated their primordial gas (e.g. Pascucci et al. 2006) so that any thermal dust emission is optically thin.

Our criteria for identifying transitional disks join consistently onto the criteria for photometric identification of Class II sources from Gutermuth et al. (2009), which are:  $[3.6] - [5.8] > 0.4$  and  $[4.5] - [8] > 0.268 \times ([3.6] - [5.8]) + 0.393$ . We also required a detection at 22 or  $24\mu\text{m}$ . These objects are designated II in Table 5.

#### 4.1.3. *Debris Disks*

Debris disks represent the final evolutionary state of circumstellar disks. By this stage, the primordial gas has fully dissipated and impacts among the planetesimals create a collisional cascade, resulting in a dusty, gas-less disk. When heated by the central star, the dust reradiates in the mid-infrared. Stars in IC 2395 with  $[8] - [24] > 0.15$  and spectral type of F or earlier or  $[8] - [24] < 1.5$  and of later spectral type were designated debris disks (D in Table 5). If no spectral type could be assigned photometrically (and none was available spectroscopically), we designate the status in Table 5 as D?. Sources 8 and 15 are two marginal cases with  $[8] - [24] = 0.15$  at significance levels of 5 and  $3.4\sigma$ , respectively. We have not included them in Table 5, but their parameters can be recovered from Tables

3 and 4 if desired. We identified 23 debris disk candidates. A number of the debris disk candidates have modest (0.15 - 0.30 magnitudes) IRAC band excesses at 8  $\mu\text{m}$ .

## 4.2. Contamination

The most likely contaminant in our identification of stars with 24  $\mu\text{m}$  excesses is confusion from random line-of-sight positional overlap with distant optically-faint but infrared-bright galaxies, planetary nebulae, and AGN. The effects of these contaminations are usually small (Megeath et al. 2004; Gutermuth et al. 2008). For example, with  $\sim 2000$  extra-galactic 24  $\mu\text{m}$  sources per square degree at 0.5 mJy (Papovich et al. 2004), for a flux less than our completeness limit but greater than our detection limit, the probability of a chance background source observed within our matching radius of 2.5'' of any single cluster member is 0.3% [ $\pi(2.5''^2)/(3600^2) \times 2000$ ] which means that in our sample of almost 300 stars the probability of one chance alignment is close to 100%, but more than a few cases is unlikely. We examined the angular offsets between the 2MASS and the IRAC and MIPS positions of our candidate IR excess stars to evaluate whether their excesses can be attributed to chance alignment. We found that the average offset between the 2MASS and IRAC coordinates is about  $0.3'' \pm 0.3''$  with a maximum separation of 0.68''. That is, the probability of a chance alignment with a 2MASS source is around 1%. For the objects with MIPS photometry, we found that the average offset between the 2MASS and MIPS coordinates is  $0.5'' \pm 0.5''$  with a large portion of the error coming from a few sources where the distance is larger than 1''. These are member candidate Nos. 37, 219, 44, 82, 198, 242, 230, and 122, with offsets respectively of 2.25'', 1.58'', 1.49'', 1.38'', 1.11'', 1.10'', 1.03'', and 1.02'' (without these sources the average error is  $0.4'' \pm 0.3''$  with no significant offset). Given the errors, an offset for a single source of 1'' is plausible while an offset of 1.5'' is unlikely but still possible; any larger offset is probably a chance alignment. Therefore, we removed star No. 37 from the sample of infrared excess sources (although its identification as a cluster member is still valid). We visually examined the images of Nos. 219, 44, and 82 and found that No. 82 is close to a bright star in an area of relatively large background confusion, also indicated by its large measurement errors; it also was removed from the infrared excess sample. No. 219 has no obvious background contamination and shows a large excess even in the IRAC bands which makes it unlikely to be a spurious detection. We are left with No. 44 as the only ambiguous candidate. However, this star is on well-behaved background, so we have accepted it. To summarize, we found two IR excess candidates (Nos. 37 and 82) that are probably contaminated, and we removed them in the final analysis.

## 5. Discussion: Place of Transitional Disks in Disk Evolution

IC 2395 includes a large proportion of transitional disks. Transitional disks were first identified from IRAS data as a class with little or no excess emission at wavelengths short of  $10\ \mu\text{m}$ , indicating little dust close to the star, but with strong excesses at longer wavelengths indicative of an optically thick outer disk (Strom et al. 1989). Multiple interpretations have been advanced for this behavior (Williams & Cieza 2011). Previous studies have invoked the presence of a planet (Rice et al. 2003; Quillen et al. 2004), dust evolution (Wilner et al. 2005), or photoevaporation (Hollenbach et al. 2000; Alexander et al. 2006; Goto et al. 2006) to explain the observed “holes”.

With the end of the *Spitzer* and WISE cryogenic missions, and publication of nearly all the cluster observations obtained with them, the pace of finding major new samples of transitional disks will slow substantially, making an update of their behavior timely. The most recent work along the same lines (Espaillat et al. 2014) utilized Upper Sco as its oldest sample, but since then questions have been raised about the age of the low-mass members of this moving group (Herczeg & Hillenbrand 2015) that may undermine it as a probe of 11-Myr-old transitional disks. IC 2395 (and other stellar clusters/associations of similar age) can provide a critical independent estimate. In the following four paragraphs, we set the scene for this analysis by discussing age scales, and then sample selection. In the next section we show that, in general, the proportion of transitional disks does not change dramatically from one cluster/association to another of similar age. This conclusion justifies our averaging of the transitional disk proportions in the following section, to derive high-weight proportions of transitional disks in young and middle-aged clusters/associations (1 - 3.5 and 4 - 6.5 Myr respectively on the traditional calibration, 1 - 6 and 8 - 13 Myr on the revised one).

We will focus on the young stellar clusters and associations listed in Table 6, for which we show ages on both the revised and the traditional calibrations. Because ages on the traditional calibration have been determined in a variety of ways, in obtaining a homogeneous set we have given priority to those selected in the review by Eric Mamajek (Mamajek 2009). Where ages on the revised calibration are not available directly, we have assigned them according to similarity in published HR diagrams for clusters/associations with directly determined ages. These cases are indicated in the notes to the table. As a test of this procedure, we evaluated Ori OB1b, which according to the HR diagram from Hernández et al. (2008), should have an age similar to those of  $\lambda$  Ori, NGC 2362, and  $\gamma$  Vel, all of which are indicated to be 10 - 12 Myr on the revised scale. We took the measurements of low-mass members of Ori OB1b from Briceño et al. (2005), adjusted them to the distance of IC 2395, and applied extinction corrections to the individual stars according to the estimates of this

parameter in Briceño et al. (2005). We then superimposed the resulting V vs. V-J diagram on the one for IC 2395 shown in Figure 5. The agreement is excellent indicating an age of  $\sim 9$  Myr for Ori OB1b, although there is more scatter for the stars in it, presumably because of the complications introduced by the larger and variable extinction. This agreement supports the age assignment on the revised calibration.

Importantly for this study, both the traditional and revised age calibrations place the cluster/associations into age groupings identically, as shown in Table 6. Therefore, our conclusions about the behavior of transitional disks will only change in timescale with a change in age calibration, but otherwise will remain identical.

A critical issue is how, in each case, to define a sample of cluster members for study. The most conservative approach is to require that the members be identified through techniques *not* involving the mid-infrared (to avoid any possibility of introducing a bias into the infrared characteristics we use to identify transitional disks). We have applied the same criteria for transitional and Class II disks as discussed above for IC 2395. Table 6 lists the ratios of transitional to (transitional + Class II) disks for each stellar cluster or association. It also shows the totals for three age ranges: 1 – 6 Myr, 8 – 13 Myr, and 14 – 17 Myr (all on the revised calibration, corresponding to 1 - 3.5, 4 - 6.5, and 7 - 16 Myr on the traditional calibration). For the young clusters within 1 kpc, the totals extend down to moderately late type, low mass stars, while for the two more distant young clusters (NGC 2244 and 2362), the infrared measurements extend down only to intermediate mass stars. Therefore, we also show the totals omitting the two distant clusters. These values are in boldface because we believe them to be the most reliable indicators of transitional disk behavior. We show similar boldface numbers for the intermediate age range, but both groupings in the oldest age range are closer than 1 kpc.

A less-conservative approach uses the *Spitzer* data to identify cluster members, yielding significantly larger numbers in the samples. The results with this approach are also tabulated for the youngest age range<sup>7</sup>; for the intermediate and old ranges, the cluster members are all identified without *Spitzer* data so this case is not shown. The results for all three levels of conservatism are identical within the errors, indicating that they are relatively robust to the member-identification approach.

---

<sup>7</sup>We do not show the values for the individual clusters.

### 5.1. Does the Proportion of Transitional Disks Vary from Cluster to Cluster?

Table 6 shows that, in general, the individual clusters/associations in the young ( $\leq 6$  Myr on the revised scale) and middle-aged (8 - 13 Myr) categories have incidences of transitional disks consistent within the errors with the averages for each group (in particular, Upper Sco seems to be in line with other clusters and associations of similar age). This is also true for the old category, but in that case with very minimal counts. To make this comparison quantitative, we use the difference from the average in units of the quoted errors for all the young and middle-aged systems. The result is a nearly perfect normal distribution, except that the number of transitional disks in  $\rho$  Oph is low at 2/123 or 1.6%. Turning to the infrared-selected sample, this cluster is still low in transitional disks, 9/249 or 3.6%, but now at less than  $3\sigma$  from the average. That is, there is no compelling evidence for variations in the fraction of transitional disks over the full set of results reported in Table 6, although the case of  $\rho$  Oph deserves further investigation.

Sicilia-Aguilar et al. (2008) have reported that the Coronet Cluster may have an abnormally high incidence of transitional disks, and indeed the counts reported for it in Table 6 are higher than average, albeit not at a statistically significant level. To understand any possible differences, we examine the seven transitional disks identified by Sicilia-Aguilar et al. (2008) in more detail. Only two of these disks are within the selection criteria for our sample - CrA-4111 and G-14. A third source on their list, G-65, has no data at  $24\ \mu\text{m}$  (Table 3 of Sicilia-Aguilar et al. (2008)) and furthermore has a  $[3.6] - [5.8]$  color of 1.01, far larger than our selection threshold of  $< 0.4$ . Two more sources from their list, CrA-466 and G-87, also have large values of  $[3.6] - [5.8]$ , 0.81 and 0.72 respectively. Two more from their list, CrA-205 and CrA-4109, are missing IRAC data used in our photometric selection; extrapolating from the existing data, they would likely be classified as transitional disks if full IRAC measurements were available. We do not add them to our sample because a similar detailed examination has not been performed for all the other clusters. However, we have included one source, G-30, which they excluded because of low signal to noise at  $24\ \mu\text{m}$  (the indicated SNR of 6.7 puts it above our WT threshold by  $\sim 1\sigma$ ; excluding it would introduce a potential bias in our method). If we added the two sources with missing IRAC data without subtracting the one with a low SNR, it would not raise the apparent excess of transitional disks to a statistically significant level. It is necessary to add *three* additional disks to the three we have identified to barely reach a  $2\text{-}\sigma$  result. We conclude that the Coronet cluster does not provide a convincing counter-example to our conclusion that the incidence of transitional disks is *not* variable for stellar groupings of similar age, within the limits of the existing data.

## 5.2. Change of Transitional Disk Proportion with Age

The results of the preceding section suggest that we can use the average incidences of transitional disks for young, middle-aged, and elderly systems without significant loss of information. There is a substantial and highly statistically significant increase in the fraction of transitional disks among those disks with strong  $24\ \mu\text{m}$  excesses, going from the young to the middle-aged clusters/associations; the elderly clusters/associations have an incidence perhaps similar to that for the middle-aged ones, but the low numbers in the elderly grouping make any firm conclusions impossible. Figure 10 shows this trend graphically. The trend of an increasing incidence of transitional disks with age has been found previously, e.g., Muzerolle et al. (2010), but with marginal statistical significance for the older clusters/associations, and by Currie & Sicilia-Aguilar (2011), again with sparse representation of older clusters/associations, and with the results summarized in the review by Espaillat et al. (2014). This trend is put on a firm statistical basis by the average results for the young and middle-aged stellar clusters/associations summarized in Table 6. In general, other studies using different criteria for identifying transitional disks will find them in different numbers (see cautions in Espaillat et al. (2014)), but our study remains valid in terms of trends because it uses a homogeneous selection throughout.

What are the implications of the substantial change in transitional disks as a fraction of strong-infrared-excess disks? There are two limiting possibilities: 1.) that there is a systematic change in disk properties with age that is reflected by an increasing probability of any given disk entering this stage; or 2.) that the disks retain similar structures but there is an increasing fraction of those remaining at any time that enters the transitional stage. An indication that the second case is closer to correct is that the relative fractions of disks with  $[8] - [24] > 1.5$ ,  $2.5$ , or  $3.5$  is virtually identical for the averages for the young and middle-aged stellar groupings, i.e., 1:  $0.98 \pm 0.21$ :  $1.78 \pm 0.42$  and 1:  $0.93 \pm 0.34$ :  $1.35 \pm 0.28$ , respectively (based on the boldfaced values in Table 6). Since the excess at  $24\ \mu\text{m}$  is an indicator for the optical depth of the disks outside the inner few AU, these statistics indicate that a minority of systems can retain disks that are still very dense in this zone for 10 Myr or a bit longer.

We therefore assume that the time to clear an optically thick disk is independent of the age of the stellar grouping to which it belongs, and that such clearing passes through a transitional disk stage, which is of similar duration for all disks (e.g., Muzerolle et al. 2010; Espaillat et al. 2014). The consequence of the increase in transitional disk incidence is then that the decay of the  $24\text{-}\mu\text{m}$ -dominant optically thick disk component of a YSO population cannot be exponential, unlike that at shorter infrared wavelengths (e.g., Ribas et al. 2014), but must start slowly and accelerate relative to an exponential.

## 6. Conclusions

The open cluster IC 2395 can add significantly to our understanding of protoplanetary and early debris disk evolution, since it is relatively close (800 pc) and at a critical age where protoplanetary disks are disappearing and debris disks begin to dominate. However, the cluster has largely been overlooked in disk studies. We report optical and infrared photometry and high resolution optical spectroscopy of the cluster, from which we:

- Increase the list of probable members to nearly 300, spanning spectral types of early B to middle M;
- Estimate an age of  $9 \pm 3$  Myr on the revised age scale, e.g. that of Bell et al. (2013); this value compares with  $6 \pm 2$  Myr on the traditional scale (Claria et al. 2003); and
- Identify 18 Class II (6.5% of the members with full IRAC data), 8 transitional disk (2.9%), and 23 debris disk candidates (8.3%).

We have combined the transitional disk information with homogeneously defined similar objects in nineteen additional young clusters and associations to quantify the evolution of this phase; finding that

- The dominant cause of variations in the proportion of transitional disks is age; most clusters of similar age have similar proportions of transitional disks among the systems with strong  $24 \mu\text{m}$  excesses. The single possible exception is  $\rho$  Oph, where transitional disks are relatively rare.
- The relative numbers of disks with different degrees of  $24 \mu\text{m}$  excess do not change significantly with age, implying that the change in the proportion of transitional disks is not driven by a systematic change of disk properties, e.g., a thinning of disks that makes them more susceptible to dissipation
- The number of disks in the transitional phase as a fraction of the total with strong  $24 \mu\text{m}$  excesses ( $[8] - [24] \geq 1.5$ ) increases from  $8.4 \pm 1.3\%$  at  $\sim 3$  Myr to  $46 \pm 5\%$  at  $\sim 10$  Myr; alternative definitions of transitional disks will yield different percentages but should show the same trend.
- Under the conventional assumption that the lifetime of the transitional stage is fixed, and given the evidence that the nature of the individual Class II and transitional disks does not change with age, this result implies that the decay in the proportion of systems with strong  $24 \mu\text{m}$  excesses cannot be exponential, but must start more slowly and finish more rapidly than the “best fit” exponential.



We have also demonstrated that IC 2395 is a rich cluster at a critical age for circumstellar disk evolution, worthy of additional study.

## 7. Acknowledgements

We thank Eric Mamajek for assistance on estimating cluster ages and Lynne Hillenbrand for a short course on the intricacies of current age determination. We also thank the anonymous referee for a detailed critique that yielded significant improvements in the paper. Partial support for this work was provided by NASA through Contract Number 1255094 issued by JPL/Caltech. LLK has been supported by the Lendület Young Researchers Program of the Hungarian Academy of Sciences. This research has made use of the SIMBAD database, operated at CDS, Strasbourg, France. This publication makes use of data products from the Two Micron All Sky Survey, which is a joint project of the University of Massachusetts and the Infrared Processing and Analysis Center/California Institute of Technology, funded by the National Aeronautics and Space Administration and the National Science Foundation. It also makes use of data products from the Wide-field Infrared Survey Explorer, which is a joint project of the University of California, Los Angeles, and the Jet Propulsion Laboratory/California Institute of Technology, funded by the National Aeronautics and Space Administration. We thank the Anglo-Australian Observatory and Cerro Tololo Inter-American Observatory for granting telescope time and for logistical support of our program.

## REFERENCES

- Alexander, R. D., Clarke, C. J., & Pringle, J. E. 2006, *MNRAS*, 369, 229
- Allen, L. E., Calvet, N., D’Alessio, P. et al. 2004, *ApJS*, 154, 363
- Allen, L. E., Megeath, S. T., Gutermuth, R. et al. 2007, *Planets and Protostars V*, eds B. Reipurth, D. Jewit, and K. Keil (Univ. Arizona Press: Tucson), 951, 361
- Balog, Z., Muzerolle, J., Rieke, G. H., Su, K. Y. L., Young, E. T., & Megeath, S. T. 2007, *ApJ*, 660, 1532
- Balog, Z., Kiss, L. L., Vinkó, J. et al. 2009, *ApJ*, 698, 1989
- Barrado y Navascués, D., & E. L. Martin, E. L. 2003, *AJ* 126, 2997
- Barsony, M., Haisch, K. E., Marsh, K. A. & McCarthy, C. 2012, *ApJ*, 751, 22

- Baumgardt, H., Dettbarn, C., & Wielen, R. 2000, *A&AS*, 146, 251
- Bell, C. P. M., Naylor, T., Mayne, N. J., Jeffries, R. D., & Littlefair, S. P. 2013, *MNRAS*, 434, 806
- Bell, C. P. M., Rees, J. M., Naylor, T. et al. 2014, *MNRAS*, 445, 3496
- Bell, C. P. M., Mamajek, E. E., & Naylor, T. 2015, *MNRAS*, 454, 593
- Bevington, P. R. & Robinson, D. K. 1992, *Data Reduction and Error Analysis for the Physical Sciences*, Second Edition, McGraw-Hill
- Briceño, C., Calvet, N., Hernández, J. et al. 2005, *AJ*, 129, 907
- Briceño, C., Hartmann, L., Hernández, J. et al. 2007, *ApJ*, 661, 1119
- Brown, A. G. A., Arenou, F., van Leeuwen, F., Lindegren, L., & Luri, X. 1997, in *ESA Special Publication*, Vol. 402, *Hipparcos - Venice '97*, 63-68
- Burgh, E. B., France, K., & Snow, T. P. 2012, *ApJ*, 756, 6
- Carpenter, J. M., Mamajek, E. E., Hillenbrand, L. A., & Meyer, M. R. 2006, *ApJL*, 651, L49
- Castelli, F., & Kurucz, R. L. 2004, *A&A*, 419, 725
- Chen, L., de Grijs, R., & Zhao, J. L. 2007, *AJ*, 134, 1368
- Cieza, L. A., Schreiber, M. R., Romero, G. A., Williams, J. P., Rebassa-Mansergas, A., & Merín, B. 2012, *ApJ*, 750, 157
- Claria, J.J., Lapasset, E., Piatti, A. E., & Ahumada, A. V. 2003, *A&A*, 409, 541
- Crawford, D. L., & Mander, J. 1966, *AJ*, 71, 114
- Currie, T., Lada, C. J., Plavchan, P., Robitaille, T. P., Irwin, J., & Kenyon, S. J. 2009, *ApJ*, 698, 1
- Currie, T., & Sicilia-Aguilar, A. 2011, *ApJ*, 732, 24
- Dahm, S. E., & Hillenbrand, L. A. 2007, *AJ*, 133, 2072 G. C., & Najita, J. 2005, *ApJ*, 621, 461
- Dias, W. S., Lépine, J. R. D., & Alessi, B. S. 2001, *A&A*, 376, 441

- Dias, W. S., Alessi, B. S., Moitinho, A., & Lépine, J. R. D. 2002, *A&A*, 389, 871
- Dias, W. S., Assafin, M., Flório, V., Alessi, B. S., & Líbero, V. 2006, *A&A*, 446, 949
- Dias, W. S., Monteiro, H., Caetano, T. D., Lépine, J. R. D., Assafin, M., & Oliveira, A. F. 2014, *A&A*, 564, A79
- Dominik, C., & Decin, G. 2003, *ApJ*, 598, 626
- Ekström, S., Georgy, C., Eggenberger, P. et al. 2012, *A&A*, 537A, 146
- Engelbracht, C. W., Blaylock, M., Su, K. Y. L. et al. 2007, *PASP*, 119, 994
- Erickson, K. L., Wilking, B. A., Meyer, M. R. et al. 2011, *AJ*, 142, 140
- Erickson, K. L., Wilking, B. A., Meyer, M. R., Kim, J. S., Sherry, W., & Freeman, M. 2015, *AJ*, 149, 103
- Espaillet, C., Muzerolle, J., Najita, J. et al. 2014, "An Observational Perspective of Transitional Disks," *Protostars and Planets VI*, ed.: H. Beuther, R. S. Klessen, C. P. Dullemond, & T. Henning, Univ. of AZ: Tucson, pp 497-520
- Evans, N. J. II, Dunham, M. M., Jorgensen, J. K. et al. 2009, *ApJS*, 181, 321
- Fazio, G. G., Hora, J. L., Allen, L. E. et al. 2004, *ApJS*, 154, 10
- Flaherty, K. M., Pipher, J. L., Megeath, S. T. et al. 2007, *ApJ*, 663, 1069
- Flaherty, K. M., & Muzerolle, J. 2008, *AJ*, 135, 966
- Gagné, M., Skinner, S. L., & Daniel, K. j. 2004, *ApJ*, 613, 393
- Gáspár, A., Rieke, G. H. & Balog, Z. 2013, *ApJ*, 768, 25
- Gautier, T. N. III, Rebull, L. M., Stapelfeldt, K. R., & Mainzer, A. 2008, *ApJ*, 683, 813
- Getman, K. V., Feigelson, E. D., Townsley, L., Bally, J., Lada, C. J., & Reipurth, Bo 2002, *ApJ*, 575, 354
- Getman, K. V., Feigelson, E. D., & Kuhn, M. A. 2014, *ApJ*, 787, 109
- Giardino, G., Favata, F., Micela, G., Sciortino, S., & Winston, E. 2007, *A&A*, 463, 275
- Girardi, L., Grebel, E. K., Odenkirchen, M., & Chiosi, C. 2004, *A&A*, 422, 205
- Gordon, K. D., Rieke, G. H., Engelbracht, C. W. et al. 2005, *PASP*, 117, 503

- Gorlova, N., Balog, Z., Rieke, G. H. et al. 2007, *ApJ*, 670, 516
- Gorlova, N., Steninhauer, A., & Lada, E. 2010, *ApJ*, 716, 634
- Goto, M., Usuda, T., Dullemond, C. P. et al. 2006, *ApJ*, 652, 758
- Gott, J. R. I., Vogeley, M. S., Podariu, S., & Ratra, B. 2001, *ApJ*, 549, 1
- Gulyaev, A. P. & Nesterov, V. V. 1992, On a catalogue of four million stars. Collection of scientific papers. (On a catalogue of four million stars. Collection of scientific papers., by Gulyaev, A. P.; Nesterov, V. V.. Gosudarstvennyj Astronomicheskij Institut im. P. K. Shternberga, Moskva (Russia) Izdatel'stvo Moskovskogo Universiteta, Moskva (Russia), 1992, 72 p., ISBN 5-211-02847-3, Price 90 Kop.)
- Gutermuth, R. A., Megeath, S. T., Muzerolle, J., Allen, L. E., Pipher, J. L., Myers, P. C., & Fazio, G. G. 2004, *ApJS*, 154, 374
- Gutermuth, R. A., Myers, P. C., Megeath, S. T. et al. 2008, *ApJ*, 674, 336
- Gutermuth, R. A., Megeath, S. T., Myers, P. C., Allen, L. E., Pipher, J. L., & Fazio, G. G. 2009, *ApJS*, 184, 18
- Haish, K. E., Lada, E. A., & Lada, C. J. 2001, *ApJ*, 553, 153
- Hartmann, L., Megeath, S. T., Allen, L. E. et al. 2005, *ApJ*, 629, 881
- Harvey, P., Merín, B., Huard, T. L. et al. 2017, *ApJ*, 663, 1149
- Herczeg, G. J., & Hillenbrand, L. A. 2015, *ApJ*, 808, 23
- Hernández, J., Hartmann, L., Megeath, T. et al. 2007a, *ApJ*, 662, 1067
- Hernández, J., Calvet, N., Briceño, C. et al. 2007b, *ApJ*, 671, 1784
- Hernández, J., Hartmann, L., Calvet, N. et al. 2008, *AJ*, 686, 1195
- Hillenbrand, L. A. 2005, *ArXiv Astrophysics e-prints*
- Hogg, D. W., Neugebauer, G., Cohen, J. G., Dickinson, M., Djorgovski, S. G., Matthews, K., & Soifer, B. T. 2000, *AJ*, 119, 1519
- Hollenbach, D. J., Yorke, H. W., & Johnstone, D. 2000, *Protostars and Planets IV*, eds. V. Mannings, A. P. Boss, and S.S. Russell (Univ. Arizona Press: Tucson), 401
- Jeffries, R. D., Jackson, R. J., Cottaar, M. et al. 2014, *Å*, 563A, 94

- Kennedy, G. M., & Kenyon, S. J. 2014, *ApJ*, 695, 1210
- Kenyon, S. J. & Hartmann, L. 1995, *ApJS*, 101, 117
- Kerschbaum, F. & Hron, J. 1994, *A&A*, 351, 533
- Kharchenko, N. V., Pakulyak, L. K., & Piskunov, A. E. 2003, *Astronomy Reports*, 47, 263
- Kharchenko, N. V. 2004, *Kinematika i Fizika Nebesnykh Tel.*, 20, 366
- Kharchenko, N. V., Piskunov, A. E., Röser, S., Schilbach, E., & Scholz, R.-D. 2005, *A&A*, 438, 1163
- Kim, K. H., Watson, D. M., Manoj, P. et al. 2013, *ApJ*, 769, 149
- Lada, C. J. 1987 in *Star Forming Regions: Proc. IAU Symp. 115*, eds. M. Peimbert and J. Jugaku (Dordrecht: D. Reidel), 1
- Lada, C. J. & Wilking, B. A. 1984, *ApJ*, 287, 610
- Lada, C. J., Muench, A. A., Luhman, K. L. et al. 2006, *AJ*, 131, 1574
- Lagrange, A.-M., Backman, D. E., & Artymowicz, P. 2000, "Planetary Material Around Main-Sequence Stars", in *PPIV*, eds. Mannings, Boss, Russell, Univ. AZ Press: Tucson, page 639
- Landolt, Arlo U. 1992, *AJ*, 104, 340
- Lejeune, T. & Schaerer, D. 2001, *A&A*, 366, 538
- López Martí, B., Jiménez-Esteban, F., Bayo, A. et al. 2013, *A&A*, 556A, 144
- Loktin, A. V. & Beshenov, G. V. 2003, *Astronomy Reports*, 47, 6
- Luhman, K. L., Stauffer, J. R., Muench, A. A. et al. 2003, *ApJ*, 593, 1093
- Luhman, K. L. 2004, *ApJ*, 602, 816
- Luhman, K. L., & Steeghs, D. 2004, *ApJ*, 609, 917
- Luhman, K. L., Lada, E. A., Muench, A. A., & Elston, R. J. 2005, *ApJ*, 618, 810
- Luhman, K. L., 2007, *ApJS*, 173, 104
- Luhman, K. L., Allen, L. E., Allen, P. R., et al. 2008, *ApJ*, 675, 1375

- Luhman, K. L., Allen, P. R., Espaillat, C., Hartmann, L., & Calvet, N. 2010, *ApJS*, 186, 111
- Luhman, K. L., & Mamajek, E. E. 2012, *ApJ*, 758, 31
- Luhman, K. L., Esplin, T. L., & Loutrel, N. P. 2016, *arXiv* 1605.08907
- Mamajek, E. E., M. R. Meyer, M. R., & Liebert, J. 2002, *AJ* 124, 1670
- Mamajek, E. E., Meyer, M. R., Hinz, P. M. et al. 2004, *ApJ*, 612, 496
- Mamajek, E. E. 2005, *ApJ*, 634, 1385
- Mamajek, E. E. 2009, in *AIP Conf. Proc.*, 1158, 3
- Mamajek, E. E. 2015, [http://www.pas.rochester.edu/~emamajek/EEM\\_dwarf\\_UBVIJHK\\_colors\\_Teff.txt](http://www.pas.rochester.edu/~emamajek/EEM_dwarf_UBVIJHK_colors_Teff.txt)
- Manara, C. F., Fedele, D., Herczeg, G. J., & Teixeira, P. S. 2015, *A&A*, 585A, 136
- Marigo, P., Girardi, L., Bressan, A., Groenewegen, M. A. T., Silva, L., & Granato, G. L. 2008, *A&A*, 482, 883
- Megeath, S. T. , Allen, L. E., Gutermuth, R. A. et al. 2004, *ApJS*, 154, 367
- Megeath, S. T., Hartmann, L., Luhman, K. et al. 2005, *ApJ*, 634, 113
- Megeath, S. T., Gutermuth, R., Muzerolle, J. et al. 2012, *AJ*, 144, 192
- Meng, H. Y. A., Rieke, G. H., Su, K. Y. L., & Gáspár, Andras 2016, to be submitted to *ApJ*
- Morris, S. L., 1985, *ApJ*, 295, 143
- Murphy, S. J., Lawson, W. A., & Bessell, M. S. 2013, *MNRAS*, 435, 1325
- Murphy, S. J., Lawson, W. A., & Bento, J. 2015, *MNRAS*, 453, 2220
- Muzerolle, J., Calvet, N., Hartmann, L. & D’Alessio, P. 2003, *ApJ*, 597, L149
- Muzerolle, J., Allen, L. E., Megeath, S. T., Hernández, J., & Gutermuth 2010, *AJ*, 708, 1107 186
- Oliveira, I., Merín, B., Pontoppidan, K. M. et al. 2009, *ApJ*, 691, 672
- Olson, B. I. 1975, *PASP*, 87, 349
- Ozawa, H., Grosso, N., & Montmerle, T. 2005, *A&A*, 438, 661

- Palla, F. & Stahler, S. W. 1999, *ApJ*, 525, 772
- Palla, F., Randich, S., Flaccomio, E., & Pallavicini, R. 2005, *ApJ*, 626, 49
- Papovich, C., Dole, H., Egami, E. et al. 2004, *ApJS*, 154, 70
- Park, B.-G., & Sung, H. 2001, *AJ*, 123, 892
- Pascucci, I., Gorti, U., Hollenbach, D. et al. 2006, *ApJ*, 651, 1177
- Paunzen, E. 2015, *a*, 580A, 23
- Pecaut, M. J., Mamajek, E. E., & Bubar, E. J. 2012, *ApJ*, 746, 154
- Pickles, A., & Depagne, É. 2010, *PASP*, 122, 1437
- Platais, I., Kozhurina-Platais, V., Barnes, S. et al. 2001, *AJ*, 122, 1486
- Quillen, A. C., Blackman, E. G., Frank, A., Varniere, P. 2004, *ApJ*, 612, L137
- Rees, J. M., Wilson, T., Bell, C. P. M., Jeffries, R. D., & Naylor, T. 2016, in "Young Stars & Planets Near the Sun," *Proc. IAU*, 314, 205
- Reach, W. T., Megeath, S. T., Cohen, M. et al. 2005, *PASP*, 117, 978
- Ribas, Á, Merín, B., Bouy, H., & Maud, L. 2014, *A&A*, 561A, 54
- Rice, W. K. M., Wood, K., Armitage, P. J., Whitney, B. A., Bjorkman, J. E. 2003, *MNRAS*, 342, 79
- Rieke, G. H., Young, E. T., Engelbracht, C. W. et al. 2004, *ApJS*, 154, 25
- Rizzuto, A. C., Ireland, M. J., & Kraus, A. L. 2015, *MNRAS*, 448, 2737
- Robitaille, T. P., Whitney, B. A., Indebetouw, R., Wood, K., & Denzmore, P. 2006, *ApJS*, 167, 256
- Schneider, A., Melis, C., & Song, I. 2012, *ApJ*, 754, 39
- Sicilia-Aguilar, A., Hartmann, L. W., Hernández, J., Briceño, C., & Calvet, N. 2005, *AJ*, 130, 188
- Sicilia-Aguilar, A., Hartmann, L., Calvet, N. et al. 2006, *ApJ*, 638, 897 2007, *ApJ*, 659, 1637
- Sicilia-Aguilar, A., Henning, T., Juhász, A., Bouwman, J., Garmire, G., & Garmire, A. 2008, *ApJ*, 687, 1145

- Sicilia-Aguilar, A., Henning, T., Kainulainen, J., & Roccatagliata, V. 2011, *ApJ*, 736, 137
- Sierchio, J. M., Rieke, G. H., Su, K. Y. L. & Gáspár, A., 2014, *ApJ*, 785, 33
- Simon, M. & Prato, L. 1995, *ApJ*, 450, 824
- Skiff, B. A. 2014, VizieR online catalog
- Skrutskie, M. F., Dutkevitch, D., Strom, S. E., Edwards, S., Strom, K. M., Shure, M. A. 1990, *AJ*, 99, 1187
- Soderblom, D. R., Hillenbrand, L. A., Jeffres, R. D., Mamajek, E. E., & Naylor, T. 2014, "Ages of Young Stars", in *Protostars and Planets VI*, eds. Beuther, Klessen, Dullemond, & Henning, University of AZ Press: Tucson, AZ, pp 219-241
- Song, I., Zuckerman, B., & Bessell, M. S. 2012, *AJ*, 144, 8
- Steinmetz, M., Zwitter, T., Siebert, A. et al. 2006, *AJ*, 132, 1645
- Stelzer, B., Preibisch, T., Alexander, F. et al. 2012, *A&A*, 537A, 135
- Strom, K. M., Strom, S. E., Edwards, S., Cabrit, S., & Skrutskie, M. F. 1989, *AJ*, 97, 1451
- Takagi, Y., Itoh, Y., Arai, A., Sai, S., & Oasa, Y. 2015, *PASJ*, 67, 87
- Urban, L. E., Rieke, G. H., Su, K. Y. L., & Trilling, D. E. 2012, *ApJ*, 750, 98
- Wang, S. W. & Looney, S. W. 2007, *ApJ*, in press
- Wang, J., Townsley, L. K., Feigelson, E. D. et al. 2008, *ApJ*, 675, 464
- Weinberger, A. J., Becklin, E. E., Song, I., & Zuckermen, B. 2011, *ApJ*, 726, 72
- Weinberger, A. J., Anglada-Escudé, G., & Boss, A. 2013, *ApJ*, 762, 118
- Werner, M. W., Roellig, T. L., Low, F. J. et al. 2004, *ApJS*, 154, 1
- Wiling, B. A., Meyer, M. r., Robinson, J. G., & Greene, T. P. 2005, *AJ*, 130, 1733
- Wiling, B. A., Gagné, M., & Allen, L. E. 2008, in "Handbook of Star Forming Regions, Vol. II, ed. B. Reipurth, Ast. Soc. Pac, p. 351
- Williams, J. P., & Cieza, L. A. 2011, *ARA&A*, 49, 67
- Wilner, D. J., d'Alessio, P., Calvet, N., Claussenm M. J., & Hartmann, L. 2005, *ApJ*, 626, L109



- Winston, E., Megeath, S. T., Wolk, S. J. et al. 2009, AJ, 137, 4777
- Wolk, S. J. & Walter, F. M. 1996, AJ, 111, 2066
- Wolk, S. J. 1996, unpublished Ph.D. thesis, State University of New York
- Wyatt, M. C. 2008, ARA&A, 46, 339
- Yasui, C., Kobayashi, N., Tokunaga, A. T., & Saito, M. 2014, MNRAS, 442, 2543
- Zacharias, N., Monet, D. G., Levine, S. E., Urban, S. E., Gaume, R., & Wycoff, G. L. 2004, BAAS, 205, #48.15
- Zwitter, T., Siebert, A., Munari, U. et al. 2008, AJ, 136, 421

---

This preprint was prepared with the AAS L<sup>A</sup>T<sub>E</sub>X macros v5.2.

Table 1. Proper Motion Studies of IC 2395

Survey	$\mu_{\alpha} \cos \delta$ mas/yr	Uncertainty mas/yr	$\mu_{\delta}$ mas/yr	Uncertainty mas/yr	Sample size	Comments
Gulyaev & Nesterov (1992)	+2.3	1.0	-1.8	1.0	8	Greater than $3\sigma$ away from this paper's result.
Baumgardt et al. (2000)	-3.6	0.6	2.2	0.5	1	
Dias et al. (2001)	-4.4	1.6	4.0	1.6	11	
Dias et al. (2002)	-4.37	1.73	4.05	1.73	14	
Loktin et al. (2003)	-4.86	0.33	3.48	0.23	33	
Kharchenko et al. (2003)	-4.21	0.63	1.73	0.63	12	
Kharchenko et al. (2004)	-4.34	0.38	2.42	0.35	15	Greater than $3\sigma$ away from this paper's result.
Dias et al. (2006)	-5.56	0.40	6.02	0.40	55	
This Paper	-3.92	0.33	3.03	0.26	11	1 clipped; proper motion values used in this analysis.
This Paper	-3.60	0.36	2.69	0.28	10	2 clipped

Table 2. General Characteristics of IC 2395 Cluster Members from Claria et al. (2003)

ID <sup>a</sup>	ID Tbl 4 <sup>b</sup>	RA (2000)	Dec (2000)	SpT	Ref.	V (mag)	B-V (mag)	$\mu_{\alpha} \cos \delta$ (mas/yr)	$\mu_{\delta}$ (mas/yr)	Other Designation <sup>c</sup>
246	1	8:40:09.9	-48:07:57.6	A5V	1	11.29	0.10	-3.4±2.9	4.2±3.8	-
232	2	8:40:18.9	-48:29:43.4	A7V	1	11.30	0.16	-8.1±1.4	5.7±1.4	CD-484010
229	3	8:40:25.6	-48:22:48.1	F7	3	12.96	0.56	-13.7±5.8	12.7±5.8	-
113	14	8:40:46.8	-48:12:42.8	B8:	2	9.60	0.05	-8.7±3.0	-1.6±3.0	JW8, CD-474208
112	16	8:40:48.2	-48:14:15.6	A4	3	11.75	0.17	-6.1±2.3	2.0±3.2	JW5, CD-474209
111	23	8:40:53.4	-48:13:31.8	B2IV	2	6.96	-0.16	-3.6±0.6	2.2±0.4	JW2, HD74234
260	-	8:40:59.8	-47:47:02.8	F0II	1	11.39	0.17	-4.6±2.1	3.9±2.0	CD-474211
118	36	8:41:04.0	-48:04:15.6	F9	3	13.31	0.61	6.6±5.1	5.8±5.1	-
119	41	8:41:13.7	-48:04:36.7	F5	3	12.77	0.49	-7.2±3.6	1.5±1.4	-
100	45	8:41:19.2	-48:13:04.2		5	14.32	0.68	...	...	-
128	-	8:41:30.4	-47:58:41.5	B9IV	2	9.92	-0.04	-1.2±2.1	6.7±1.3	L57,HD74338
129	-	8:41:35.3	-47:57:51.3	A1	3	11.12	0.09	-2.4±1.9	2.4±1.4	CD-474225
50	60	8:41:35.8	-48:04:24.1	A3	3	11.30	0.12	-2.9±3.0	0.5±1.4	L54
220	63	8:41:37.3	-48:20:47.8	G2	3	13.03	0.64	-8.0±5.8	7.2±5.8	-
41	77	8:41:44.9	-48:09:35.8	F0	3	12.17	0.38	-4.6±2.2	2.2±1.4	L51
40	83	8:41:50.5	-48:09:17.6	F6	3	13.20	0.45	1.7±3.0	-1.7±2.7	L50
39	92	8:41:55.2	-48:09:12.2	A3	3	11.49	0.15	-6.0±1.4	4.4±1.4	CD-474238
266	96	8:41:55.7	-47:52:12.6	B9/A0V	2	9.84	-0.02	-4.9±1.7	5.1±1.8	HD74402
263	107	8:41:59.5	-47:48:17.7	B9V	1	10.29	-0.05	-4.6±1.3	3.4±1.5	CD-474240
78	114	8:42:04.9	-48:11:43.3	A3	3	11.88	0.17	-4.3±1.4	5.5±2.3	L49
83	121	8:42:07.5	-48:14:40.9	B3V	2	8.23	-0.06	-4.1±1.2	4.4±1.5	L6, HD74436 <sup>d</sup>
80	122	8:42:08.2	-48:13:16.5	F7	3	13.12	0.58	-6.1±5.8	2.8±5.8	-
216	124	8:42:09.5	-48:20:56.1	F3	3	12.68	0.44	-4.9±5.8	8.1±5.8	-
5	131	8:42:11.8	-48:06:33.0	B9:	2	10.39	0.00	-3.4±1.4	4.7±2.0	L43,CD-474247
38	137	8:42:12.9	-48:09:34.5	G1	3	13.60	0.66	...	...	-
6	138	8:42:14.3	-48:06:55.9	B9	3	11.28	0.09	-4.4±1.4	4.0±1.4	CPD-472576, L44
211	139	8:42:14.4	-48:27:09.2	B5V	2	9.46	-0.04	-1.5±1.7	0.8±1.2	HD74456
2	142	8:42:15.8	-48:04:20.0	A5	3	11.70	0.29	-2.2±3.2	5.3±2.4	L18
1	143	8:42:16.2	-48:05:56.7	B1.5Vn	2	5.49	-0.18	-3.8±0.9	2.7±0.8	HD74455 <sup>e</sup> , V* HX Vel
3	148	8:42:17.8	-48:03:53.1	B9V	4	10.74	0.03	-6.8±2.5	1.1±1.4	L15, CD-474253
135	171	8:42:26.4	-47:58:22.1	A6	3	12.49	0.32	-4.6±1.4	7.2±1.6	L20
57	180	8:42:30.1	-47:59:17.9	F9	3	13.29	0.63	-7.0±2.7	8.7±2.5	-
35	188	8:42:33.5	-48:10:27.8	A4	3	11.91	0.22	-5.9±2.3	6.9±2.3	-
34	-	8:42:34.8	-48:09:48.9	B2V:	2	7.27	-0.16	-3.7±0.8	2.9±0.7	L3, HD74531
136	193	8:42:35.2	-47:55:47.4	B8	3	11.02	0.06	-6.4±1.7	3.7±1.4	CD-474260
17	195	8:42:36.5	-48:04:30.9	B3IV-V	2	8.71	-0.11	-5.3±1.7	4.4±1.6	L8, HD74530
18	189	8:42:36.6	-48:05:04.1	B8	3	10.61	0.03	-9.4±2.7	0.8±3.2	L34, CD-474262
21	200	8:42:37.0	-48:08:12.3	A0	3	11.56	0.12	-8.3±2.8	4.7±1.7	L28, CD-474264
205	-	8:42:39.5	-48:23:59.8	G1	3	13.13	0.68	-6.3±5.8	-1.8±5.8	-
25	207	8:42:42.1	-48:05:17.0	A5	3	11.07	0.15	-8.7±1.7	1.3±1.4	L33,CD-474265
24	-	8:42:42.4	-48:06:27.2	A1	3	11.17	0.10	-8.5±2.7	5.4±1.7	L31, CD-474266
23	209	8:42:43.0	-48:07:55.7	A0	3	11.51	0.12	-4.0±1.6	4.6±1.4	L29, CD-474267
141	212	8:42:44.5	-47:51:02.5	F6	3	12.69	0.49	-9.3±2.5	6.1±2.2	-
27	-	8:42:46.4	-48:05:25.5	B9Ve	2	9.49	-0.03	-2.5±1.3	1.7±1.7	L11, HD74559 <sup>d</sup>
29	220	8:42:47.2	-48:08:04.2	F4	3	12.69	0.54	-9.1±5.1	13.3±5.1	L26
73	221	8:42:47.9	-48:13:31.9	B6/8V	2	9.25	-0.09	-4.5±1.3	1.9±1.9	L21, HD74581
74	222	8:42:48.0	-48:13:40.4	B/A	2	9.93	0.02	-4.0±1.5	-1.9±2.4	-
31	228	8:42:53.1	-48:07:41.2	B3V	2	8.66	-0.03	-1.5±1.4	3.8±1.2	L7, HD74580
72	242	8:43:00.2	-48:13:06.6	B7V	4	10.42	-0.02	-5.9±1.3	4.8±1.3	L14, CD-474274
70	-	8:43:04.3	-48:11:03.7	B8V	2	8.91	-0.04	-6.0±0.9	5.1±0.7	L9, HD74621
268	255	8:43:06.5	-48:18:16.2	G6	3	14.52	0.70	-6.9±5.9	5.3±5.8	-
202	-	8:43:18.8	-48:20:42.9	B3V	2	8.87	-0.11	-5.7±1.3	2.6±1.1	HD74662
67	277	8:43:29.1	-48:02:54.9	A1	3	10.99	0.04	-4.0±1.4	3.1±1.5	CD-474286
175	283	8:43:41.3	-48:09:33.1	F3	3	12.84	0.48	-5.9±2.9	2.6±2.6	-
163	287	8:44:07.8	-48:01:14.6	A7V	1	11.80	0.18	-4.9±1.8	4.4±2.8	CD-474298
180	288	8:44:11.4	-48:10:44.4	F8	3	13.06	0.62	-8.0±5.8	1.1±5.8	-
192	-	8:44:26.6	-48:27:05.7	A5III	1	11.64	0.24	-6.3±1.4	7.5±3.3	CD-474307

<sup>a</sup>From Claria et al. (2003)<sup>b</sup>If no cross-reference to Table 4 is provided, we do not confirm the membership assignment.<sup>c</sup>CD or CPD = photographic plates from the Annals of the Cape Observatory, L = Lynga, HD = Henry Draper<sup>d</sup>Probable binary

<sup>e</sup> Likely ellipsoidal variable (Morris 1985), hence binary

Note. — (i) Celestial coordinates are from 2MASS; (ii) optical photometry from Claria et al. (2003); uncertainties described therein; (iii) proper motions from NOMAD; Zacharias et al. (2004); (iv) mean cluster proper motion derived in § 3.1.1 is  $\mu_\alpha \cos \delta = -3.9 \pm 0.4$  mas/yr and  $\mu_\delta = 3.0 \pm 0.4$  mas/yr. Spectral type references: 1, Pickles & Depagne (2010); 2, Skiff (2014); 3, from photometry (see text); 4, from H $\beta$  photometry (Paunzen 2015) calibrated through (Crawford & Mander 1966).

Table 3. Optical Photometry of Cluster Members

ID	RA(2000) (deg)	DEC(2000) (deg)	SpT <sup>a</sup>	U mag	(err) (mag)	B (mag)	(err) (mag)	V (mag)	(err) (mag)	R (mag)	(err) (mag)	I (mag)	(err) (mag)
1	130.04111	-48.13267	A1	11.463	–	11.251	–	11.114	–	–	–	–	–
2	130.07856	-48.49538	A1	11.602	–	11.32	–	11.116	–	–	–	–	–
3	130.10667	-48.38002	F7	13.549	–	13.381	–	12.783	–	–	–	–	–
4	130.13353	-48.15396	–	–	–	–	–	–	–	–	–	–	–
5	130.16329	-48.35785	K8	17.685	0.014	17.052	0.009	15.836	0.011	15.122	0.012	14.41	0.022
6	130.16755	-47.80875	M7	–	–	–	–	19.652	0.036	18.143	0.016	16.566	0.029
7	130.17279	-48.08578	M0	19.469	0.058	18.233	0.013	16.791	0.008	15.777	0.015	14.822	0.013
8	130.17401	-47.97556	A8	11.835	0.015	11.591	0.005	11.285	0.011	11.098	0.011	10.903	0.014
9	130.18154	-47.97577	–	–	–	19.158	0.026	17.594	0.013	16.484	0.007	15.25	0.01
10	130.18426	-47.89005	M6	–	–	–	–	19.25	0.024	17.964	0.013	16.485	0.008
11	130.19016	-48.13	–	–	–	20.278	0.078	18.862	0.019	17.682	0.013	16.3	0.01
12	130.19292	-47.92146	–	–	–	18.96	0.02	17.398	0.01	16.357	0.007	15.235	0.006
13	130.19294	-48.09262	K0	14.968	0.002	14.502	0.003	13.623	0.006	13.09	0.008	12.606	0.007
14	130.19516	-48.21189	–	9.272	0.028	9.556	0.023	9.493	0.024	9.412	0.013	9.357	0.012
15	130.19645	-47.95963	F1	12.633	0.006	12.232	0.003	11.824	0.005	11.581	0.008	11.371	0.008
16	130.20083	-48.23767	A4	11.972	0.035	12.255	0.072	11.768	0.025	11.477	0.039	11.351	0.037
17	130.20201	-48.0119	–	–	–	–	–	19.122	0.03	17.931	0.018	16.481	0.018
18	130.2088	-47.85571	K8	17.796	0.021	16.683	0.013	15.487	0.014	14.719	0.017	14.045	0.012
19	130.21083	-47.93254	K4	16.493	0.006	15.783	0.004	14.699	0.007	14.044	0.007	13.457	0.007
20	130.21435	-48.12297	M4	–	–	–	–	19.315	0.02	18.071	0.015	16.579	0.01
21	130.21711	-47.82916	M4	–	–	19.266	0.028	17.756	0.008	16.572	0.007	15.241	0.017
22	130.22224	-48.30987	–	–	–	–	–	19.717	0.037	18.431	0.015	16.857	0.015
23	130.22255	-48.22551	–	5.942	0.061	7.677	0.2	7.631	0.101	–	–	6.725	0.086
24	130.225	-48.39803	–	–	–	–	–	20.657	0.058	19.055	0.019	17.2	0.012
25	130.22738	-47.89508	M6	–	–	–	–	19.93	0.041	18.405	0.017	16.581	0.014
26	130.23338	-48.04948	M3	–	–	19.848	0.048	18.217	0.014	17.109	0.008	15.857	0.006
27	130.23468	-47.89904	–	–	–	19.429	0.029	17.84	0.015	16.689	0.01	15.383	0.013
28	130.23669	-48.08591	M6	–	–	–	–	19.186	0.023	17.878	0.009	16.305	0.009
29	130.24285	-47.88766	M6	–	–	–	–	19.444	0.038	18.141	0.019	16.562	0.016
30	130.24851	-48.22288	M4	20.751	0.158	19.854	0.05	18.267	0.013	17.066	0.008	15.624	0.005
31	130.24887	-48.27729	M3	–	–	20.049	0.046	18.525	0.021	17.387	0.007	16.036	0.01
32	130.24976	-48.00943	K3	16.332	0.005	15.627	0.005	14.619	0.005	14.04	0.006	13.505	0.012
33	130.25073	-48.1446	–	–	–	–	–	20.415	0.07	18.957	0.021	17.272	0.017
34	130.25523	-47.99615	–	–	–	19.099	0.026	17.603	0.008	16.61	0.012	15.561	0.013
35	130.2598	-48.39655	M4	–	–	–	–	19.193	0.022	17.958	0.012	16.465	0.013
36	130.26646	-48.07101	F9	14.159	0.003	13.944	0.005	13.282	0.005	12.895	0.008	12.545	0.008
37	130.28096	-48.31279	M6	20.63	0.099	19.877	0.032	18.303	0.017	17.1	0.008	15.634	0.014
38	130.29027	-48.05354	M0	–	–	19.72	0.038	18.157	0.013	17.033	0.009	15.815	0.007
39	130.29346	-48.24735	A4	11.62	0.006	11.851	0.013	11.685	0.006	11.552	0.008	11.41	0.011
40	130.30281	-48.30906	–	–	–	–	–	19.184	0.028	17.986	0.01	16.552	0.013
41	130.3069	-48.07686	F5	13.316	0.003	13.173	0.004	12.641	0.006	12.323	0.005	12.034	0.005
42	130.3076	-47.85229	M0	–	–	19.514	0.032	17.96	0.017	16.85	0.01	15.717	0.011
43	130.31617	-48.07088	K5	18.049	0.012	16.949	0.007	15.698	0.006	14.941	0.007	14.265	0.008
44	130.32777	-47.94247	M6	20.797	0.124	19.828	0.039	18.201	0.012	16.989	0.008	15.541	0.006
45	130.33013	-48.21782	–	15.237	0.003	15.026	0.004	14.337	0.005	13.906	0.005	13.471	0.005
46	130.33425	-48.01932	M1	–	–	19.601	0.033	17.951	0.01	16.837	0.009	15.598	0.006
47	130.34054	-47.91004	M6	–	–	–	–	19.91	0.039	18.509	0.011	16.737	0.009
48	130.35021	-48.11476	–	–	–	19.027	0.023	17.568	0.008	16.473	0.008	15.228	0.005
49	130.35659	-47.80632	M6	–	–	20.451	0.067	18.723	0.027	17.376	0.011	15.803	0.01
50	130.35859	-48.24266	M3	–	–	19.97	0.042	18.438	0.02	17.273	0.012	15.912	0.013

Table 3—Continued

ID	RA (2000) (deg)	DEC(2000) (deg)	SpT <sup>a</sup>	U mag	B (mag)	(err) (mag)	V (mag)	(err) (mag)	R (mag)	(err) (mag)	I (mag)	(err) (mag)
51	130.36452	-47.93229	K7	19.054	0.026	–	16.244	0.009	15.403	0.007	14.714	0.007
52	130.36982	-48.0752	M4	–	–	–	17.827	0.033	16.763	0.005	15.597	0.005
53	130.37517	-48.17687	M6	–	–	–	18.725	–	17.5	0.009	16.141	0.006
54	130.38432	-48.06913	M6	–	–	–	19.121	–	17.705	0.012	16.032	0.007
55	130.385	-47.87392	M6	–	–	–	19.193	0.085	17.927	0.018	16.442	0.008
56	130.38717	-48.02066	M4	–	–	–	18.567	0.056	17.358	0.01	15.893	0.006
57	130.38908	-48.24433	–	16.735	0.006	–	15.043	0.01	14.428	0.008	13.863	0.011
58	130.39047	-48.00595	M3	–	–	–	18.254	–	17.095	0.008	15.744	0.006
59	130.39743	-48.18454	M4	–	–	–	18.571	0.017	17.437	0.009	16.12	0.009
60	130.39926	-48.07337	A3	11.501	0.004	–	11.111	0.009	11.055	0.01	10.965	0.012
61	130.40133	-48.09466	–	–	–	–	19.588	0.034	18.293	0.013	16.714	0.009
62	130.40297	-48.16009	–	19.328	0.039	–	16.797	0.007	15.837	0.006	14.88	0.006
63	130.40549	-48.34661	G2	13.738	0.003	–	12.894	0.009	12.499	0.009	12.139	0.008
64	130.4077	-47.93177	M6	–	–	–	18.631	0.019	17.447	0.01	16.069	0.006
65	130.40883	-47.97562	M6	–	–	–	18.001	0.016	16.845	0.007	15.572	0.008
66	130.40947	-47.80299	M6	–	–	–	19.125	0.021	17.727	0.008	16.022	0.007
67	130.41169	-47.91742	G2	14.021	0.003	–	12.625	0.008	12.189	0.012	11.832	0.006
68	130.41494	-47.95245	–	–	–	–	20.119	–	18.643	0.015	16.974	0.01
69	130.41879	-47.8669	M6	–	–	–	18.556	0.016	17.359	0.011	15.939	0.01
70	130.42058	-48.32122	K5	17.677	0.008	–	15.462	0.006	14.72	0.009	14.042	0.012
71	130.42212	-47.92717	–	18.83	0.024	–	16.104	0.008	15.219	0.01	14.403	0.007
72	130.42264	-48.04642	M5	–	–	–	18.496	0.015	17.321	0.009	15.957	0.007
73	130.43183	-48.06353	M6	–	–	–	19.745	0.038	18.395	0.015	16.712	0.008
74	130.43366	-48.09705	G6	14.116	0.002	–	12.906	0.004	12.426	0.005	11.97	0.006
75	130.43452	-48.03746	M6	–	–	–	19.238	0.022	17.942	0.01	16.375	0.01
76	130.43642	-48.07252	M6	–	–	–	18.443	0.017	17.189	0.008	15.638	0.007
77	130.43713	-48.15996	F0	12.7	0.006	–	12.001	0.006	11.792	0.012	11.562	0.007
78	130.43779	-48.24184	K5	16.984	0.005	–	15.123	0.004	14.49	0.009	13.859	0.017
79	130.43919	-48.01921	M2	19.676	0.047	–	16.788	0.006	15.724	0.007	14.614	0.007
80	130.44379	-48.28019	–	–	–	–	20.614	0.088	19.097	0.019	17.285	0.021
81	130.44411	-48.33692	M5	–	–	–	18.552	0.018	17.395	0.012	16.011	0.013
82	130.45622	-48.12308	–	–	–	–	20.327	0.075	18.964	0.027	17.227	0.014
83	130.4606	-48.15488	F6	13.598	0.003	–	13.043	0.005	12.741	0.005	12.418	0.005
84	130.46658	-48.19344	M6	–	–	–	19.167	0.025	17.665	0.008	15.928	0.007
85	130.46871	-48.12927	M0	–	–	–	18.1	0.014	16.882	0.009	15.468	0.005
86	130.46939	-48.14062	M4	–	–	–	17.671	0.029	16.568	0.005	15.386	0.005
87	130.47019	-47.97116	–	–	–	–	18.893	0.024	17.681	0.008	16.229	0.008
88	130.47197	-47.98656	K4	16.866	0.009	–	14.921	0.009	14.268	0.005	13.655	0.004
89	130.47275	-47.88406	K5	19.186	0.026	–	16.731	0.013	15.836	0.01	14.995	0.011
90	130.47304	-48.37222	M3	–	–	–	18.064	0.04	16.917	0.009	15.636	0.011
91	130.47504	-48.29206	M5	–	–	–	18.873	0.022	17.637	0.012	16.161	0.012
92	130.48015	-48.15339	A3	11.659	0.007	–	11.308	0.006	11.217	0.009	11.084	0.012
93	130.48058	-47.91023	M6	–	–	–	18.594	0.016	17.348	0.009	15.944	0.005
94	130.4814	-47.85101	M6	–	–	–	18.136	0.01	17.008	0.008	15.803	0.005
95	130.482	-47.92538	–	17.883	0.011	–	15.335	0.01	14.504	0.017	13.771	0.02
96	130.48222	-47.87016	B7	9.784	0.007	–	9.65	0.008	9.623	0.014	9.626	0.011
97	130.48235	-48.11474	–	18.678	0.02	–	16.077	0.005	15.241	0.003	14.505	0.003
98	130.48289	-47.98434	M1	–	–	–	18.504	0.02	17.325	0.011	15.949	0.006
99	130.48379	-47.93894	M6	–	–	–	19.502	0.038	18.182	0.016	16.627	0.01
100	130.48392	-48.23105	M6	–	–	–	19.44	0.034	18.126	0.014	16.509	0.008

Table 3—Continued

ID	RA (2000) (deg)	DEC(2000) (deg)	SpT <sup>a</sup>	U mag	(err) (mag)	B (mag)	(err) (mag)	V (mag)	(err) (mag)	R (mag)	(err) (mag)	I (mag)	(err) (mag)
101	130.48719	-48.27705	K5	17.141	0.005	16.165	0.005	15.092	0.01	14.44	0.006	13.819	0.009
102	130.48939	-47.88853	M6	—	—	—	—	19.335	0.036	17.902	0.013	16.208	0.009
103	130.49114	-48.03883	K7	19.642	0.037	18.336	0.02	16.89	0.012	15.983	0.016	15.141	0.013
104	130.49318	-47.84533	K5	18.067	0.011	16.566	0.005	15.242	0.006	14.476	0.003	13.829	0.004
105	130.49445	-48.25725	K5	19.095	0.038	17.409	0.006	16.058	0.007	15.201	0.004	14.402	0.008
106	130.49729	-47.99005	M5	—	—	20.006	0.046	18.48	0.02	17.204	0.009	15.644	0.007
107	130.49802	-47.80492	B5	10.317	0.009	10.053	0.004	10.08	0.007	10.03	0.009	10.044	0.012
108	130.4981	-48.28121	K7	18.146	0.009	16.653	0.007	15.275	0.01	14.419	0.006	13.661	0.007
109	130.49969	-48.29562	—	—	—	—	—	20.399	0.078	18.871	0.016	17.218	0.014
110	130.50042	-48.012	—	—	—	—	—	—	—	—	—	—	—
111	130.50084	-48.086	M6	—	—	20.374	0.043	18.751	0.02	17.558	0.011	16.129	0.007
112	130.50467	-48.00283	M6	—	—	21.318	0.119	19.493	0.032	18.197	0.033	16.558	0.028
113	130.52028	-48.06779	M4	—	—	20.334	0.04	18.884	0.017	17.611	0.013	16.087	0.007
114	130.52043	-48.19535	A3	12.105	0.004	11.902	0.002	11.678	0.008	11.596	0.02	11.462	0.008
115	130.52097	-47.79497	M6	—	—	20.953	0.124	19.201	0.026	17.885	0.017	16.404	0.02
116	130.52116	-48.10053	M5	—	—	—	—	19.445	0.023	18.154	0.015	16.575	0.011
117	130.52117	-48.12712	M6	20.906	0.113	19.807	0.025	18.174	0.014	16.92	0.009	15.402	0.006
118	130.52257	-47.90689	—	—	—	—	—	20.794	0.115	19.274	0.026	17.41	0.012
119	130.52434	-48.0064	—	—	—	—	—	17.783	0.014	16.601	0.019	15.087	0.038
120	130.52733	-48.27716	M6	—	—	—	—	19.985	0.052	18.421	0.013	16.571	0.011
121	130.53145	-48.24471	—	7.952	0.01	8.244	0.055	9.827	0.263	9.155	0.098	8.171	0.028
122	130.53398	-48.22125	F7	13.784	0.005	13.553	0.007	12.945	0.003	12.59	0.011	12.259	0.009
123	130.53875	-48.20716	—	—	—	—	—	20.625	0.07	19.118	0.024	17.354	0.013
124	130.53961	-48.34891	F3	13.115	0.007	12.992	0.007	12.523	0.007	12.235	0.005	11.973	0.006
125	130.54101	-48.13182	M6	—	—	—	—	19.792	0.045	18.451	0.021	16.782	0.008
126	130.54268	-48.09797	M5	—	—	20.69	0.122	18.754	0.02	17.499	0.011	16.066	0.008
127	130.54306	-47.78288	M5	—	—	20.165	0.049	18.57	0.017	17.33	0.017	15.93	0.018
128	130.54515	-47.82073	M6	—	—	20.425	0.064	18.827	0.019	17.541	0.008	16.053	0.007
129	130.54864	-48.1435	—	18.636	0.016	17.493	0.007	16.193	0.008	15.352	0.008	14.544	0.008
130	130.54883	-48.01179	—	19.999	0.046	20.079	0.039	18.918	0.018	17.641	0.013	16.063	0.014
131	130.54911	-48.10916	A0	10.205	0.003	10.233	0.005	10.196	0.005	10.162	0.005	10.146	0.008
132	130.54935	-48.35825	—	18.162	0.015	16.908	0.008	15.456	0.005	14.522	0.005	13.609	0.006
133	130.55006	-48.24302	—	—	—	—	—	—	—	—	—	—	—
134	130.55077	-47.93385	M6	—	—	19.945	0.06	18.404	0.043	17.101	0.042	15.577	0.064
135	130.5535	-48.08714	—	16.434	0.005	15.672	0.004	14.61	0.007	13.95	0.006	13.304	0.005
136	130.55352	-48.22897	—	—	—	—	—	19.722	0.037	18.403	0.017	16.788	0.014
137	130.55393	-48.15959	G1	14.349	0.003	14.125	0.005	13.474	0.008	13.054	0.008	12.676	0.007
138	130.55945	-48.11552	B9	11.391	0.004	11.211	0.006	11.081	0.005	11.029	0.006	10.975	0.01
139	130.56005	-48.45256	—	9.019	0.017	9.319	0.016	9.327	0.018	9.308	0.02	9.28	0.024
140	130.5623	-48.13295	—	—	—	—	—	20.001	0.043	18.577	0.019	16.937	0.011
141	130.5624	-47.80244	M5	—	—	—	—	18.537	0.035	17.207	0.031	15.678	0.043
142	130.56567	-48.07223	A5	12.079	0.006	11.8	0.004	11.502	0.004	11.329	0.008	11.18	0.007
143	130.56747	-48.09907	—	—	—	—	—	8.32	0.119	7.877	0.117	7.074	0.124
144	130.56877	-47.78455	M0	18.929	0.023	17.56	0.008	16.213	0.012	15.368	0.014	14.644	0.014
145	130.56956	-48.02019	M1	—	—	19.547	0.024	17.98	0.012	16.849	0.01	15.59	0.008
146	130.56967	-48.15525	M5	—	—	20.717	0.082	19.117	0.021	17.75	0.013	16.085	0.008
147	130.57163	-48.24849	M7	—	—	—	—	20.625	0.03	19.175	0.018	17.338	0.01
148	130.57428	-48.06475	B9	10.648	0.002	10.579	0.005	10.52	0.003	10.482	0.007	10.469	0.008
149	130.57547	-48.05382	M6	—	—	—	—	19.355	0.031	17.96	0.013	16.194	0.007
150	130.57648	-48.16748	M2	19.661	0.03	18.282	0.011	16.798	0.01	15.802	0.01	14.87	0.006

Table 3—Continued

ID	RA (2000) (deg)	DEC(2000) (deg)	SpT <sup>a</sup>	U mag	(err) (mag)	B (mag)	(err) (mag)	V (mag)	(err) (mag)	R (mag)	(err) (mag)	I (mag)	(err) (mag)
151	130.57925	-48.13683	G8	14.412	0.004	14.011	0.005	13.18	0.004	12.676	0.01	12.213	0.007
152	130.57955	-47.80367	–	16.676	0.005	15.7	0.005	14.373	0.005	13.55	0.004	12.802	0.005
153	130.58436	-48.17559	–	21.844	0.276	21.298	0.112	19.767	0.031	18.402	0.018	16.767	0.01
154	130.58478	-48.10274	M6	–	–	20.458	0.048	19.076	0.023	17.696	0.016	16.049	0.011
155	130.5895	-48.12004	–	–	–	–	–	20.676	0.083	19.065	0.028	17.073	0.013
156	130.59121	-48.35601	M4	20.777	0.12	19.63	0.035	17.956	0.061	16.74	0.009	15.279	0.012
157	130.59283	-48.33745	M6	–	–	–	–	19.89	0.016	18.549	0.012	16.9	0.014
158	130.59527	-48.07796	M6	–	–	19.934	0.03	18.362	0.016	17.172	0.012	15.769	0.009
159	130.59672	-48.06534	–	–	–	–	–	20.557	0.069	18.867	0.022	17.142	0.013
160	130.59718	-48.04992	–	–	–	19.413	0.021	17.849	0.013	16.675	0.011	15.324	0.008
161	130.59786	-48.1875	M0	19.731	0.037	18.598	0.016	17.138	0.012	16.15	0.014	15.142	0.011
162	130.5984	-48.42842	K8	18.822	0.028	17.51	0.01	16.111	0.006	15.245	0.009	14.469	0.011
163	130.59884	-48.01535	M0	19.135	0.018	17.829	0.01	16.419	0.006	15.508	0.007	14.662	0.007
164	130.60181	-48.04307	M6	–	–	–	–	19.34	0.028	18.078	0.017	16.487	0.009
165	130.60423	-48.21719	–	–	–	–	–	19.781	0.036	18.479	0.02	16.835	0.01
166	130.60658	-48.27244	–	–	–	–	–	–	–	–	–	–	–
167	130.60801	-48.1922	M6	–	–	19.768	0.031	18.214	0.016	17.05	0.012	15.707	0.007
168	130.60823	-48.15611	M4	20.813	0.084	19.802	0.031	18.182	0.014	17.034	0.01	15.707	0.007
169	130.60917	-48.29816	M6	–	–	–	–	19.839	0.014	18.457	0.014	16.808	0.011
170	130.60959	-48.36235	–	20.368	0.115	19.234	0.029	17.681	0.006	16.59	0.007	15.427	0.009
171	130.61014	-47.9728	A6	12.919	0.007	12.589	0.007	12.259	0.006	12.056	0.01	11.862	0.006
172	130.61262	-48.06911	M5	20.945	0.113	20.021	0.034	18.413	0.014	17.188	0.011	15.762	0.011
173	130.61416	-48.14957	–	–	–	–	–	20.451	0.053	19.017	0.023	17.215	0.013
174	130.61477	-48.12699	M5	20.724	0.088	19.403	0.023	17.859	0.01	16.788	0.009	15.598	0.007
175	130.61499	-48.17745	–	14.822	0.011	14.113	0.014	13.091	0.02	12.473	0.034	11.919	0.027
176	130.61643	-48.23233	–	–	–	–	–	19.439	0.032	18.147	0.011	16.628	0.01
177	130.61766	-47.93393	–	–	–	–	–	20.068	0.05	18.663	0.021	17.052	0.009
178	130.61961	-48.15551	K3	16.475	0.004	15.685	0.004	14.644	0.005	14.011	0.005	13.447	0.005
179	130.61974	-48.32554	–	–	–	–	–	20.183	0.008	18.652	0.013	16.874	0.01
180	130.62532	-47.9883	F9	13.989	0.003	13.71	0.003	13.1	0.008	12.689	0.005	12.315	0.007
181	130.6254	-48.0099	M6	–	–	–	–	19.802	0.037	18.432	0.014	16.772	0.009
182	130.62635	-48.37638	M6	–	–	–	–	19.421	0.029	17.869	0.009	16.021	0.01
183	130.63384	-48.14099	–	20.39	0.057	19.555	0.029	17.951	0.017	16.682	0.02	15.19	0.018
184	130.63442	-48.15695	M6	–	–	–	–	18.983	0.019	17.672	0.011	16.202	0.007
185	130.63459	-48.051	M2	20.283	0.049	19.247	0.019	17.713	0.012	16.537	0.013	15.178	0.007
186	130.63819	-48.22063	M6	–	–	19.971	0.032	18.349	0.014	17.153	0.008	15.806	0.007
187	130.63914	-48.26608	–	–	–	–	–	19.287	0.039	18.062	0.013	16.64	0.007
188	130.63954	-48.17439	A4	12.188	0.006	11.955	0.007	11.709	0.005	11.589	0.006	11.458	0.007
189	130.63987	-48.21314	–	–	–	20.751	0.06	19.477	0.027	18.173	0.01	16.559	0.007
190	130.64049	-48.33692	M6	–	–	–	–	19.977	0.008	18.634	0.016	16.908	0.008
191	130.64235	-48.16692	F1	12.25	0.008	12.057	0.008	11.62	0.004	11.353	0.005	11.108	0.008
192	130.64576	-48.36393	K1	15.658	0.007	15.075	0.007	14.119	0.007	13.556	0.008	13.069	0.01
193	130.64675	-47.92984	B8	11.05	0.006	10.869	0.01	10.769	0.011	10.713	0.013	10.675	0.01
194	130.64868	-48.06196	M4	–	–	20.038	0.036	18.494	0.014	17.282	0.01	15.902	0.007
195	130.65226	-48.07524	B2	8.048	0.004	8.439	0.028	8.504	0.01	8.653	0.069	8.6	0.008
196	130.65228	-48.28875	K0	15.341	0.007	14.769	0.008	13.829	0.008	13.288	0.007	12.823	0.009
197	130.65228	-48.13372	K6	17.622	0.007	16.545	0.005	15.305	0.008	14.549	0.007	13.883	0.006
198	130.65266	-48.08447	B8	10.564	0.003	10.48	0.004	10.409	0.005	10.374	0.006	10.362	0.008
199	130.65276	-48.10229	M1	19.069	0.017	17.801	0.008	16.429	0.008	15.515	0.007	14.626	0.006
200	130.6541	-48.13675	A0	11.734	0.004	11.496	0.003	11.332	0.005	11.269	0.004	11.209	0.009

Table 3—Continued

ID	RA (2000) (deg)	DEC(2000) (deg)	SpT <sup>a</sup>	U mag	(err) (mag)	B (mag)	(err) (mag)	V (mag)	(err) (mag)	R (mag)	(err) (mag)	I (mag)	(err) (mag)
201	130.6573	-48.21142	—	19.303	0.025	18.048	0.011	16.588	0.005	15.657	0.005	14.753	0.004
202	130.65844	-47.99303	M6	20.773	0.07	21.129	0.083	19.639	0.033	18.143	0.024	16.421	0.007
203	130.66161	-48.05106	—	20.694	0.073	19.563	0.026	17.991	0.012	15.771	0.01	15.33	0.008
204	130.66723	-48.18991	—	20.826	0.086	19.704	0.024	18.049	0.012	16.906	0.01	15.619	0.006
205	130.67026	-48.30506	M6	—	—	—	—	19.246	19.351	17.922	0.007	16.386	0.007
206	130.67482	-48.09828	M4	—	—	20.127	0.029	18.616	0.016	17.406	0.011	15.979	0.008
207	130.67538	-48.08806	A5	11.327	0.003	11.075	0.006	10.897	0.005	10.807	0.01	10.709	0.01
208	130.6764	-47.97152	M6	—	—	20.663	0.078	19.233	0.036	17.957	0.01	16.466	0.006
209	130.67932	-48.13215	A0	11.667	0.005	11.443	0.004	11.295	0.006	11.227	0.005	11.181	0.011
210	130.68044	-48.3464	K4	15.972	0.004	15.532	0.007	14.648	14.753	14.057	0.005	13.48	0.005
211	130.68077	-48.07929	M6	—	—	20.596	0.061	19.072	0.018	17.772	0.01	16.279	0.007
212	130.6855	-47.8507	F6	13.242	0.007	12.998	0.005	12.484	0.009	12.12	0.009	11.814	0.008
213	130.68681	-48.01668	—	19.858	0.035	20.203	0.035	18.971	0.019	17.65	0.014	16.023	0.006
214	130.6886	-48.15538	M5	—	—	19.749	0.027	18.145	0.014	16.989	0.007	15.688	0.006
215	130.68983	-48.08909	—	—	—	17.028	0.009	15.923	0.009	14.797	0.007	14.797	0.007
216	130.69152	-48.18824	M5	19.244	0.061	18.487	0.02	19.939	0.037	18.507	0.017	16.794	0.009
217	130.69166	-48.15731	M6	—	—	20.441	0.044	18.829	0.022	17.567	0.009	16.06	0.008
218	130.69378	-48.21757	K4	18.874	0.017	17.68	0.007	16.252	0.004	15.3	0.006	14.298	0.006
219	130.69404	-48.27368	M6	—	—	—	—	19.111	19.216	17.779	0.043	16.151	0.049
220	130.69659	-48.13451	F4	13.209	0.004	13.021	0.005	12.485	0.007	12.155	0.008	11.851	0.006
221	130.69967	-48.22552	B3	8.538	0.012	8.936	0.018	9.008	0.004	9.002	0.011	9.027	0.015
222	130.69981	-48.2279	B7	9.795	0.014	9.77	0.018	9.719	0.003	9.693	0.007	9.654	0.019
223	130.70182	-48.25902	—	19.427	0.027	18.083	0.013	16.687	16.792	15.803	0.006	14.961	0.008
224	130.70532	-47.98901	M3	—	—	19.466	0.033	17.976	0.015	16.944	0.007	15.972	0.007
225	130.70785	-48.23628	M6	—	—	20.045	0.034	18.53	0.016	17.259	0.008	15.686	0.008
226	130.71111	-48.10315	—	20.033	0.041	19.117	0.022	17.579	0.007	16.418	0.008	15.107	0.005
227	130.71711	-48.21714	M2	—	—	19.43	0.022	17.855	0.01	16.666	0.006	15.269	0.006
228	130.7211	-48.1281	—	8.165	0.003	8.42	0.019	8.444	0.007	8.354	0.046	8.428	0.012
229	130.72409	-48.2766	M6	—	—	19.942	0.051	18.353	18.458	17.143	0.007	15.786	0.01
230	130.72669	-48.14452	M6	19.927	0.033	20.077	0.029	18.85	0.02	17.54	0.011	15.928	0.007
231	130.72688	-48.40444	M3	—	—	20.075	0.054	18.532	18.637	17.371	0.007	16.124	0.009
232	130.72719	-48.10849	K4	17.926	0.008	16.868	0.006	15.64	0.006	14.846	0.005	14.056	0.007
233	130.72764	-48.20899	—	20.57	0.057	19.246	0.019	17.634	0.011	16.484	0.006	15.114	0.007
234	130.72867	-48.00384	M5	—	—	20.6	0.066	18.986	0.03	17.785	0.019	16.269	0.016
235	130.73342	-48.24763	M3	—	—	19.576	0.049	17.993	18.098	16.9	0.006	15.702	0.005
236	130.73568	-48.16783	M6	21.016	0.077	20.188	0.04	18.681	0.021	17.411	0.015	15.884	0.009
237	130.73768	-48.10828	—	—	—	—	—	19.636	0.034	18.335	0.018	16.679	0.01
238	130.73799	-48.14174	M5	—	—	20.701	0.058	19.104	0.02	17.804	0.014	16.311	0.007
239	130.74118	-48.08785	M4	—	—	—	—	19.172	0.024	17.822	0.012	16.297	0.009
240	130.74316	-48.22264	—	20.611	0.055	20.307	0.041	18.792	0.018	17.465	0.01	15.861	0.009
241	130.74466	-48.41864	—	20.406	0.086	19.248	0.022	17.784	17.889	16.701	0.008	15.447	0.012
242	130.75099	-48.2185	B8	10.091	0.009	10.209	0.007	10.186	0.006	10.156	0.006	10.113	0.01
243	130.75645	-48.18456	M5	—	—	20.411	0.043	18.864	0.019	17.584	0.009	16.112	0.006
244	130.75672	-47.83584	M2	19.79	0.031	18.412	0.012	16.921	0.009	15.901	0.008	14.935	0.008
245	130.75759	-48.40117	—	—	—	—	—	19.386	19.491	18.049	0.011	16.478	0.007
246	130.75851	-48.24496	M5	—	—	19.91	0.055	18.334	18.439	17.075	0.007	15.578	0.004
247	130.75894	-48.27816	M6	—	—	19.9	0.05	18.415	17.255	17.075	0.011	15.914	0.012
248	130.75929	-48.14733	M5	—	—	—	—	18.951	0.024	17.728	0.01	16.22	0.008
249	130.75979	-48.29715	M5	—	—	20.346	0.085	18.867	18.972	17.589	0.01	16.154	0.011
250	130.76245	-48.09072	M6	—	—	—	—	19.851	0.032	18.447	0.014	16.779	0.011



Table 3—Continued

ID	RA (2000) (deg)	DEC(2000) (deg)	SpT <sup>a</sup>	U mag	(err) (mag)	B (mag)	(err) (mag)	V (mag)	(err) (mag)	R (mag)	(err) (mag)	I (mag)	(err) (mag)
251	130.76506	-47.98093	M4	20.072	0.055	19.006	0.018	17.465	0.011	16.321	0.008	15.019	0.007
252	130.76669	-47.90915	M6	—	—	—	—	19.899	0.045	18.296	0.012	16.512	0.008
253	130.76926	-48.19912	F4	12.337	0.006	12.131	0.006	11.61	0.005	11.281	0.004	10.963	0.006
254	130.77305	-48.21655	M5	—	—	20.515	0.051	19.049	0.023	17.523	0.01	15.683	0.006
255	130.77715	-48.3045	G6	15.265	0.004	14.894	0.005	14.187	14.292	13.733	0.008	13.286	0.013
256	130.77866	-47.99617	M6	—	—	—	—	19.37	0.04	17.905	0.04	16.45	0.019
257	130.77901	-48.24989	—	—	—	—	—	20.465	20.57	19.096	0.015	17.287	0.011
258	130.79416	-48.41302	—	—	—	—	—	20.486	20.591	18.736	0.015	17.032	0.009
259	130.79544	-47.92458	M3	—	—	19.986	0.044	18.398	0.016	17.109	0.009	15.699	0.009
260	130.79786	-48.1705	M4	20.905	0.072	19.949	0.03	18.47	0.016	17.268	0.009	15.905	0.005
261	130.79973	-48.16979	M0	20.359	0.05	19.259	0.017	17.672	0.006	16.557	0.008	15.27	0.005
262	130.8083	-47.88947	K1	15.425	0.025	15.092	0.019	14.372	0.014	13.844	0.018	13.377	0.022
263	130.81026	-47.88939	A1	10.325	0.017	10.474	0.023	10.387	0.018	10.377	0.032	10.254	0.03
264	130.81077	-47.91597	M5	—	—	—	—	19.007	0.027	17.687	0.015	16.033	0.019
265	130.8125	-48.25545	M6	—	—	—	—	19.135	19.24	17.83	0.007	16.29	0.007
266	130.81962	-47.98082	M6	—	—	—	—	19.991	0.056	18.615	0.019	16.916	0.014
267	130.82009	-48.16689	M5	20.814	0.064	19.315	0.017	17.724	0.009	16.626	0.007	15.447	0.005
268	130.82298	-47.86301	G7	14.804	0.004	14.252	0.004	13.367	0.007	12.914	0.007	12.498	0.01
269	130.8235	-48.30886	—	—	—	—	—	19.031	19.136	17.792	0.012	16.235	0.011
270	130.83251	-48.18364	M6	—	—	—	—	20.213	0.052	18.774	0.023	16.998	0.015
271	130.8433	-47.89883	K2	16.214	0.006	15.601	0.004	14.609	0.005	14.07	0.005	13.555	0.007
272	130.84862	-48.12332	K4	17.945	0.009	16.616	0.005	15.384	0.004	14.617	0.006	13.973	0.006
273	130.85428	-48.09275	M5	—	—	—	—	18.299	0.016	17.134	0.007	15.783	0.013
274	130.85686	-47.96414	K6	17.353	0.008	16.553	0.007	15.322	0.008	14.639	0.007	13.952	0.009
275	130.8602	-48.3569	—	11.919	0.004	11.751	0.004	11.273	0.015	10.991	0.012	10.706	0.012
276	130.86751	-48.25191	A1	18.073	0.016	16.682	0.009	15.223	0.006	14.339	0.004	13.5	0.006
277	130.87107	-48.04859	A1	11.024	—	10.893	—	10.809	—	—	—	—	—
278	130.87289	-48.0782	M3	—	—	18.656	0.024	17.104	0.007	16.003	0.007	14.737	0.011
279	130.89333	-48.21946	M6	—	—	—	—	20.073	0.068	18.77	0.024	17.066	0.01
280	130.90405	-47.93553	M1	—	—	19.233	0.028	17.663	0.011	16.631	0.005	15.399	0.009
281	130.90883	-48.14464	K4	16.85	0.01	15.84	0.005	14.723	0.008	14.041	0.006	13.434	0.008
282	130.91268	-48.21247	M5	—	—	20.014	0.042	18.499	0.018	17.303	0.009	15.879	0.008
283	130.92262	-48.15919	F3	13.358	0.005	13.109	0.004	12.61	0.006	12.299	0.005	11.995	0.007
284	130.94884	-47.88982	M2	—	—	19.895	0.041	18.367	0.014	17.236	0.008	15.892	0.008
285	130.96059	-48.26624	—	16.245	0.005	15.266	0.004	14.043	0.008	13.362	0.006	12.691	0.008
286	131.00331	-48.13297	M6	—	—	—	—	20.115	0.07	18.556	0.015	16.694	0.012
287	131.03263	-48.02072	A7	12.221	0.068	11.957	0.011	11.767	0.01	11.588	0.02	11.422	0.015
288	131.04764	-48.17899	F8	13.829	0.007	13.513	0.005	12.882	0.008	12.496	0.009	12.129	0.014
289	131.05665	-48.32706	F9	13.575	0.006	13.326	0.005	12.721	0.01	12.37	0.013	11.995	0.018
290	131.09737	-48.25454	—	—	—	16.23	0.005	14.806	0.008	13.985	0.01	13.196	0.011
291	131.10527	-48.19339	M6	—	—	—	—	19.863	0.058	18.386	0.017	16.716	0.014
292	131.10828	-48.09993	G2	14.197	0.004	13.612	0.004	12.965	0.007	12.534	0.007	12.08	0.01
293	131.12079	-48.1723	—	18.009	0.021	16.724	0.009	15.258	0.007	14.316	0.007	13.428	0.009
294	131.12082	-48.17047	G2	13.893	0.006	13.239	0.006	12.394	0.007	11.917	0.006	11.488	0.01
295	131.1272	-48.2551	M0	—	—	17.817	0.008	16.232	0.012	15.208	0.01	14.072	0.012

<sup>a</sup>All spectral types in this table are estimated from photometry (see text for details)

Note. — 2MASS celestial coordinates are used except for ID 110 where IRAC coordinates are used.



Table 4. Infrared Photometry of Cluster Members

ID	J <sup>a</sup> (mag)	(err) (mag)	H <sup>a</sup> (mag)	(err) (mag)	K <sub>S</sub> <sup>a</sup> (mag)	(err) (mag)	[3.6] (mag)	(err) (mag)	(4.5) (mag)	(err) (mag)	[5.8] (mag)	(err) (mag)	[8.0] (mag)	(err) (mag)	[24] (mag)	(err) (mag)
1	10.931	0.024	10.887	0.021	10.87	0.021	–	–	10.86	0.004	–	–	10.729	0.012	–	–
2	10.861	0.023	10.837	0.024	10.81	0.019	–	–	–	–	–	–	–	–	–	–
3	11.812	0.027	11.466	0.024	11.414	0.023	–	–	–	–	–	–	–	–	–	–
4	15.07	0.049	14.308	0.048	13.813	0.052	13.351	0.01	13.175	0.012	13.09	0.043	12.38	0.044	–	–
5	13.304	0.024	12.776	0.029	12.592	0.026	–	–	12.601	0.009	–	–	12.491	0.044	–	–
6	14.965	0.049	14.301	0.058	13.969	0.067	–	–	–	–	–	–	–	–	9.231	0.016
7	13.679	0.027	12.978	0.022	12.699	0.026	12.695	0.007	12.656	0.009	12.624	0.03	12.603	0.053	–	–
8	10.593	0.023	10.506	0.021	10.459	0.023	10.495	0.003	10.448	0.004	10.395	0.008	10.396	0.009	10.245	0.029
9	13.849	0.029	13.102	0.035	12.878	0.037	12.67	0.007	12.609	0.009	12.528	0.028	12.541	0.052	–	–
10	15.044	0.049	14.323	0.048	14.011	0.064	–	–	–	–	–	–	–	–	–	–
11	15.015	0.043	14.279	0.042	14.016	0.056	14.047	0.014	13.749	0.015	13.968	0.106	13.545	0.139	–	–
12	14.182	0.033	13.534	0.035	13.328	0.043	13.286	0.012	13.151	0.011	13.071	0.045	13.252	0.076	–	–
13	11.946	0.026	11.429	0.022	11.33	0.024	11.398	0.004	11.404	0.005	11.346	0.013	11.23	0.017	–	–
14	9.275	0.027	9.211	0.022	9.202	0.021	9.224	0.002	9.344	0.003	9.238	0.005	9.182	0.005	8.028	0.034
15	11.024	0.023	10.849	0.021	10.828	0.021	10.802	0.003	10.965	0.005	10.778	0.01	10.745	0.012	10.591	0.043
16	11.296	0.026	11.248	0.022	11.209	0.023	–	–	11.2	0.005	11.181	0.014	11.275	0.02	–	–
17	14.98	0.039	14.367	0.028	14.04	0.063	13.995	0.022	13.831	0.021	13.683	0.09	13.545	0.113	–	–
18	13.088	0.026	12.393	0.025	12.287	0.026	–	–	–	–	–	–	–	–	–	–
19	12.628	0.028	12.053	0.024	11.966	0.026	11.933	0.005	11.897	0.006	11.854	0.018	11.878	0.032	–	–
20	15.044	0.049	14.375	0.042	14.187	0.075	13.95	0.012	13.924	0.02	13.834	0.074	13.878	0.158	–	–
21	13.856	0.026	13.11	0.027	12.782	0.032	–	–	–	–	–	–	–	–	9.731	0.022
22	15.244	0.071	14.686	0.119	14.407	0.082	–	–	14.141	0.019	–	–	14.022	0.169	–	–
23	7.21	0.021	7.281	0.044	7.326	0.027	7.575	0.002	7.485	0.003	7.488	0.002	7.45	0.002	7.42	0.01
24	15.355	0.044	14.818	0.051	14.511	0.103	–	–	14.008	0.018	–	–	13.976	0.13	–	–
25	14.845	0.032	14.226	0.051	13.963	0.06	13.485	0.011	13.303	0.015	13.018	0.049	12.547	0.053	9.752	0.022
26	14.55	0.043	13.831	0.038	13.584	0.05	13.486	0.011	13.453	0.016	13.315	0.06	13.448	0.091	–	–
27	14.054	0.024	13.342	0.028	13.088	0.033	12.878	0.008	12.83	0.01	12.779	0.043	12.749	0.058	–	–
28	14.785	0.036	14.094	0.042	13.854	0.057	13.557	0.011	13.498	0.012	13.386	0.058	13.317	0.096	–	–
29	15.125	0.04	14.47	0.053	14.071	0.062	13.906	0.012	13.824	0.018	13.546	0.061	13.014	0.068	9.141	0.013
30	14.212	0.032	13.501	0.033	13.291	0.038	13.131	0.009	13.042	0.011	12.956	0.04	13.162	0.092	–	–
31	14.71	0.038	13.928	0.039	13.663	0.049	–	–	13.505	0.014	–	–	13.59	0.102	–	–
32	12.753	0.022	12.224	0.028	12.092	0.023	12.061	0.005	12.016	0.006	12.095	0.023	11.87	0.029	–	–
33	15.72	0.06	15.026	0.065	14.689	0.103	14.543	0.017	14.408	0.025	14.522	0.13	14.419	0.285	–	–
34	14.443	0.026	13.699	0.028	13.543	0.039	13.706	0.011	13.566	0.015	13.302	0.053	13.144	0.07	–	–
35	15.011	0.045	14.341	0.056	14.085	0.062	–	–	13.928	0.018	–	–	13.643	0.1	–	–
36	12.122	0.027	11.795	0.031	11.769	0.033	11.734	0.005	11.689	0.006	11.631	0.021	11.547	0.027	9.862	0.024
37	14.158	0.032	13.413	0.029	13.261	0.042	–	–	12.94	0.01	–	–	12.711	0.066	–	–
38	14.52	0.029	13.722	0.021	13.524	0.041	13.528	0.01	13.445	0.013	13.382	0.047	13.214	0.09	–	–
39	11.282	0.026	11.188	0.022	11.157	0.023	11.131	0.004	11.169	0.005	11.18	0.014	11.205	0.026	–	–
40	15.255	0.054	14.482	0.063	14.218	0.065	13.833	0.013	14.113	0.024	13.971	0.085	14.518	0.293	–	–
41	11.677	0.023	11.498	0.022	11.396	0.023	11.398	0.004	11.503	0.005	11.261	0.015	11.304	0.019	–	–
42	14.542	0.033	13.819	0.037	13.587	0.046	13.564	0.01	13.549	0.015	13.619	0.07	13.37	0.096	–	–
43	13.355	0.032	12.693	0.029	12.5	0.029	12.503	0.008	12.457	0.011	12.322	0.029	12.347	0.056	–	–
44	14.125	0.029	13.374	0.021	13.137	0.033	12.877	0.008	12.958	0.01	12.781	0.039	12.859	0.057	11.165	0.072
45	12.879	0.024	12.552	0.023	12.468	0.029	12.45	0.008	12.418	0.01	12.364	0.029	12.393	0.057	–	–
46	14.37	0.035	13.624	0.029	13.336	0.04	13.365	0.009	13.333	0.014	13.088	0.05	13.378	0.084	–	–
47	15.038	0.05	14.379	0.067	14.083	0.062	13.795	0.017	13.768	0.023	13.564	0.073	13.653	0.12	–	–
48	13.813	0.043	13.109	0.051	12.835	0.038	12.621	0.008	12.541	0.01	12.412	0.032	12.568	0.057	–	–
49	14.406	0.044	13.557	0.038	13.292	0.039	13.112	0.009	13.179	0.014	12.961	0.052	12.926	0.07	–	–
50	14.587	0.028	13.846	0.029	13.65	0.051	13.519	0.011	13.388	0.013	13.372	0.057	13.712	0.127	–	–

Table 4—Continued

ID	J <sup>a</sup> (mag)	(err) (mag)	H <sup>a</sup> (mag)	(err) (mag)	K <sub>S</sub> <sup>a</sup> (mag)	(err) (mag)	[3.6] (mag)	(err) (mag)	[4.5] (mag)	(err) (mag)	[5.8] (mag)	(err) (mag)	[8.0] (mag)	(err) (mag)	[24] (mag)	(err) (mag)
51	13.8	0.029	13.132	0.035	12.967	0.034	12.892	0.007	13.014	0.011	12.99	0.046	12.935	0.067	—	—
52	14.339	0.032	13.671	0.025	13.36	0.044	13.262	0.021	13.254	0.022	13.338	0.064	13.085	0.062	—	—
53	14.735	0.032	14.049	0.036	13.864	0.058	13.57	0.013	13.59	0.016	13.447	0.077	13.645	0.136	—	—
54	14.374	0.029	13.68	0.031	13.42	0.043	13.176	0.01	13.254	0.013	13.107	0.055	13.04	0.075	—	—
55	15.066	0.043	14.281	0.046	14.106	0.064	13.899	0.012	13.889	0.02	13.792	0.083	13.91	0.136	—	—
56	14.47	0.06	13.783	0.041	13.502	0.041	13.383	0.015	13.39	0.017	13.209	0.047	13.24	0.082	—	—
57	12.954	0.022	12.439	0.022	12.382	0.029	12.395	0.006	12.425	0.008	12.389	0.03	12.366	0.044	—	—
58	14.326	0.03	13.679	0.038	13.392	0.035	13.274	0.009	13.167	0.014	13.163	0.049	13.011	0.058	—	—
59	14.72	0.026	14.017	0.039	13.792	0.047	13.628	0.012	13.609	0.014	13.554	0.065	13.726	0.101	—	—
60	10.805	0.023	10.686	0.023	10.661	0.023	10.774	0.003	10.721	0.004	10.588	0.009	10.618	0.013	—	—
61	15.123	0.037	14.555	0.039	14.123	0.066	14.088	0.083	14.068	0.055	14.128	0.164	13.764	0.189	—	—
62	13.762	0.022	12.991	0.027	12.853	0.03	12.615	0.007	12.606	0.01	12.506	0.033	12.633	0.054	—	—
63	11.645	0.022	11.32	0.023	11.221	0.021	11.412	0.004	11.203	0.004	11.215	0.013	11.181	0.016	10.753	0.048
64	14.846	0.041	14.064	0.045	13.733	0.049	13.639	0.024	13.557	0.033	13.534	0.087	13.843	0.142	—	—
65	14.269	0.032	13.588	0.036	13.329	0.037	13.104	0.008	13.264	0.013	12.996	0.042	13.116	0.064	—	—
66	14.448	0.037	13.762	0.04	13.523	0.041	13.213	0.01	13.32	0.013	13.034	0.054	13.324	0.1	—	—
67	11.408	0.023	11.04	0.023	10.971	0.023	10.986	0.003	10.989	0.004	10.852	0.011	10.893	0.016	10.785	0.066
68	15.449	0.047	14.725	0.06	14.465	0.084	14.32	0.016	14.21	0.023	14.177	0.097	13.95	0.104	—	—
69	14.664	0.044	13.949	0.058	13.744	0.05	13.464	0.012	13.367	0.015	13.256	0.071	13.387	0.116	—	—
70	13.094	0.022	12.46	0.025	12.328	0.026	12.242	0.006	12.223	0.008	12.12	0.029	12.022	0.033	—	—
71	13.365	0.023	12.714	0.022	12.478	0.026	12.326	0.006	12.334	0.009	12.204	0.028	12.129	0.046	10.713	0.047
72	14.599	0.03	13.926	0.027	13.669	0.047	13.471	0.01	13.454	0.013	13.399	0.061	13.348	0.084	—	—
73	15.161	0.049	14.422	0.052	14.111	0.062	13.971	0.014	13.931	0.022	13.839	0.102	13.564	0.116	—	—
74	—	—	—	—	10.989	0.019	10.983	0.021	11.035	0.02	10.914	0.067	10.865	0.039	—	—
75	14.921	0.046	14.214	0.055	13.991	0.059	13.721	0.012	13.677	0.017	13.574	0.059	13.591	0.105	—	—
76	14.101	0.026	13.388	0.025	13.198	0.035	12.901	0.009	12.85	0.011	12.82	0.048	12.694	0.068	—	—
77	11.28	0.023	11.171	0.023	11.065	0.023	11.072	0.006	11.075	0.005	11.085	0.014	10.992	0.033	—	—
78	13.076	0.024	12.511	0.031	12.324	0.03	12.243	0.006	12.287	0.008	12.145	0.026	12.176	0.033	—	—
79	13.413	0.036	12.696	0.036	12.483	0.03	12.381	0.011	12.357	0.013	12.286	0.032	12.341	0.052	—	—
80	15.618	0.075	15.055	0.12	14.473	0.09	14.063	0.015	13.784	0.018	13.361	0.058	12.884	0.057	9.728	0.024
81	14.604	0.045	13.897	0.06	13.767	0.058	13.474	0.019	13.438	0.019	13.397	0.075	13.548	0.126	—	—
82	15.348	0.058	14.787	0.065	14.412	0.092	—	—	—	—	—	—	—	—	—	—
83	11.973	0.023	11.808	0.025	11.742	0.024	11.694	0.005	11.663	0.006	11.604	0.022	11.359	0.022	10.503	0.047
84	14.199	0.029	13.494	0.038	13.269	0.03	13	0.009	12.963	0.013	12.986	0.042	12.919	0.07	—	—
85	13.978	0.026	13.278	0.038	13.015	0.044	12.992	0.014	12.805	0.013	12.957	0.081	13.079	0.105	—	—
86	14.118	0.024	13.406	0.027	13.298	0.036	13.025	0.011	13.057	0.015	12.911	0.064	13.047	0.09	—	—
87	14.918	0.036	14.268	0.051	13.929	0.061	13.891	0.013	13.647	0.017	13.81	0.086	13.626	0.102	—	—
88	12.826	0.024	12.224	0.025	12.101	0.029	12.066	0.005	12.015	0.007	11.939	0.02	11.978	0.036	—	—
89	13.902	0.027	13.357	0.032	13.188	0.038	13.051	0.01	13.096	0.013	13.027	0.042	13.025	0.067	—	—
90	14.286	0.024	13.481	0.022	13.356	0.044	13.233	0.009	13.139	0.011	13.146	0.039	13.115	0.067	—	—
91	14.668	0.036	13.973	0.044	13.815	0.048	13.514	0.013	13.426	0.015	13.583	0.086	13.521	0.116	—	—
92	10.961	0.023	10.938	0.029	10.867	0.027	10.89	0.004	10.869	0.005	10.789	0.016	10.892	0.022	10.666	0.057
93	14.519	0.074	13.8	0.148	13.543	0.086	13.265	0.015	13.37	0.022	13.182	0.057	13.2	0.086	—	—
94	14.39	0.05	13.782	0.057	13.367	0.045	13.041	0.008	13.107	0.012	12.994	0.049	13.036	0.07	—	—
95	12.827	0.024	12.142	0.026	11.948	0.024	11.883	0.005	11.957	0.006	11.861	0.02	11.795	0.032	—	—
96	9.734	0.022	9.767	0.024	9.723	0.019	9.915	0.003	9.731	0.003	9.732	0.006	9.772	0.006	9.317	0.018
97	13.614	0.023	12.871	0.022	12.705	0.026	12.588	0.009	12.615	0.012	12.528	0.052	12.377	0.064	—	—
98	14.661	0.042	13.889	0.032	13.697	0.041	13.642	0.012	13.478	0.014	13.38	0.058	13.473	0.101	—	—
99	15.134	0.047	14.363	0.058	14.119	0.064	13.925	0.013	13.93	0.019	13.852	0.069	13.956	0.165	—	—
100	15.078	0.044	14.285	0.052	14.085	0.066	13.829	0.012	13.771	0.017	13.614	0.077	13.582	0.114	—	—

Table 4—Continued

ID	J <sup>a</sup> (mag)	(err) (mag)	H <sup>a</sup> (mag)	(err) (mag)	K <sub>S</sub> <sup>a</sup> (mag)	(err) (mag)	[3.6] (mag)	(err) (mag)	[4.5] (mag)	(err) (mag)	[5.8] (mag)	(err) (mag)	[8.0] (mag)	(err) (mag)	[24] (mag)	(err) (mag)
101	12.989	0.023	12.396	0.023	12.287	0.032	12.166	0.005	12.245	0.007	12.149	0.025	12.103	0.03	–	–
102	14.594	0.035	13.919	0.035	13.579	0.046	13.317	0.009	13.073	0.011	12.858	0.04	12.362	0.045	10.235	0.038
103	14.099	0.028	13.409	0.027	13.263	0.043	13.185	0.011	13.214	0.014	13.252	0.062	13.173	0.082	–	–
104	12.911	0.03	12.309	0.032	12.162	0.031	12.061	0.006	12.092	0.007	12.021	0.024	12.039	0.047	–	–
105	13.361	0.023	12.699	0.031	12.48	0.033	12.509	0.007	12.451	0.008	12.351	0.025	12.418	0.042	–	–
106	14.21	0.036	13.562	0.038	13.271	0.035	13.086	0.009	12.99	0.011	12.959	0.051	12.904	0.06	–	–
107	10.232	0.022	10.311	0.026	10.295	0.019	10.366	0.002	10.363	0.003	10.34	0.008	10.311	0.008	9.409	0.03
108	12.842	0.027	12.16	0.026	12.013	0.024	11.92	0.005	11.988	0.006	11.87	0.02	11.918	0.041	–	–
109	15.523	0.051	14.859	0.063	14.539	0.084	14.21	0.014	13.888	0.018	13.612	0.079	12.874	0.059	9.663	0.019
110	15.903	0.077	15.253	0.113	14.728	0.123	14.544	0.02	14.193	0.023	13.746	0.082	13.207	0.066	10.559	0.043
111	14.777	0.047	14.018	0.069	13.757	0.057	13.614	0.012	13.576	0.019	13.779	0.11	13.614	0.131	–	–
112	15.099	0.045	14.47	0.055	14.074	0.074	13.907	0.013	13.752	0.017	13.601	0.066	13.639	0.126	–	–
113	14.59	0.036	13.832	0.026	13.658	0.047	13.499	0.012	13.492	0.017	13.331	0.061	13.15	0.068	–	–
114	11.388	0.027	11.284	0.022	11.232	0.021	11.334	0.004	11.241	0.004	11.312	0.014	11.21	0.018	–	–
115	15.001	0.042	14.233	0.047	14.026	0.062	13.797	0.012	13.702	0.016	13.693	0.068	13.727	0.106	–	–
116	15.079	0.033	14.473	0.049	14.202	0.065	13.952	0.015	13.964	0.02	13.566	0.102	13.611	0.13	–	–
117	14.075	0.027	13.349	0.038	13.013	0.033	12.916	0.009	12.85	0.011	12.817	0.046	12.96	0.077	–	–
118	15.776	0.072	15.117	0.077	14.651	0.101	14.534	0.021	14.37	0.023	13.878	0.084	14.508	0.198	–	–
119	13.69	0.026	13.052	0.032	12.802	0.037	12.576	0.007	12.644	0.009	12.35	0.029	12.44	0.057	–	–
120	14.857	0.042	14.126	0.054	13.85	0.066	13.547	0.014	–	–	13.348	0.07	13.556	0.19	–	–
121	8.21	0.019	8.167	0.024	8.189	0.024	8.331	0.002	–	–	8.178	0.003	8.186	0.003	8.213	0.01
122	11.912	0.03	11.625	0.028	11.567	0.026	11.726	0.005	11.589	0.006	11.586	0.017	11.552	0.032	10.681	0.055
123	15.715	0.068	14.787	0.077	14.661	0.117	14.172	0.015	14.189	0.022	14.175	0.122	13.705	0.128	–	–
124	11.667	0.026	11.449	0.031	11.387	0.024	11.428	0.004	11.361	0.005	11.377	0.014	11.299	0.021	8.852	0.013
125	15.305	0.048	14.724	0.081	14.335	0.088	14.145	0.017	14.152	0.024	14.032	0.103	13.962	0.195	–	–
126	14.751	0.032	13.957	0.046	13.696	0.05	13.599	0.013	13.547	0.015	13.538	0.07	13.417	0.094	–	–
127	14.552	0.03	13.849	0.026	13.586	0.041	13.408	0.01	13.38	0.013	13.222	0.061	13.432	0.087	–	–
128	14.733	0.029	14.088	0.038	13.696	0.04	13.548	0.01	13.546	0.014	13.602	0.066	13.581	0.123	–	–
129	13.551	0.032	12.837	0.028	12.648	0.031	12.507	0.006	12.527	0.008	12.467	0.032	12.389	0.06	–	–
130	14.556	0.033	13.885	0.04	13.652	0.052	13.15	0.009	12.884	0.01	12.532	0.025	11.996	0.036	9.366	0.016
131	10.21	0.026	10.067	0.021	10.03	0.021	10.062	0.002	10.073	0.003	10.108	0.008	10.036	0.008	10.336	0.046
132	12.451	0.022	11.732	0.022	11.543	0.023	11.553	0.005	11.395	0.005	11.323	0.014	11.276	0.022	–	–
133	15.817	0.111	14.981	0.125	14.588	0.116	14.467	0.024	14.246	0.033	14.127	0.125	13.158	0.082	–	–
134	14.138	0.029	13.486	0.037	13.216	0.037	12.963	0.008	12.92	0.01	12.79	0.044	12.862	0.051	–	–
135	12.619	0.026	11.967	0.021	11.779	0.019	11.594	0.005	11.606	0.005	11.574	0.018	11.565	0.029	–	–
136	15.222	0.043	14.49	0.059	14.244	0.069	14.126	0.016	13.877	0.017	13.974	0.097	13.962	0.115	–	–
137	12.255	0.026	11.881	0.022	11.834	0.024	11.892	0.006	11.781	0.006	11.684	0.023	11.785	0.032	–	–
138	11.016	0.027	10.98	0.021	10.964	0.021	10.897	0.004	10.787	0.004	10.459	0.009	9.906	0.007	6.88	0.007
139	9.268	0.024	9.172	0.025	9.123	0.021	9.146	0.002	9.299	0.003	9.12	0.004	9.18	0.006	9.105	0.014
140	15.224	0.048	14.634	0.049	14.375	0.083	13.757	0.015	13.42	0.015	13.165	0.051	12.558	0.054	9.91	0.025
141	14.166	0.038	13.439	0.032	13.199	0.044	13.031	0.01	12.979	0.011	12.928	0.042	13.06	0.084	–	–
142	11.117	0.026	10.946	0.024	10.901	0.023	10.93	0.004	10.945	0.004	10.877	0.011	10.767	0.011	8.393	0.009
143	5.812	0.018	5.899	0.024	5.915	0.02	6.118	0.002	6.155	0.003	6.197	0.002	6.085	0.001	6.07	0.007
144	13.633	0.047	13.052	0.055	12.799	0.04	12.646	0.007	12.75	0.01	12.574	0.027	12.758	0.064	–	–
145	14.369	0.026	13.651	0.028	13.412	0.043	13.354	0.009	13.342	0.013	13.073	0.045	13.057	0.071	–	–
146	14.536	0.03	13.856	0.026	13.601	0.041	13.387	0.011	13.232	0.014	13.148	0.046	12.914	0.082	–	–
147	15.677	0.057	15.035	0.063	14.713	0.105	14.294	0.016	14.082	0.021	13.743	0.072	13.038	0.084	10.055	0.03
148	10.505	0.022	10.432	0.021	10.418	0.019	10.451	0.003	10.439	0.004	10.383	0.008	10.403	0.01	10.122	0.027
149	14.624	0.035	13.913	0.043	13.767	0.05	13.387	0.011	13.281	0.013	13.313	0.064	12.797	0.077	–	–
150	13.849	0.027	13.104	0.03	12.868	0.031	12.824	0.007	12.84	0.009	12.76	0.04	12.744	0.071	–	–

Table 4—Continued

ID	J <sup>a</sup> (mag)	(err) (mag)	H <sup>a</sup> (mag)	(err) (mag)	K <sub>S</sub> <sup>a</sup> (mag)	(err) (mag)	[3.6] (mag)	(err) (mag)	([4.5] (mag)	(err) (mag)	[5.8] (mag)	(err) (mag)	[8.0] (mag)	(err) (mag)	[24] (mag)	(err) (mag)
151	11.686	0.027	11.216	0.022	11.074	0.019	11.077	0.004	11.073	0.004	11.028	0.011	11.01	0.017	10.304	0.036
152	11.821	0.021	11.21	0.024	11.037	0.019	10.934	0.003	10.934	0.004	10.871	0.012	10.846	0.012	—	—
153	15.157	0.045	14.459	0.051	14.202	0.07	14.06	0.015	14.02	0.02	13.8	0.09	13.64	0.128	—	—
154	14.586	0.027	13.799	0.026	13.646	0.038	13.372	0.014	13.278	0.014	13.267	0.086	13.352	0.079	—	—
155	15.237	0.034	14.58	0.063	14.155	0.068	13.946	0.016	13.873	0.019	13.172	0.158	13.818	0.155	—	—
156	13.824	0.028	13.104	0.022	12.873	0.031	12.733	0.008	12.621	0.009	12.571	0.031	12.581	0.05	—	—
157	15.365	0.039	14.729	0.058	14.554	0.044	14.155	0.017	14.176	0.021	14.231	0.117	13.874	0.108	—	—
158	14.482	0.03	13.639	0.04	13.416	0.044	13.29	0.009	13.222	0.013	13.075	0.05	12.908	0.08	—	—
159	15.68	0.057	14.869	0.079	14.689	0.106	14.43	0.018	14.167	0.024	14.051	0.102	13.217	0.084	10.32	0.031
160	14.052	0.022	13.364	0.021	13.107	0.031	12.833	0.01	12.823	0.011	12.799	0.041	12.758	0.065	—	—
161	14.006	0.034	13.217	0.035	13.031	0.04	13.015	0.009	12.973	0.01	12.782	0.043	12.798	0.1	—	—
162	13.514	0.022	12.856	0.022	12.692	0.019	12.588	0.015	12.495	0.017	12.503	0.097	12.521	0.074	—	—
163	13.694	0.06	12.952	0.065	12.727	0.047	12.707	0.007	12.7	0.009	12.715	0.034	12.473	0.043	—	—
164	14.898	0.041	14.202	0.046	14.191	0.096	13.661	0.011	13.602	0.015	13.507	0.061	12.997	0.06	9.964	0.025
165	15.331	0.044	14.72	0.076	14.388	0.094	14.254	0.016	14.119	0.018	14.049	0.108	13.922	0.121	—	—
166	—	—	—	—	14.557	0.1	14.139	0.018	13.954	0.023	13.708	0.087	12.93	0.073	9.646	0.021
167	14.477	0.034	13.722	0.073	13.428	0.057	13.261	0.01	13.248	0.015	13.085	0.05	13.158	0.137	—	—
168	14.42	0.032	13.583	0.032	13.431	0.04	13.341	0.012	13.264	0.015	13.216	0.048	13.259	0.113	—	—
169	15.287	0.048	14.639	0.067	14.263	0.078	14.062	0.016	13.97	0.018	13.8	0.077	13.93	0.214	—	—
170	14.237	0.03	13.471	0.036	13.31	0.039	13.045	0.009	13.148	0.013	13.075	0.046	13.02	0.099	—	—
171	11.685	0.026	11.617	0.034	11.539	0.029	11.509	0.005	11.484	0.005	11.508	0.015	11.541	0.017	—	—
172	14.511	0.049	13.692	0.057	13.468	0.052	13.373	0.016	13.2	0.02	13.3	0.062	13.18	0.108	—	—
173	15.351	0.045	14.751	0.062	14.438	0.086	14.027	0.014	13.805	0.017	13.403	0.061	12.944	0.097	10.122	0.033
174	14.422	0.039	13.696	0.043	13.49	0.044	13.276	0.019	13.274	0.018	13.376	0.082	13.203	0.147	—	—
175	11.192	0.024	10.632	0.022	10.492	0.021	10.566	0.004	10.542	0.004	10.48	0.009	10.442	0.014	10.877	0.059
176	15.168	0.057	14.545	0.074	14.331	0.09	14.322	0.018	14.001	0.019	13.805	0.103	13.876	0.142	—	—
177	—	—	14.819	0.088	14.517	0.12	—	—	—	—	—	—	13.658	0.102	—	—
178	12.814	0.026	12.178	0.024	12.027	0.021	12.073	0.005	12.1	0.007	11.907	0.021	11.884	0.041	—	—
179	15.163	0.045	14.327	0.049	14.045	0.062	13.756	0.016	13.756	0.018	13.887	0.117	13.749	0.204	—	—
180	11.977	0.023	11.727	0.021	11.617	0.019	11.578	0.004	11.655	0.005	11.562	0.016	11.567	0.021	—	—
181	15.354	0.044	14.743	0.06	14.41	0.09	14.128	0.014	14.158	0.022	14.32	0.12	14.265	0.204	—	—
182	14.313	0.039	13.687	0.049	13.404	0.041	13.151	0.009	13.023	0.012	12.985	0.045	13.013	0.069	—	—
183	13.762	0.032	13.019	0.035	12.693	0.033	12.485	0.009	12.443	0.009	12.337	0.03	12.454	0.071	—	—
184	14.874	0.033	14.07	0.053	13.791	0.052	13.58	0.012	13.732	0.017	13.603	0.098	13.376	0.318	—	—
185	13.87	0.026	13.158	0.022	12.865	0.023	12.823	0.007	12.819	0.009	12.824	0.047	12.589	0.048	—	—
186	14.493	0.029	13.773	0.042	13.572	0.049	13.311	0.012	13.358	0.016	13.218	0.065	13.401	0.117	—	—
187	15.182	0.081	14.465	0.085	14.384	0.094	—	—	—	—	—	—	—	—	—	—
188	11.387	0.027	11.278	0.024	11.209	0.021	11.319	0.005	11.334	0.005	11.264	0.014	11.335	0.023	10.57	0.057
189	15.083	0.037	14.242	0.049	13.875	0.06	13.431	0.01	13.211	0.012	12.894	0.041	12.514	0.059	10.088	0.031
190	15.345	0.044	14.627	0.063	14.363	0.07	14.123	0.016	13.988	0.021	13.848	0.103	14.156	0.294	—	—
191	10.89	0.026	10.675	0.024	10.611	0.023	10.605	0.006	10.65	0.005	10.556	0.011	10.603	0.02	10.269	0.034
192	12.388	0.024	11.916	0.027	11.775	0.024	11.756	0.006	11.752	0.006	11.743	0.022	11.65	0.036	—	—
193	10.743	0.026	10.766	0.022	10.742	0.025	10.752	0.004	10.807	0.005	10.759	0.01	10.641	0.012	9.702	0.022
194	14.587	0.04	13.882	0.044	13.662	0.053	13.485	0.013	13.434	0.013	13.41	0.063	13.344	0.079	—	—
195	8.886	0.021	8.938	0.022	8.963	0.021	9.083	0.002	9.012	0.003	9.072	0.004	9.031	0.004	8.803	0.025
196	12.218	0.026	11.696	0.022	11.601	0.023	11.645	0.005	11.626	0.006	11.591	0.015	11.688	0.042	—	—
197	13.126	0.03	12.441	0.026	12.297	0.024	12.241	0.007	12.168	0.008	12.157	0.027	12.205	0.055	—	—
198	10.469	0.026	10.406	0.024	10.368	0.019	10.471	0.004	10.545	0.004	10.413	0.009	10.314	0.011	8.292	0.01
199	13.53	0.026	12.779	0.022	12.609	0.027	12.513	0.006	12.518	0.008	12.382	0.029	12.444	0.044	—	—
200	11.224	0.024	11.159	0.021	11.132	0.021	11.165	0.004	11.148	0.005	11.125	0.012	11.142	0.039	9.63	0.022

Table 4—Continued

ID	J <sup>a</sup> (mag)	(err) (mag)	H <sup>a</sup> (mag)	(err) (mag)	K <sub>S</sub> <sup>a</sup> (mag)	(err) (mag)	[3.6] (mag)	(err) (mag)	([4.5] (mag)	(err) (mag)	[5.8] (mag)	(err) (mag)	[8.0] (mag)	(err) (mag)	[24] (mag)	(err) (mag)
201	13.745	0.026	13.001	0.022	12.817	0.029	12.662	0.007	12.661	0.009	12.503	0.033	12.448	0.094	—	—
202	14.903	0.035	14.239	0.032	14.005	0.05	13.727	0.011	13.667	0.015	13.54	0.068	13.426	0.08	—	—
203	14.012	0.029	13.255	0.03	13.012	0.03	12.821	0.007	12.807	0.01	12.772	0.034	12.72	0.055	—	—
204	14.458	0.033	13.593	0.032	13.49	0.047	13.683	0.016	13.289	0.015	13.158	0.055	12.892	0.095	—	—
205	14.88	0.037	14.085	0.047	13.829	0.049	13.668	0.011	13.611	0.015	13.487	0.07	13.308	0.095	—	—
206	14.655	0.057	13.958	0.085	13.673	0.051	13.555	0.011	13.502	0.014	13.582	0.086	13.33	0.117	—	—
207	10.597	0.032	10.373	0.022	10.296	0.021	10.297	0.003	10.316	0.003	10.292	0.008	10.231	0.009	10.159	0.029
208	15.22	0.045	14.363	0.055	14.341	0.075	14.04	0.015	13.967	0.02	14.092	0.099	13.821	0.136	—	—
209	11.179	0.024	11.093	0.021	11.079	0.023	11.097	0.004	11.031	0.004	11.053	0.012	11.141	0.036	—	—
210	12.608	0.024	12.15	0.021	11.993	0.019	11.861	0.005	11.843	0.006	11.847	0.019	11.748	0.03	—	—
211	14.951	0.047	14.231	0.044	14.054	0.062	13.723	0.012	13.656	0.015	13.641	0.073	13.472	0.093	—	—
212	11.532	0.029	11.25	0.029	11.139	0.027	11.247	0.004	11.282	0.005	11.072	0.014	11.038	0.016	—	—
213	14.421	0.035	13.689	0.042	13.207	0.039	12.722	0.008	12.339	0.008	12.049	0.024	11.208	0.026	8.309	0.01
214	14.435	0.035	13.708	0.034	13.426	0.041	13.32	0.011	13.302	0.013	13.159	0.059	13.082	0.172	—	—
215	13.563	0.075	12.865	0.062	12.626	0.04	12.473	0.017	12.511	0.016	12.454	0.049	11.899	0.045	6.61	0.008
216	15.223	0.046	14.486	0.065	14.411	0.079	14.075	0.015	13.927	0.02	14.045	0.126	13.789	0.185	—	—
217	14.666	0.036	13.936	0.03	13.75	0.047	13.469	0.013	13.457	0.016	13.424	0.085	13.479	0.304	—	—
218	13.129	0.024	12.429	0.021	12.224	0.026	12.359	0.006	12.101	0.007	12.07	0.025	12.077	0.051	—	—
219	14.651	0.039	13.955	0.049	13.739	0.051	13.368	0.01	13.264	0.013	13.082	0.054	12.482	0.079	10.255	0.035
220	11.577	0.023	11.328	0.022	11.292	0.023	11.219	0.004	11.27	0.005	11.263	0.019	11.234	0.054	—	—
221	9.327	0.032	9.327	0.038	9.353	0.024	9.45	0.004	9.467	0.003	9.504	0.005	9.413	0.018	9.65	0.026
222	9.767	0.024	9.754	0.022	9.759	0.021	9.871	0.003	9.876	0.003	9.781	0.006	9.879	0.017	—	—
223	14.042	0.039	13.345	0.044	13.147	0.039	13.002	0.009	12.944	0.011	12.803	0.063	12.593	0.076	—	—
224	14.827	0.036	14.096	0.045	13.848	0.062	13.751	0.012	13.743	0.017	13.824	0.085	14.061	0.173	—	—
225	14.265	0.026	13.597	0.03	13.344	0.038	13.064	0.009	13.003	0.012	12.935	0.051	12.874	0.142	—	—
226	13.758	0.029	13.058	0.022	12.855	0.037	12.598	0.007	12.629	0.01	12.582	0.043	12.652	0.13	—	—
227	14.008	0.035	13.24	0.03	13.02	0.04	12.969	0.008	12.846	0.01	12.726	0.045	13.119	0.133	—	—
228	8.524	0.019	8.491	0.036	8.458	0.021	8.538	0.002	8.542	0.002	8.523	0.004	8.507	0.003	8.495	0.014
229	14.344	0.032	13.596	0.037	13.376	0.038	13.177	0.011	13.163	0.012	13.125	0.066	13.558	0.138	—	—
230	14.408	0.026	13.719	0.043	13.459	0.04	13.161	0.01	12.907	0.01	12.568	0.045	12.001	0.095	9.328	0.02
231	14.927	0.024	14.345	0.044	14.056	0.062	13.852	0.013	13.836	0.016	13.619	0.068	13.81	0.128	—	—
232	13.108	0.023	12.469	0.022	12.27	0.024	12.445	0.006	12.142	0.007	12.057	0.027	11.94	0.065	—	—
233	13.802	0.028	13.115	0.034	12.836	0.031	12.622	0.007	12.702	0.009	12.59	0.043	12.577	0.127	—	—
234	14.893	0.043	14.204	0.053	13.92	0.064	13.744	0.011	13.86	0.019	13.703	0.071	13.691	0.11	—	—
235	14.554	0.032	13.843	0.037	13.618	0.045	13.495	0.013	13.452	0.015	13.665	0.091	14.243	0.511	—	—
236	14.423	0.046	13.714	0.053	13.522	0.083	13.213	0.009	13.089	0.016	13.128	0.083	13.28	0.192	—	—
237	15.196	0.047	14.567	0.045	14.17	0.06	14.1	0.013	13.952	0.018	13.876	0.084	13.936	0.159	—	—
238	14.997	0.043	14.286	0.038	14.108	0.071	13.867	0.014	13.778	0.018	13.665	0.088	13.714	0.41	—	—
239	14.88	0.04	14.242	0.045	13.98	0.069	13.796	0.013	13.701	0.015	13.848	0.083	13.501	0.087	—	—
240	14.333	0.023	13.532	0.035	13.169	0.041	12.624	0.011	12.319	0.009	11.926	0.023	11.283	0.036	8.859	0.014
241	14.306	0.03	13.733	0.037	13.466	0.045	13.42	0.01	13.307	0.013	13.233	0.058	13.372	0.096	—	—
242	10.208	0.023	10.174	0.022	10.139	0.019	10.144	0.003	10.218	0.004	10.19	0.008	10.191	0.015	9.852	0.024
243	14.759	0.032	14.082	0.037	13.771	0.058	13.617	0.011	13.532	0.015	13.604	0.082	13.608	0.205	—	—
244	13.895	0.03	13.103	0.022	12.966	0.038	12.863	0.008	12.879	0.012	12.879	0.039	12.793	0.069	—	—
245	14.955	0.052	14.172	0.081	13.96	0.06	13.371	0.01	13.136	0.012	12.879	0.039	12.406	0.046	9.742	0.022
246	14.204	0.023	13.534	0.022	13.297	0.033	13.082	0.009	13.05	0.012	12.962	0.044	13.093	0.138	—	—
247	14.674	0.035	13.932	0.054	13.659	0.043	13.46	0.011	13.463	0.017	13.31	0.061	12.95	0.104	—	—
248	14.88	0.053	14.26	0.082	14.006	0.072	13.756	0.019	13.786	0.019	13.671	0.138	13.631	0.371	—	—
249	14.819	0.029	14.088	0.021	13.818	0.058	13.672	0.011	13.561	0.015	13.479	0.063	13.305	0.12	—	—
250	15.238	0.043	14.501	0.056	14.303	0.073	13.988	0.016	13.994	0.022	14.073	0.093	13.746	0.154	—	—

Table 4—Continued

ID	J <sup>a</sup> (mag)	(err) (mag)	H <sup>a</sup> (mag)	(err) (mag)	K <sub>S</sub> <sup>a</sup> (mag)	(err) (mag)	[3.6] (mag)	(err) (mag)	([4.5] (mag)	(err) (mag)	[5.8] (mag)	(err) (mag)	[8.0] (mag)	(err) (mag)	[24] (mag)	(err) (mag)
251	–	–	–	–	13.014	0.051	12.516	0.01	12.561	0.013	–	–	11.937	0.027	–	–
252	14.914	0.037	14.379	0.063	13.999	0.063	13.687	0.017	13.525	0.023	13.482	0.065	12.998	0.062	–	–
253	10.726	0.024	10.503	0.026	10.408	0.019	10.376	0.003	10.414	0.004	10.347	0.009	12.046	0.021	9.498	0.023
254	14.059	0.028	13.513	0.026	13.265	0.039	12.939	0.01	12.794	0.011	12.769	0.047	12.462	0.141	–	–
255	12.724	0.022	12.357	0.024	12.238	0.024	12.191	0.005	12.258	0.007	12.172	0.023	12.24	0.048	–	–
256	14.991	0.044	14.351	0.07	14.065	0.071	13.824	0.012	13.593	0.016	13.391	0.069	12.616	0.05	9.498	0.047
257	15.567	0.059	14.905	0.085	14.691	0.102	14.047	0.017	13.663	0.02	13.382	0.07	13.012	0.095	10.964	0.068
258	15.351	0.059	14.647	0.059	14.577	0.096	14.102	0.017	13.98	0.019	14.195	0.138	13.77	0.181	–	–
259	14.346	0.024	13.706	0.029	13.37	0.043	13.272	0.009	13.159	0.011	13.169	0.051	12.93	0.076	–	–
260	14.548	0.023	13.799	0.032	13.661	0.061	13.458	0.011	13.423	0.014	13.346	0.073	13.55	0.206	–	–
261	14.231	0.041	13.542	0.04	13.43	0.053	13.249	0.011	13.137	0.015	13.057	0.062	13.001	0.127	–	–
262	12.564	0.049	12.12	0.049	11.987	0.036	12.018	0.008	11.862	0.007	–	–	–	–	–	–
263	10.163	0.03	10.142	0.031	10.109	0.026	10.188	0.003	10.135	0.003	10.19	0.008	10.132	0.008	10.163	0.03
264	14.361	0.034	13.646	0.041	13.402	0.041	13.21	0.009	13.3	0.013	13.099	0.044	13.151	0.076	–	–
265	14.923	0.04	14.192	0.044	13.984	0.059	13.683	0.011	13.655	0.014	13.535	0.071	13.759	0.135	–	–
266	15.422	0.051	14.789	0.072	14.48	0.089	14.243	0.017	14.204	0.022	14.206	0.103	14.261	0.202	–	–
267	14.356	0.028	13.619	0.046	13.47	0.047	13.235	0.011	13.309	0.016	13.207	0.062	13.41	0.162	–	–
268	11.825	0.024	11.349	0.022	11.356	0.021	11.313	0.004	11.338	0.005	11.247	0.016	11.259	0.018	–	–
269	14.822	0.024	14.162	0.043	13.905	0.064	13.802	0.012	13.579	0.015	13.77	0.072	13.534	0.116	–	–
270	15.446	0.054	14.859	0.073	14.649	0.106	14.203	0.019	14.178	0.023	13.977	0.105	14.617	0.936	–	–
271	12.761	0.024	12.261	0.022	12.15	0.019	12.238	0.006	12.156	0.007	12.085	0.021	11.998	0.041	–	–
272	13.254	0.023	12.602	0.022	12.483	0.026	12.549	0.008	12.475	0.008	12.506	0.036	12.433	0.042	–	–
273	14.488	0.037	13.779	0.045	13.524	0.044	13.365	0.011	13.391	0.015	13.483	0.064	13.216	0.09	–	–
274	12.935	0.036	12.293	0.039	12.154	0.033	12.069	0.006	12.114	0.007	12.095	0.026	12.041	0.044	–	–
275	10.424	0.023	10.251	0.025	10.159	0.019	10.16	0.002	10.193	0.003	10.284	0.008	10.041	0.007	10.029	0.027
276	12.671	0.026	12.021	0.025	11.842	0.023	11.753	0.004	11.904	0.007	11.704	0.018	11.652	0.038	–	–
277	10.623	0.023	10.576	0.025	10.532	0.021	10.487	0.003	10.433	0.004	10.425	0.009	10.425	0.011	10.04	0.027
278	13.715	0.048	13.149	0.031	12.84	0.045	12.65	0.009	12.647	0.011	12.548	0.035	12.573	0.061	–	–
279	15.436	0.059	14.85	0.078	14.611	0.097	14.267	0.027	14.258	0.034	14.093	0.103	13.885	0.162	–	–
280	14.118	0.026	13.502	0.031	13.261	0.041	13.104	0.009	13.078	0.012	12.941	0.04	12.827	0.065	–	–
281	12.744	0.026	12.147	0.023	12.004	0.023	12.075	0.005	11.933	0.006	11.894	0.021	11.857	0.027	9.637	0.019
282	14.569	0.032	13.752	0.027	13.606	0.039	13.436	0.01	13.368	0.012	13.387	0.064	13.42	0.128	–	–
283	11.79	0.026	11.59	0.022	11.49	0.023	11.66	0.005	11.508	0.005	11.529	0.016	11.426	0.019	9.515	0.019
284	14.345	0.024	13.66	0.033	13.334	0.035	13.311	0.009	13.329	0.013	13.083	0.042	13.132	0.056	–	–
285	11.8	0.024	11.174	0.023	11.005	0.021	10.986	0.004	11.341	0.005	10.95	0.011	10.897	0.012	11.094	0.069
286	15.025	0.034	14.387	0.056	14.175	0.069	13.762	0.012	13.665	0.015	13.407	0.054	13.592	0.105	–	–
287	11.105	0.022	11.085	0.023	11.013	0.021	11.048	0.004	11.026	0.004	11.028	0.011	10.987	0.018	10.747	0.054
288	11.855	0.028	11.56	0.027	11.445	0.029	11.532	0.005	11.463	0.006	11.378	0.016	11.453	0.026	–	–
289	11.589	0.024	11.349	0.022	11.245	0.023	11.251	0.004	11.196	0.005	11.36	0.014	11.248	0.019	–	–
290	12.194	0.024	11.557	0.022	11.365	0.019	11.275	0.004	11.31	0.005	11.238	0.013	11.209	0.022	–	–
291	15.263	0.05	14.575	0.067	14.348	0.086	14.042	0.016	14.024	0.022	13.97	0.072	13.91	0.149	–	–
292	11.637	0.023	11.328	0.021	11.264	0.019	11.237	0.004	11.236	0.005	11.125	0.013	11.184	0.022	–	–
293	12.672	0.024	12.023	0.025	11.851	0.027	11.745	0.006	11.72	0.007	11.687	0.017	11.645	0.03	–	–
294	11.135	0.03	10.771	0.039	10.697	0.03	10.671	0.004	10.76	0.005	10.713	0.011	10.643	0.015	10.745	0.058
295	13.13	0.024	12.528	0.027	12.3	0.024	12.134	0.005	12.083	0.006	12.027	0.022	12.048	0.027	–	–

<sup>a</sup>JHK photometry from 2MASS



Table 5. Disk Candidates in IC 2395

ID	SpT	[3.6]-[5.8] (mag)	err (mag)	[4.5]-[8] (mag)	err (mag)	[8]-[24] (mag)	err (mag)	Disk Type
14	–	-0.014	0.005	0.162	0.006	1.154	0.034	D?
25	M6	0.467	0.050	0.756	0.055	2.795	0.057	II
29	M6	0.36	0.062	0.81	0.070	3.873	0.069	T
36	F9	0.103	0.022	0.142	0.028	1.685	0.036	D?
41	F5	0.137	0.016	0.199	0.020	0.829	0.042	D
44	–	0.096	0.040	0.099	0.058	1.694	0.092	WT
63	G2	0.197	0.014	0.022	0.016	0.428	0.051	D
71	–	0.122	0.029	0.205	0.047	1.416	0.066	D?
80	–	0.702	0.060	0.9	0.060	3.156	0.062	II
83	F6	0.09	0.023	0.304	0.023	0.856	0.052	D
96	B9/A0V	0.183	0.007	-0.041	0.007	0.455	0.019	D
102	M6	0.459	0.041	0.711	0.046	2.127	0.059	II
107	B9V	0.026	0.008	0.052	0.009	0.902	0.031	D
109	–	0.598	0.080	1.014	0.062	3.211	0.062	II
110	–	0.798	0.084	0.986	0.070	2.648	0.079	II
122	F7	0.14	0.018	0.037	0.033	0.871	0.064	D
124	F3	0.051	0.015	0.062	0.022	2.447	0.025	D
130	–	0.618	0.027	0.888	0.037	2.63	0.039	II
133	–	0.34	0.127	1.088	0.088	3.167	0.086	T
138	B9	0.438	0.010	0.881	0.008	3.026	0.010	II
140	–	0.592	0.053	0.862	0.056	2.648	0.060	II
142	A5	0.053	0.012	0.178	0.012	2.374	0.014	D
147	–	0.551	0.074	1.044	0.087	2.983	0.089	II
148	B9V	0.068	0.009	0.036	0.011	0.281	0.029	D
151	–	0.049	0.012	0.063	0.017	0.706	0.040	D?
159	–	0.379	0.104	0.95	0.087	2.897	0.090	T
164	M6	0.154	0.062	0.605	0.062	3.033	0.065	T
166	–	0.431	0.089	1.024	0.077	3.284	0.076	II
173	–	0.624	0.063	0.861	0.098	2.822	0.102	II
188	A4	0.055	0.015	-0.001	0.024	0.765	0.061	D
189	–	0.537	0.042	0.697	0.060	2.426	0.067	II
191	F1	0.049	0.013	0.047	0.021	0.334	0.039	D
193	B8	-0.007	0.011	0.166	0.013	0.939	0.025	D
195	B3IV-V	0.011	0.004	-0.019	0.005	0.228	0.025	D?
198	B8	0.058	0.010	0.231	0.012	2.022	0.015	D
200	A0	0.04	0.013	0.006	0.039	1.512	0.045	D
213	–	0.673	0.025	1.131	0.027	2.899	0.028	II
215	–	0.019	0.052	0.612	0.048	5.289	0.046	T
219	M6	0.286	0.055	0.782	0.080	2.227	0.086	WT
230	M6	0.593	0.046	0.906	0.096	2.673	0.097	II
240	–	0.698	0.025	1.036	0.037	2.424	0.039	II
242	B7V	-0.046	0.009	0.027	0.016	0.339	0.028	D
245	–	0.492	0.040	0.73	0.048	2.664	0.051	II
253	F4	0.029	0.009	0.168	0.021	0.748	0.031	D
256	M6	0.433	0.070	0.977	0.052	3.118	0.069	II
257	–	0.665	0.072	0.651	0.097	2.048	0.117	II
277	A1	0.062	0.009	0.008	0.012	0.385	0.029	D
281	K4	0.181	0.022	0.076	0.028	2.22	0.033	WT
283	F3	0.131	0.017	0.082	0.020	1.911	0.027	D

Table 6. Proportion of Transitional Disk Candidates Among Known Members of Clusters and Associations

Cluster or Association (1)	Revised Age (Myr) (2)	Ref. age (3)	Trad. Age (Myr) (4)	Ref. age (5)	Ref. Mship (6)	Trans./Total [8]-[24]>1.5 (7)	% (8)	Trans./Total [8]-[24]>2.5 (9)	% (10)	Trans./Total [8]-[24]>3.5 (11)	% (12)	Ref. photometry
Coronet	-	-	0.5 - 1	15	15	3/13	14 ± 10	2/8	25 ± 18	1/2	50 ± ...	15
$\rho$ Oph	0.5 - 3	1	1 - 2	16	35	2/123	1.6 ± 1.2	2/90	2.2 ± 1.6	0/24	0 ± ...	47
NGC 2068/70	-	-	~ 2	17	17	7/51	14 ± 5	7/40	17 ± 7	5/7	71 ± 32	17
NGC 2244	~ 2	2	~ 2	18	36	15/95	16 ± 4	13/78	17 ± 5	7/31	23 ± 9	48
Serpens	0.5 - 3	3	1 - 3	19	37	6/79	7.6 ± 3.1	3/67	4.5 ± 2.6	2/28	7 ± ...	49
Taurus	3 - 4	4	1.5	20	38	10/152	6.6 ± 2.1	8/129	6.2 ± 2.2	6/54	11 ± 5	38
NGC 1333	~ 6	5	1	20, 21	39	2/44	4.5 ± 3.2	1/31	3.2 ± ...	1/9	11 ± ...	47
Chameleon I	~ 6	6	2.6	23	40	4/27	15 ± 8	3/20	15 ± 9	2/5	40 ± ...	23
IC 348	~ 6	2	2.5	22	41	11/65	17 ± 5	8/47	17 ± 6	7/30	23 ± 9	50
$\sigma$ Ori	~ 6	2	~ 3	24	24	2/6	33 ± ...	2/4	50 ± ...	1/1	100 ± ...	24
Totals	-	-	-	-	-	62/653	9.5 ± 1.2	49/514	9.5 ± 1.4	32/191	17 ± 3	-
<b>Dist &lt; 1kpc</b>	-	-	-	-	-	<b>47/560</b>	<b>8.4 ± 1.3</b>	<b>36/436</b>	<b>8.3 ± 1.4</b>	<b>25/160</b>	<b>16 ± 3</b>	-
IR Members	-	-	-	-	-	112/1473	7.6 ± 0.7	83/1163	7.1 ± 0.8	54/470	11.5 ± 1.6	-
IC 2395	9	7	6	25	7	8/26	31 ± 11	5/19	26 ± 12	2/2	100 ± ...	7
Ori OB1b	~ 9	10	4 - 6	27	27	5/14	36 ± 16	3/11	27 ± 16	1/2	50 ± ...	27
TW Hya	10	8, 9	8	26	42	6/10	60 ± 25	6/10	60 ± 25	3/3	100 ± 60	51
Upper Sco	11	11	5	28	43	51/103	50 ± 7	42/90	47 ± 7	26/45	57 ± 11	52
$\epsilon$ Cha	~ 11	12	~ 6	49	49	4/9	44 ± 22	3/7	43 ± 25	2/5	40 ± 28	51
$\eta$ Cha	11	8	~ 6	31	44	1/6	17 ± ...	1/6	17 ± ...	1/1	100 ± ...	31
NGC 2362	12	2	5	32	45	8/18	44 ± 16	8/14	57 ± 20	2/3	67 ± 47	42
$\gamma$ Vel	~ 12	13	~ 5	33	33	7/16	44 ± 17	3/7	43 ± 25	1/1	100 ± ...	33
Totals	-	-	-	-	-	90/202	45 ± 5	71/164	43 ± 5	38/62	61 ± 10	-
<b>Dist &lt; 1kpc</b>	-	-	-	-	-	<b>81/178</b>	<b>46 ± 5</b>	<b>62/144</b>	<b>43 ± 6</b>	<b>35/58</b>	<b>60 ± 10</b>	-
Ori OB1a	~ 15	14	7 - 10	27	27	1/3	33 ± ...	1/2	50 ± ...	1/1	100 ± ...	27
LCC/UCL	16 - 17	11	16	34	46	3/4	75 ± 43	1/2	50 ± ...	0/1	0	51
Totals	-	-	-	-	-	4/7	57 ± 29	2/4	50 ± 35	1/2	50 ± ...	-

Column (1): Cluster designation; Column (2): Adopted age; Column (3): Reference(s) for age (1 - Erickson et al. (2011) and Takagi et al. (2015), 2 - Bell et al. (2013), 3 - Erickson et al. (2015) find an age similar to that of  $\rho$  Oph, with both estimates using the same technique, 4 - Rees et al. (2016), 5 - Luhman et al. (2016) show age is similar to or younger than that of IC 348, which has an age from Bell et al. (2013), 6 - Luhman et al. (2008) and discussion therein shows the age is similar to that of IC 348, which has an age from Bell et al. (2013), 7 - this work, 8 - Bell et al. (2015), 9 - Weinberger et al. (2013); the estimate by Herczeg & Hillenbrand (2015) is consistent but slightly younger, 10 - see text, 11 - Pecaut et al. (2012), 12 - Luhman (2004) finds the age to be similar to that of  $\eta$  Cha, which is estimated at 11 Myr by Bell et al. (2015), 13 - Jeffries et al. (2014); Hernández et al. (2008) also show this association to be similar in age to NGC 2362 and Orion OB1b, 14 - the lack of stars earlier than B1 (E. E. Mamajek, private communication) indicates  $\sim 15$  Myr, and the placement of the sub-association 25 Ori on the HR diagram showing it to be significantly older than Ori OB1b (Briceño et al. 2007) - see also Wolk (1996), 15 - Sicilia-Aguilar et al. (2008, 2011), 16 - Wilking et al. (2005), 17 - Flaherty & Muzerolle (2008), 18 - Park & Sung (2002), 19 - Winston et al. (2009); Gorlova et al. (2010), 20 - Barrado y Navascués & Martin (2003), 21 - Luhman et al. (2003, 2016); Lada et al. (2006), 22 - Gutermuth et al. (2008); Winston et al. (2009), 23 - Luhman (2004); Luhman et al. (2008), 24 - Hernández et al. (2007a), 25 - Claria et al. (2003), 26 - Barrado y Navascués & Martin (2003), 27 - Briceño et al. (2005); Hernández et al. (2007b), 28 - Carpenter et al. (2006), 29 - Murphy et al. (2013), 30 - Luhman (2004), 31 - Luhman (2004); Megeath et al. (2005), 32 - Dahm & Hillenbrand (2007), 33 - Hernández et al. (2008), 34 - Mamajek et al. (2002); Column (4): Reference(s) for membership (35 - Gagné et al. (2004); Wilking et al. (2005); Ozawa et al. (2005); Barsony et al. (2012), 36 - Chen et al. (2007); Wang et al. (2008), 37 - Giardino et al. (2007); Winston et al. (2009); Erickson et al. (2015), 38 - Luhman et al. (2010), 39 - Getman et al. (2002); Winston et al. (2009), 40 - Luhman (2007); López Martí et al. (2013), 41 - Luhman et al. (2003, 2005); Stelzer et al. (2012), 42 - Schneider et al. (2015), 43 - Luhman & Mamajek (2012); Rizzuto et al. (2015), 44 - Megeath et al. (2005) and Gautier et al. (2008), 45 - (Currie et al. 2009), 46 - Pecaut et al. (2012); Song et al. (2012) Column (5) Number of transition disks over total of 24  $\mu$  bright disks; Column (6) Percentage of transitional disks with nominal errors; Columns (7 - 10): Same for increasing excess thresholds; Column (11): Reference(s) for photometry (47 - Evans et al. (2009), 48 - (Balog et al. 2007), 49 - Harvey et al. (2007), 50 - Getman et al. (2002); Winston et al. (2009), 51 - WISE, 52 - Luhman & Mamajek (2012) plus WISE, )

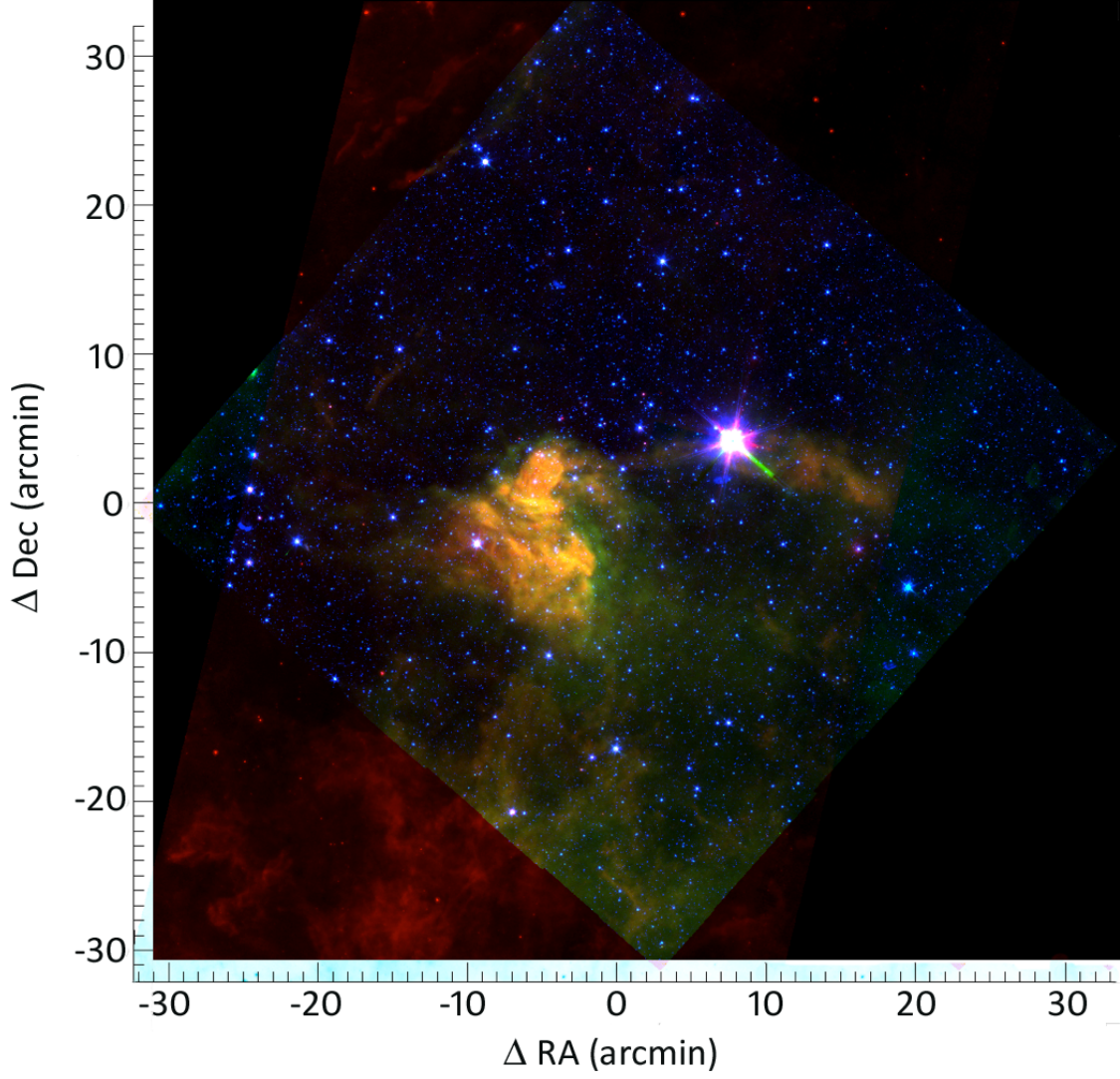


Fig. 1.— IC 2395 three color composite image composed of IRAC wavelengths  $3.6\,\mu\text{m}$  (blue) and  $8.0\,\mu\text{m}$  (green) and MIPS  $24\,\mu\text{m}$  (red). The coordinates are relative to  $\text{RA} = 130.6111$ ,  $\text{DEC} = -48.1690$ . Likely contributors to the emission in the  $8.0\,\mu\text{m}$  channel are silicate grains and aromatic molecules, seen as the bright green areas.

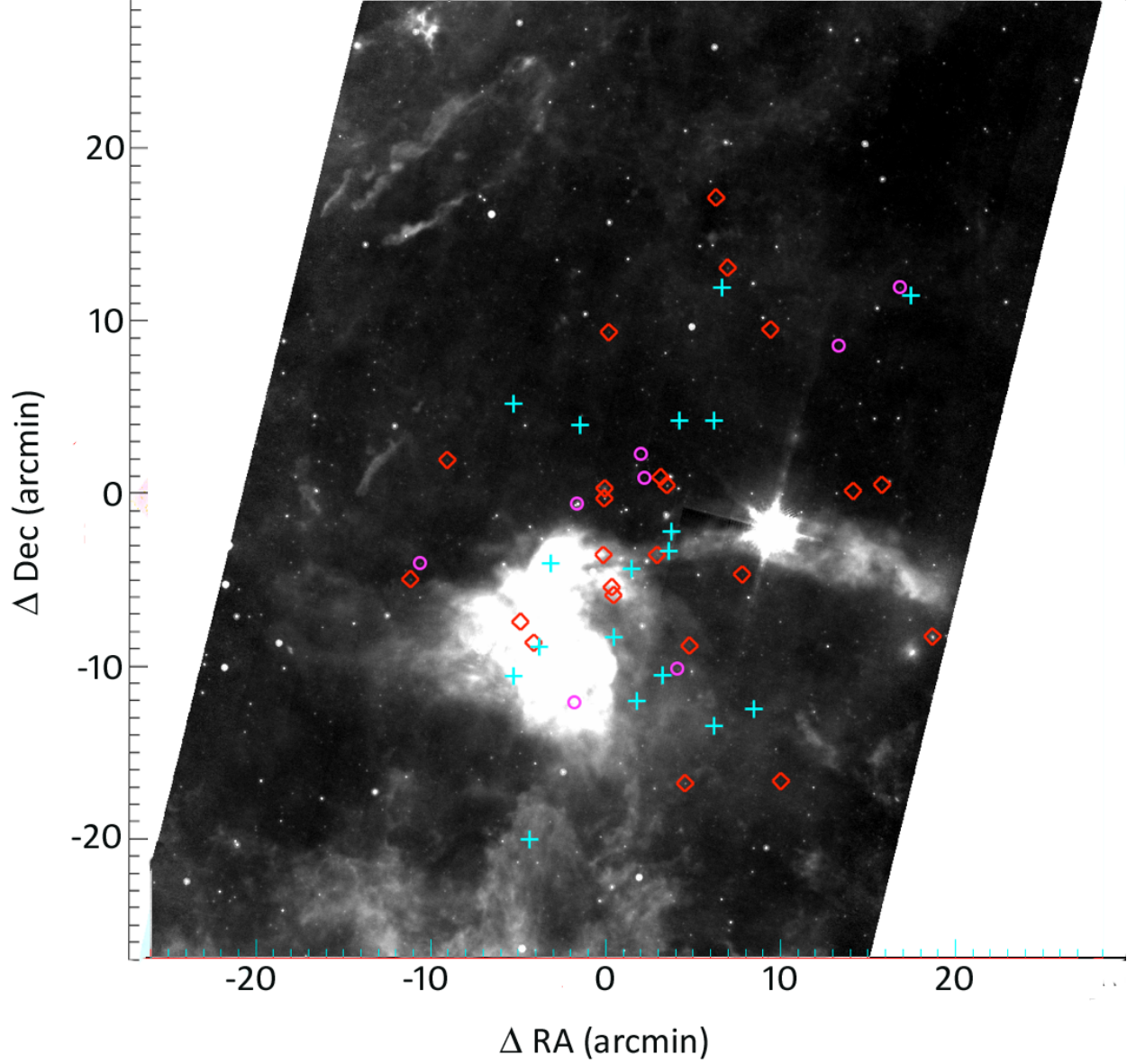


Fig. 2.— The central  $\sim 60' \times 40'$  mosaic of IC 2395 taken with the MIPS  $24\mu\text{m}$  channel. The coordinates are relative to  $\text{RA} = 130.6389$ ,  $\text{DEC} = -48.0688$ . Sources with disks are identified with symbols: *cyan crosses* represent Class II candidates, *magenta circles* represent transition disk candidates, and *red diamonds* represent debris disk candidates. The point source FWHM is  $5.7''$  and the platescale is  $1.25''/\text{pixel}$ .

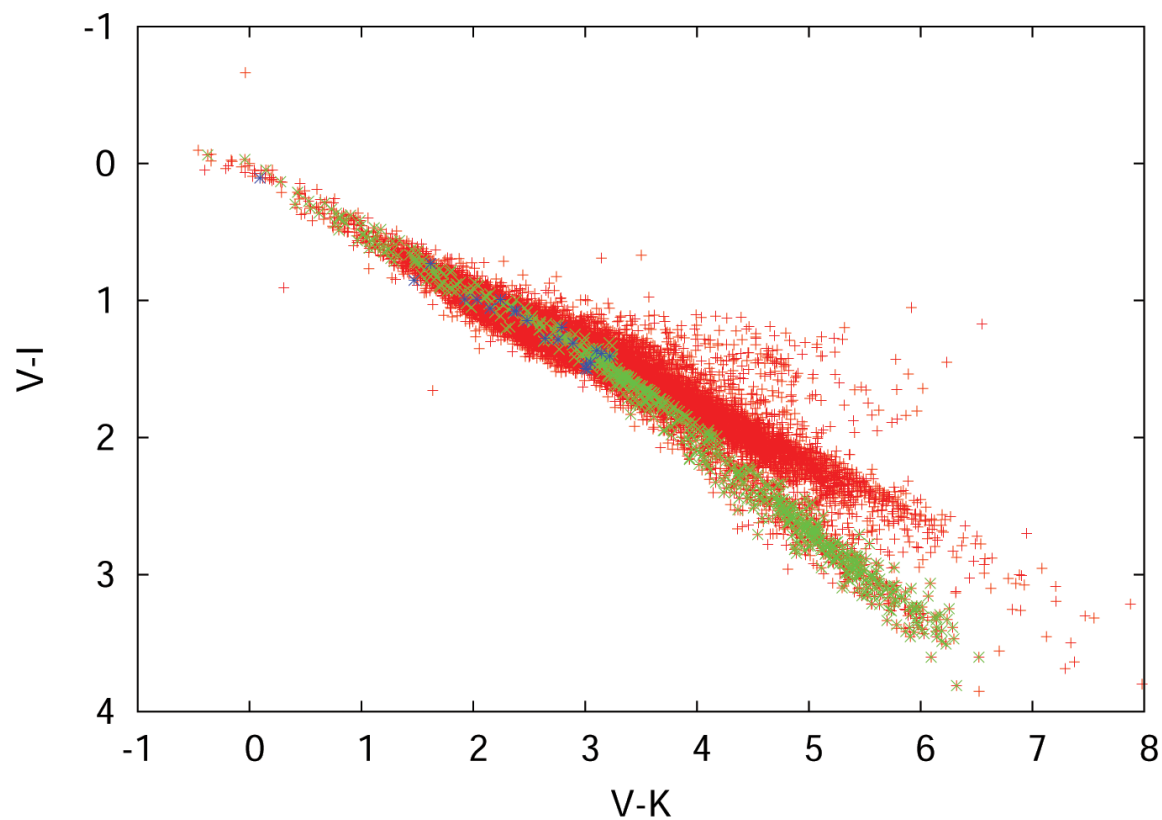


Fig. 3.— Optical - near-infrared CC diagram of IC 2395 cluster member candidates (green symbols) selected for the spectroscopic survey together with the complete sample of the photometric data (red symbols). Blue symbols show the stars with IR excess that may not be cluster members but were included in the spectroscopic sample.

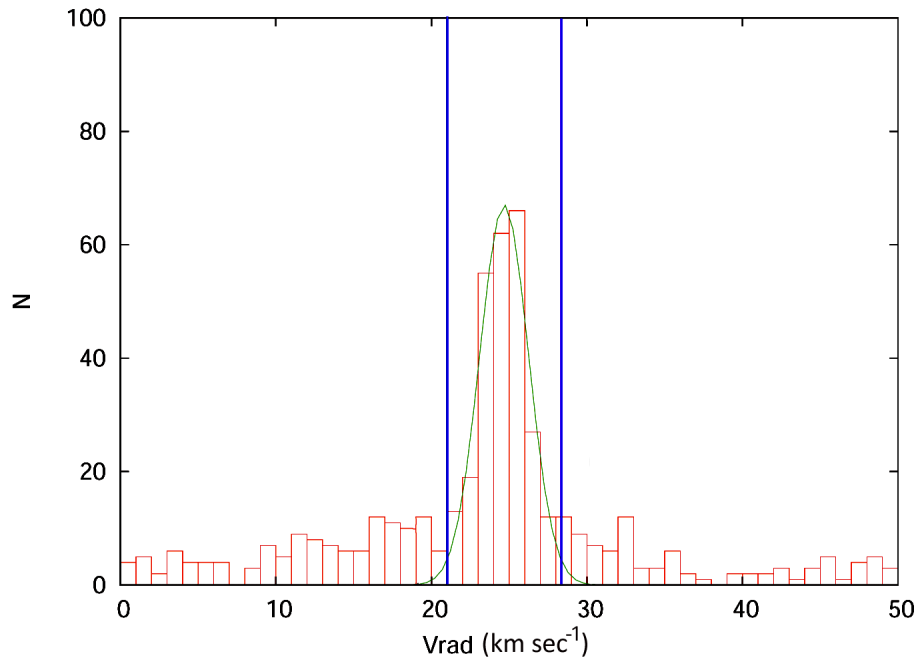


Fig. 4.— Radial velocity distributions toward IC 2395. The Gaussian fit is centered at 24.7 km/s. The vertical blue lines indicate  $\pm$  one full width at half maximum above and below the center velocity. This velocity range was used to identify cluster members; it corresponds to  $\pm 2.4 \sigma$ .

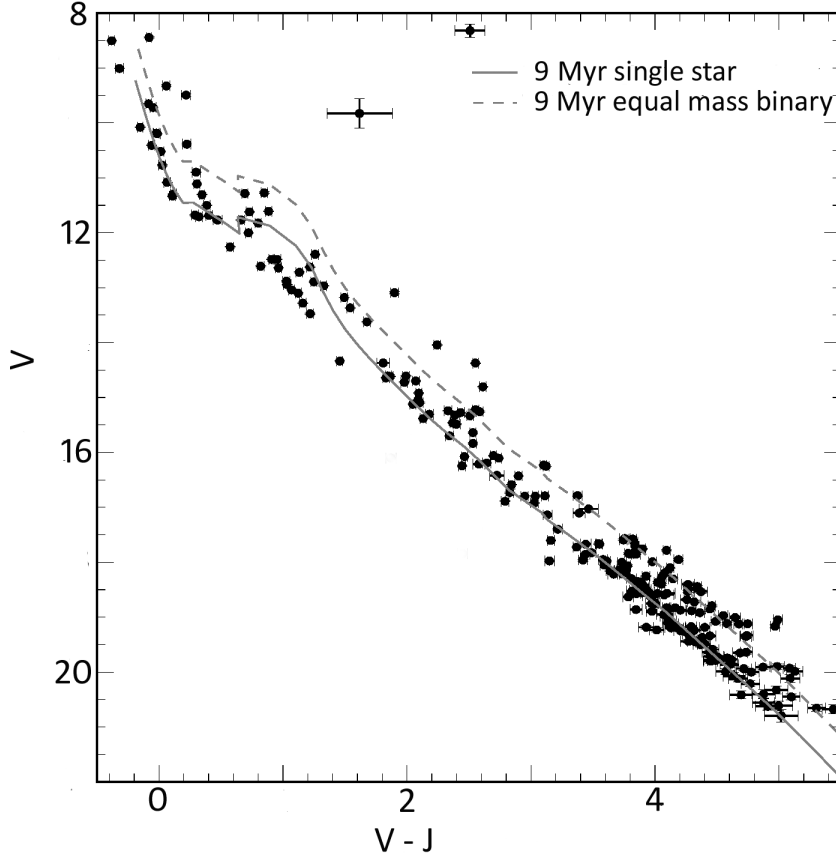


Fig. 5.—  $V$ ,  $V-J$  CM diagram with semi-empirical (see Bell et al. (2014) for details) model isochrones using the Dartmouth interior models. The red solid isochrone is for 9 Myr; it has been reddened by  $E(B-V)=0.09$  and shifted in distance assuming a modulus of 9.5. The dashed line is the same but shifted 0.75 mag higher i.e. where we would expect the equal mass binaries to lie.

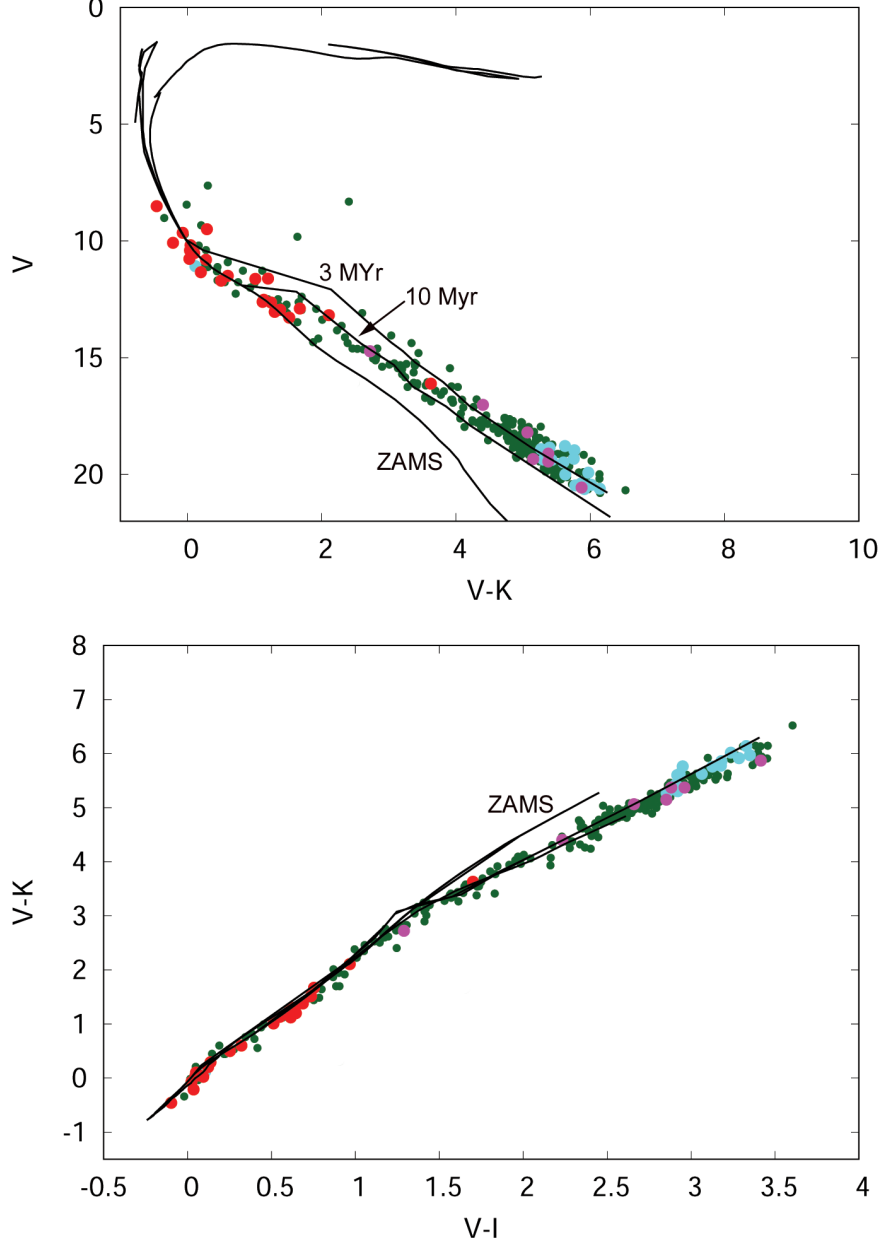


Fig. 6.— Optical - near-infrared CM and CC diagrams of IC 2395 cluster members. Green dots: members without IR excess, red: debris disk candidates, magenta: transitional disk candidates, cyan: class II candidates. Black lines show the 10- and 3Myr isochrones (Palla & Stahler 1999) (traditional age scale) and the ZAMS (Marigo et al. 2008).



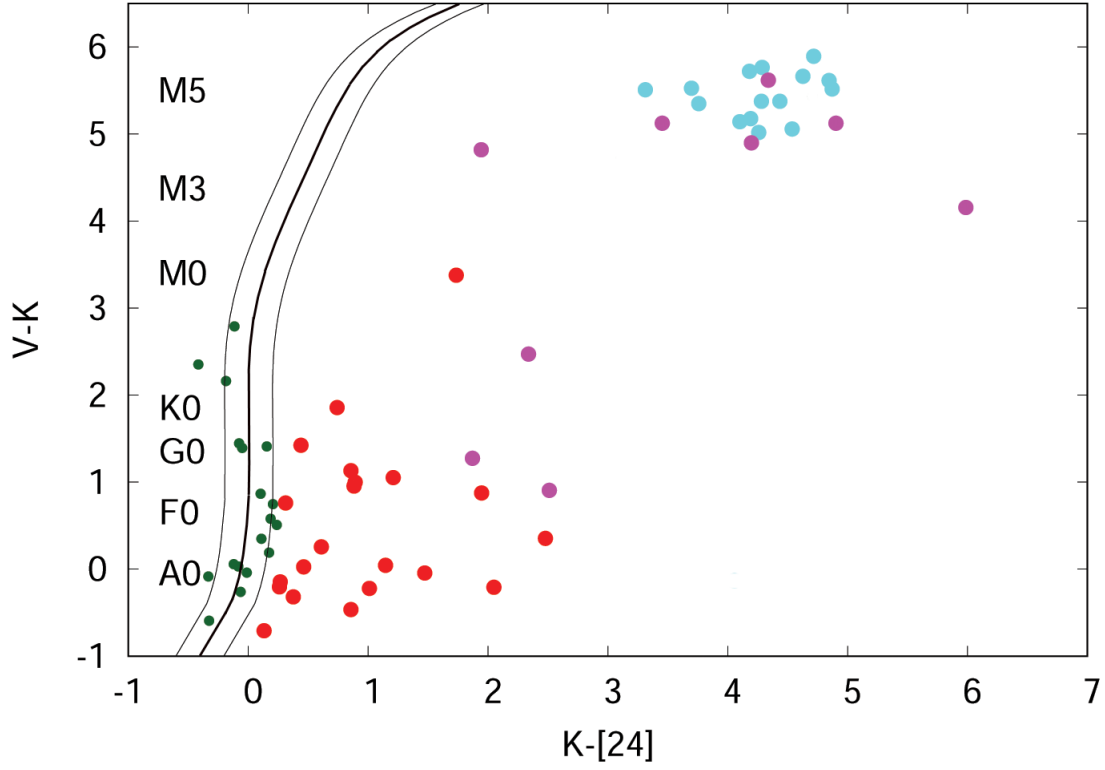


Fig. 7.— Dereddened  $V-K$  versus  $K_s-[24.0]$  CC diagram. Symbols are as in Figure 6. The black line represent the photospheric colours of main sequence stars (Urban et al. 2012), while the bounding lines are the typical range of uncertainties in projecting the color from shorter wavelengths (including random and systematic errors).

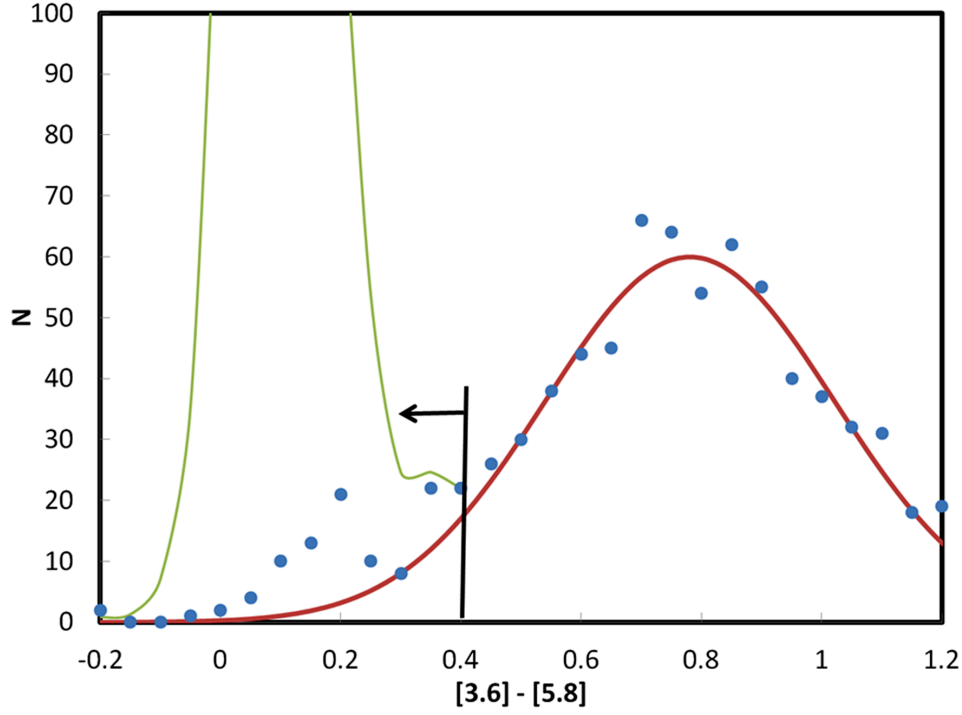


Fig. 8.— Selection criterion for transition disks using IRAC colors. The points show the distribution of the colors for all the objects with  $[8] - [24] > 1.5$  in all the clusters under study (see text), to which we have fitted a Gaussian (solid red line) confined to the upper 2/3 of the points to avoid biasing the fit with the wings of the distribution. The thin green line shows the distribution for the sources with smaller  $[24]$  excess emission. The vertical line shows the criterion adopted to identify transitional disk candidates (i.e.,  $[3.6] - [5.8] < 0.4$ ).

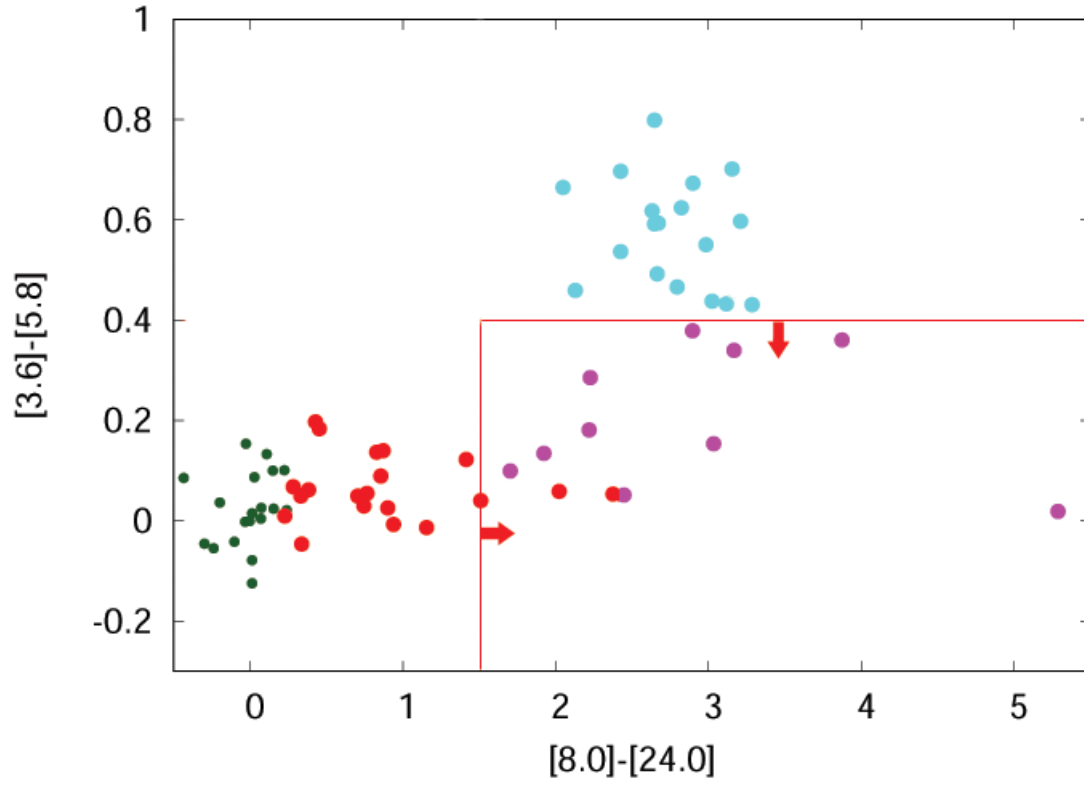


Fig. 9.— Color-color diagram illustrating the selection criteria (**within the red box**) for transitional disks (i.e.,  $[3.6] - [5.8] < 0.4$  &  $[8] - [24] > 1.5$ ) applied to IC 2395. Symbols are as in Figures 6 and 7.

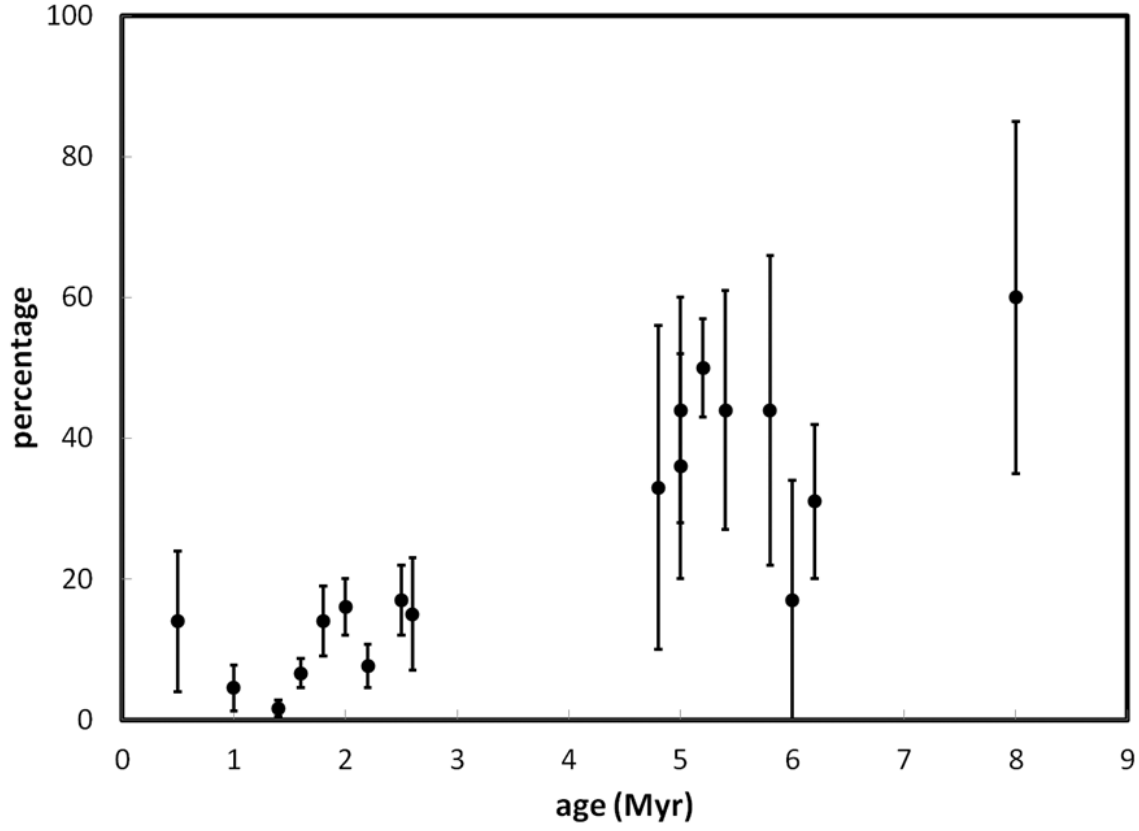


Fig. 10.— Percentage of transitional disks vs. age. defined as  $\text{No. Transitional} / (\text{No. Transitional} + \text{No. Class II}) * 100$ . This graph uses the traditional age scale because it is more complete for the relevant clusters/associations.